Parametric Studies and Effect of Scale-up on Heat Transfer Characteristics of Circulating Fluidized Beds

Lakshminath Bezbaroa Central Library ★ IIT Guwahati

A Thesis Submitted in
Partial Fulfillment of the Requirements
for the Degree of

Doctor of Philosophy

by

Patil Ranjit Shankarrao

Centre for Energy
Indian Institute of Technology Guwahati
April 2011

TH-1848_Shankarrao

THESIS
Lakshminath Bezbaroa Central Library
Indian Institute of Technology Guwahati
ACC. No. TH...1848.....
Date.....28/3/19.....

621.042
SHA/P
P11

CERTIFICATE

It is certified that the work contained in the thesis entitled Parametric Studies and Effect of Scale-up on Heat Transfer Characteristics of Circulation Fluidized beds by Patil Ranjit S., a research scholar in the Centre for Energy, Indian Institute of Technology Guwahati, India, for the award of the degree of the Doctor of Philosophy has been carried out under our supervision and this work has not been submitted elsewhere for a degree.

30/4/11

Dr. Manmohan Pandey
Professor,
Department of Mechanical Engineering,
Indian Institute of Technology Guwahati.

April 2011

30/4/11

Dr. Pinakeswar Mahanta
Professor – Dept. of Mech. Engg.,
Head – Centre for Energy,
Indian Institute of Technology Guwahati.

April 2011

TH-1848_Shankarrao

Acknowledgement

I express my deepest gratitude to my supervisors, Prof. Pinakeswar Mahanta and Prof. Manmohan Pandey for their inestimable guidance and support, for the constant inspiration. I drew from their critical thinking and approach, and for providing an excellent working atmosphere. Their thoughtful suggestions and ideas were vital for the framework and outcome of this research. It has been a rewarding experience for me in working with them all these years, and has inspired me enough in different aspects of research and life, for the years to come.

I would like to thank my doctoral committee members, Prof. Anoop K. Dass, Dr. Anugrah Singh and Dr. P. Muthukumar for their valuable suggestions and encouragement during my research work.

I would like to acknowledge Indian Institute of Technology Guwahati (Centre for Energy and Dept. of Mech. Engg.) for providing the funds and facilities for carrying out my research.

I would like to thank Mr. Rahul Praghanmor, Mr. Monoj Baruah, Mr. Yambem Volga Singh, Mr. Balwinder Singh, Mr. Chinmay Mittal, Mr. Pankaj Sharma for their help in my research work. I extend my thanks to Mr. Nalini Sharma - Biogas Development Training Centre (BDTC), Mr. Madan - pipe fitting and water supply department of IIT Guwahati and Mr. D. Chetry and other staff members of central workshop of IIT Guwahati for their lot of help during the fabrication and assembly of experimental setup.

I am thankful to many friends across different IITs and IIT Guwahati. Special mention to Mr. Pankaj Kalita (Scientific Officer), Mrs. L. Barbora (Scientific Officer), Mr. D. Huzuri, Mrs. A. Rajbanshi of Centre for Energy - IIT Guwahati, for being with me in good and as well as difficult times through these years. Many thanks to Mr. Siba Shankar Mohapatra and teammates in the sports field for their friendship and company.

I am very grateful to my beloved parents – Shri. Shankarrao K. Patil and Mrs. Kusum S. Patil, Mrs. Kamal S. Patil, my sisters, all other relatives, and my wife Mrs. Archana R. Patil and my Son Omkar R. Patil for their immeasurable love, understanding, and unwavering support, which has made this feat possible.

Patil Ranjit S.

Patil Ranjit S.

TH-1848_Shankarrao

Synopsis

Coal is the principal energy source in India because of its large deposits and availability. Coal has been extensively used in Indian power sector. Out of the total installed capacity of 147,965 MW, coal was in use to produce 93,725 MW (63.34%) during the year 2009. However, majority of coal in India contains high ash (as high as 45%) and sulphur (3-5%). With the existing technology, carbon dioxide, oxides of nitrogen and sulphur emitted by majority of the coal based power plants in India are significant attributing to environmental pollution. Therefore there is a great need for an alternative technology which can utilize this type of coal with its improved combustion and reducing pollution. A circulating fluidized bed (CFB) is a relatively new and alternate technology gaining popularity in power generation because of its capability of burning wide range of fuels including coal, wood wastes, agricultural wastes, kerosene etc, its environmental compatibility i.e efficient sulphur removal, low NO_x emission and high combustion efficiency. These factors led to the development of CFB steam generators. Research then began on the various aspects related with CFB.

Recently majority of the work on hydrodynamics and heat transfer characteristics were reported on a single riser of CFB unit operated under fast fluidization mode. Very few researchers have reported about hydrodynamics and heat transfer characteristics, those changes abruptly with change in dimensions (scale-up) of circular riser. Moreover, now a days' industry prefers fast fluidization with rectangular or square cross section CFB riser for power generation. Another important integral component of CFB unit is cyclone separator. Cyclone separator in the circulating fluidized bed boiler handles a large volume of gas at high temperature. The unburned char particles entrained through the riser passes through the cyclone separator along with volatile and flue gases. Extent of combustion inside the cyclone separator is small due to less residence time and insufficient oxygen. However, additional combustion of carbon monoxide and the volatiles often occur in the cyclone separator. The outer skin temperature of the cyclone separator is relatively high incurring excessive heat losses due to natural convection and radiation. Recovery of the heat has been accomplished in many cases by circulation of cool water or saturated steam to convert it into superheated steam. There is still scope to increase the capacity of the CFB boiler through extraction of heat from the cyclone

TH-1848_Shankarrao

separator. From the literature review it is evident that most of the work has been completed on hydrodynamics and bed-to-wall heat transfer characteristics for a single cyclone separator.

Therefore, present work is focused to perform parametric studies and effect of scale-up on heat transfer characteristics of risers and cyclone separators of CFB. To accomplish the aim, three CFB units of same height and different dimensions of square cross section were fabricated. CFD simulations using Fluent 6.3.26 were also performed for heated portion of the riser. Effect of parameters like sand inventory, sand particle size, superficial velocity of air and also the effect of risers' cross sectional area and cyclone separators' barrel diameter on heat transfer characteristics were predicted. Numerous numbers of experiments were conducted and subsequently the empirical correlation models were also developed for the risers and cyclone separators. Hence this study will be more promising and helpful for design and fabrication of the new CFBs.

In the present work, a flow regime study was carried out on the CFB riser of cross section 0.15 m × 0.15 m. Effect of superficial velocity of air on variation of pressure drop and suspension density along the riser column was studied. Study on wall-to-bed heat transfer characteristics for risers of three different CFB units of different cross sections 0.15 m × 0.15 m, 0.20 m × 0.20 m, and 0.25 m × 0.25 m has been completed. Risers of all the CFB units are of same height 2.85 m. To accomplish the scale-up study, experiments were conducted on each CFB setup for five different non-dimensional air velocities ($U^* = 5, 5.5, 6, 6.6$ and 8) and two different weights of sand inventory per unit area of the distributor plate ($P = 1750$ N/m^2 and $P = 3050$ N/m^2). Sand particles with average size of 460 μm were used in all the experiments. Effect of parameter like riser cross section on the axial variation of heat transfer coefficients and off axial distribution of bed temperature was compared for all the three beds. Effect of other operating parameters like velocity of air and sand inventory on heat transfer characteristics were also predicted for individual CFB setup. The results obtained were compared with available literatures.

In individual CFB setup, effect of superficial velocity and sand inventory on distribution of bed temperature across the riser and heat transfer coefficient along the riser height was studied. In all the setups it was observed that the bed temperature

TH-1848_Shankarrao

decreases with increase in cross section of the riser and superficial velocity of air in the riser column, and increase with increases in sand inventory. Heat transfer coefficient increases with increase in cross section of the riser and sand inventory, and decreases with increase in superficial velocity of air.

Based on the scale-up study correlations on bed Nusselt number were obtained separately for lower splash region, middle splash region and for the portion of riser covering all regions i.e lower splash, middle splash and upper splash region. A best-fit equation having non-dimensional numbers was obtained and constants of correlation were obtained with the help of Findfit function of Mathematica 5.2. Experimental results with the prediction of correlation showing maximum rms deviation of ±11.66- 21.73%.

CFD simulations using Fluent 6.3.26 were also completed to study the effect of superficial velocity of air, particle size, sand inventory and bed cross section area on heat transfer characteristics. 3D CFD simulations were performed using the Fluent 6.3.26 on steady state wall-to-bed heat transfer characteristics of CFB riser of cross section 0.15 m × 0.15 m and height 2.85 m for heated portion (heater) of same cross section of riser and height of 0.6 m, located at 0.6 m and 1.8 m above the distributor plate which is the lower splash region and upper splash region of CFB, respectively. Further simulations on upper splash region of height 0.6 m, located at 1.8 m above the distributor plate were accomplished for risers of cross section 0.30 m × 0.30 m.

Modelling and meshing were done with Gambit software - version 2.4.6. The wall of heater was maintained at the constant heat flux q" = 1000 W/m^2. RNG k-ε model was used for turbulence modelling. Eulerian model with Gidaspow phase interaction scheme was used to simulate the two phase flow (air + sand mixture flow).

Effect of particle size on heat transfer characteristics of lower splash region was predicted using six particle sizes falling in the range of Geldart *B* type particles (60 µm, 100 µm, 160 µm, 260 µm, 360 µm, 460 µm) at sand inventory of 7 kg and superficial velocity of air as 2.5 m/s for the heater of cross section 0.15 m × 0.15 m.

Effect of superficial velocity of air and sand inventory on heat transfer characteristics was predicted with respect to lower splash region of riser of cross section 0.15 m × 0.15 m for two superficial velocities of air (2.5 m/s and 4 m/s) and two sand inventories (4 kg and 7 kg) for particle size of 460 µm.

Effect of riser cross section on heat transfer characteristics was predicted with respect to upper splash region of risers of cross section 0.15 m × 0.15 m and 0.30 m ×

TH-1848_Shankarrao

0.30 m for two superficial velocities of air (2.5 m/s and 4 m/s) at 3050 N/m^2 (weight of sand inventory per unit area of distributor plate) and sand particle size of 460 μm is used during the simulation.

It is observed that bed temperature and heat transfer coefficient increases with increase in sand inventory and decreases with increase in particle size. Bed temperature and heat transfer coefficient also decreases with increase in superficial velocity of air. Bed temperature decreases and heat transfer coefficient increases with increase in cross section of risers. Results obtained from CFD simulations and experimental results obtained from available CFB setup of IIT Guwahati were in good agreement.

Heat transfer behaviour in the cylindrical portion of cyclone separators having different size of barrel diameter belonging to three different CFB units also has been studied. Steady state experiments were carried out by providing heat in the lower splash region of the riser of a CFB and consequently examining bed-to-wall heat transfer in the cyclone separator. To study the effect of scale-up (increase in barrel diameter of cyclone separators) on heat transfer characteristics, experiments were conducted under similar operating conditions on three CFB setups. Cyclone separator's design ratios i.e ratios of various dimensions of cyclone separator with respect to cyclone barrel diameter were maintained same in each cyclone separator belonging to the three different CFB setups. Experiments were conducted on each CFB setup for five non-dimensional air velocities (U^* = 5, 5.5, 6, 6.6 and 8) at two different weights of sand inventory per unit area of the distributor plate (P = 1750 N/m^2 and 3050 N/m^2).

Effect of parameters like superficial velocity of air and sand inventory on heat transfer characteristics was investigated for individual cyclone separator. Local heat transfer coefficient along the height of cylindrical portion of cyclone separators were evaluated and compared. Also, bed temperature across the barrel diameter of all cyclone separators were measured and compared. In all the cyclone separators, it is observed that the bed temperature decreases with increase in cyclone's barrel diameter and superficial velocity of air. It increases with increases in sand inventory. Heat transfer coefficient increases with increase in barrel diameter of the cyclone separator and inventory of sand. It decreases with increase superficial velocity of air.

Based on the scale-up study, correlation on Nusselt number was obtained for cyclone separators. A best-fit equation having four non-dimensional numbers fitting 60 experimental data points was obtained and constants of the correlation was obtained with

the help of Findfit function of Mathematica 5.2. Experimental results with the prediction of correlation showing maximum rms deviation of ± 14.31%.

The thesis is organised in seven chapters. Chapter 1 deals with the introduction. Chapter 2 presents the literature review and scope for the present investigations. In Chapter 3, details about the experimental setups and procedure are explained. Chapter 4 includes experimental results and discussions on parametric study and effect of scale-up on heat transfer characteristics of circulating fluidized bed risers. Chapter 5 includes computational study (modelling and simulation) using Fluent 6.3.26 on CFB risers. Chapter 6 deals with experimental results and discussions on parametric study and effect of scale-up on heat transfer characteristics of cyclone separators. Conclusions and future scope are presented in Chapter 7.

TH-1848_Shankarrao

Contents

TH-1848_Shankarrao

TH-1848_Shankarrao

List of Figures

TH-1848_Shankarrao

TH-1848_Shankarrao

TH-1848_Shankarrao

TH-1848_Shankarrao

List of Tables

TH-1848_Shankarrao

Nomenclature

A_S	Surface Area of Heater, m^2
A_{Sc}	Surface Area of Cyclone Separator, m^2
A_B and A_D	Cross Section Area of Heater or Bed or Riser and Graduated Column or Sand Measuring Section, m^2
B1	CFB riser of cross section 0.15 m × 0.15 m
B2	CFB riser of cross section 0.20 m × 0.20 m
B3	CFB riser of cross section of 0.25 m × 0.25 m
b	Width of Heater, m
b1	Width of Heater of B1, m
b2	Width of Heater of B2, m
b3	Width of Heater of B3, m
C1, C2, C3	Smaller, Medium and Larger Cyclone Separator with D_C = 0.27 m, 0.36 m and 0.45 m respectively
D	Distance from the Distributor Plate to the off-axis Section AA of the Heater, m
D_C	Cyclone Separator's Barrel Diameter, m
d_p	Average Diameter of Sand Particles, m
d_p^*	Non-dimensional Particle Size
G_s	Solid Circulation Rate (Solid Mass Flux), $kg.m^{-2}.s^{-1}$
H	Height of the Heater, m
H_B, H_b	Height of the Static Sand Inventory of the Fluidized Bed, m
H_C	Height of the Cyclone ($L_C + Z_C$), m
H_D, B	Hydraulic Diameter of CFB Bed [H_{D1} = b1, H_{D2} = b2, H_{D3} = b3], m
H_r	Total Height of the Riser, m
h, h_y	Local Heat Transfer Coefficient - Riser, $Wm^{-2}K^{-1}$

TH-1848_Shankarrao

h_{avg}	Average Heat Transfer Coefficient - Riser, W $m^{-2}K^{-1}$
h_c	Local Heat Transfer Coefficient – Cyclone Separator, $Wm^{-2}K^{-1}$
Δh	Difference of Height in Manometric Fluid, cm of Water
k_g	Thermal Conductivity of Gas (Air), $Wm^{-1}K^{-1}$
L	Lower Splash Region in the Riser of CFB
Lc	Length of Cylindrical Portion of Cyclone Separator, m
L_m	Distance between Two Consecutive Pressure Taps (0.6 m approx. for all CFB units)
M	Middle Splash Region in the Riser of CFB
Nu_B	Bed Nusselt Number, $(h. H_D/k_g)$
P	Weight of Static Sand Inventory Mounted per unit Area of Distributor Plate, N/m^2
ΔP_b	Pressure Drop in terms of cm of Water
Q	Heat Supplied at Heater, W
Q_0	Flow Rate or Discharge through Orifice Meter, m^3
q_1	Amount Heat Carried by Air + Sand Mixture which was Calculated at the Inlet of Cyclone Separator, W
q_2, q_3	(q_2) and (q_3) are the Heat Carried by Air and Sand, respectively, Measured at the Two Outlets of Cyclone Separator – Top Outlet (Chimney) and Bottom Outlet of Cyclone Separator, respectively, W
q"	Heat Flux for the Cyclone Separator, W/m^2
Re_B	Reynolds Number - Riser, $(U' H_D \rho_g/\mu_g)$
Re_C	Reynolds Number – Cyclone Separator, $(U_C D_C \rho_g/\mu_g)$
T_B, T_b	Bulk Mean Temperature of Bed or Mixture (Air + Sand) Flow - Riser, K
T_{Bc}	Bulk Mean Temperature of Air + Sand Mixture Flow - Cyclone Separator, K
T_S	Wall Temperature of Heater - Riser, K
T_{Sc}	Wall Temperature of Cyclone Separator, K
U	Upper Splash Region in the Riser of CFB

TH-1848_Shankarrao

u_g	Gas (Air) Velocity, m/s
U'	Superficial Velocity of Air, m/s
U_{mf}	Minimum Fluidizing Air Velocity, m/s
U*	Non-dimensional Velocity Parameter, (Ratio of Superficial Velocity of Air {U'}to Minimum Fluidizing Air Velocity {U_{mf}})
u^*	Non-dimensional Particle Velocity
X	Distance Measured from Left Hand Side of Wall of Heater to the Thermocouple End, m
$[A_B/A_S]$	Non-dimensional Area Parameter, (Ratio of Cross section Area of Heater or Riser {A_B} to the Surface Area of the Heater {A_S})
$[H_B/H_D]$	Aspect Ratio, (Ratio of Height of The Static Sand Inventory of the Fluidized Bed {H_B}to the Hydraulic Diameter of Bed {H_D})
$H^*=$ $[H_m/H_r]$	Non-dimensional Height Parameter, (Ratio of Height from the Distributor Plate to the Thermocouple Location in the Heater {H_m, in correlation eq. (4.3) and eq. (4.4)} to the Total Height of the Riser {H_r}). In correlation eq. (4.5) {H_m} is the of Height from the Distributor Plate to the Midpoint of Heater
[r/R]	(r/R) is the Ratio of Distance (r) of the Thermocouple Location with respect to (T2-T6) Measured from the Centre of Each Cyclone Separator to the Radius (R) of that Cyclone (refer Fig. 3.5)
[X/b]	Non-dimensional Distance across the Heater
$[Y/D_C]$	Non-dimensional Distance (Y/D_C) is the Ratio of Distance (Y) of the Thermocouple Location with respect to (T7-T11) as shown in Fig. 3.5, measured from the inlet of the Cyclone Separator, Normalized with Respect to the Cyclone Barrel Diameter (D_C)
$[Y/H_C]$	Non-dimensional Distance (Y/H_C) is the Ratio of Distance (Y) of the Thermocouple Location with respect to (T7-T11) as shown in Fig. 3.5, measured from the inlet of the Cyclone Separator, Normalized with Respect to the Height of the Cyclone (H_C)

Greek Symbols

ρ_g	Density of Gas (Air), kg m^{-3}
ρ_{sus}	Supension Density of Mixture (Air + Sand), kg m^{-3}
μ_g	Viscosity of Gas (Air), kg m^{-1} s^{-1}
ε, ε_{mf}	Voidage, Voidage at Minimum Fluidization

TH-1848_Shankarrao

Abbreviations

CFB	Circulating Fluidized Bed
FCC	Face Centred Cubic
ID	Inside Diameter
MS	Mild Steel
OD	Outside Diameter
rms	Root Mean Square

TH-1848_Shankarrao

Chapter 1

Introduction

TH-1848_Shankarrao

Chapter 1

Introduction

1.1 Motivation

Coal is the principal source of energy in India because of its large deposits and availability. Coal is extensively used in Indian power sector. Out of the total installed capacity of 147,965 MW, coal was in use to produce 93,725 MW (63.34%) during the year 2009 (Goyal, 2009). However, majority of coal in India contains high ash (as high as 45%) and sulphur (3-5%) (Goyal, 2009). High ash content in coal is responsible for the derating of the power plant. Moreover, emissions of oxides of carbon, nitrogen and sulphur are significantly high from power plants, where coal with high ash content has been used with conventional technology. Therefore, there is a great need of an alternative technology to utilize this type of coal for improving combustion and reducing the pollution. Circulating fluidized bed (CFB) is one of the promising technologies to deal with the combustion of coal with high ash and sulphur. Apart from using coal as a fuel, CFB technology can be used for combustion of wide range of fuels including wood wastes, agricultural wastes, biomass etc. Further, this technology is popular for environmental compatibility in terms of sulphur capture and reduction of oxides of nitrogen. CFB technology has been used in power production for last few decades. However, many of the issues related to hydrodynamics and heat transfer on scale-up of CFB is yet to be explored. Hence, present work is taken up to investigate behavior of CFB in terms of bed geometry and operating parameters.

1.2 Regimes of Fluidization

Fluidization is the phenomenon by which solid particles are transformed into a fluid like state through suspension in a gas or liquid (Fig. 1.1). Fluidized bed may have different flow structures depending upon the flow velocity of fluid imposed on the bed. Various regimes of fluidization are described as follows.

TH-1848_Shankarrao

1) Fixed Bed: When the fluid is passed through bottom of bed at a low flow rate, the fluid merely percolates through the void spaces between stationary particles. This is called a fixed bed as shown in Fig. 1.1 (a).

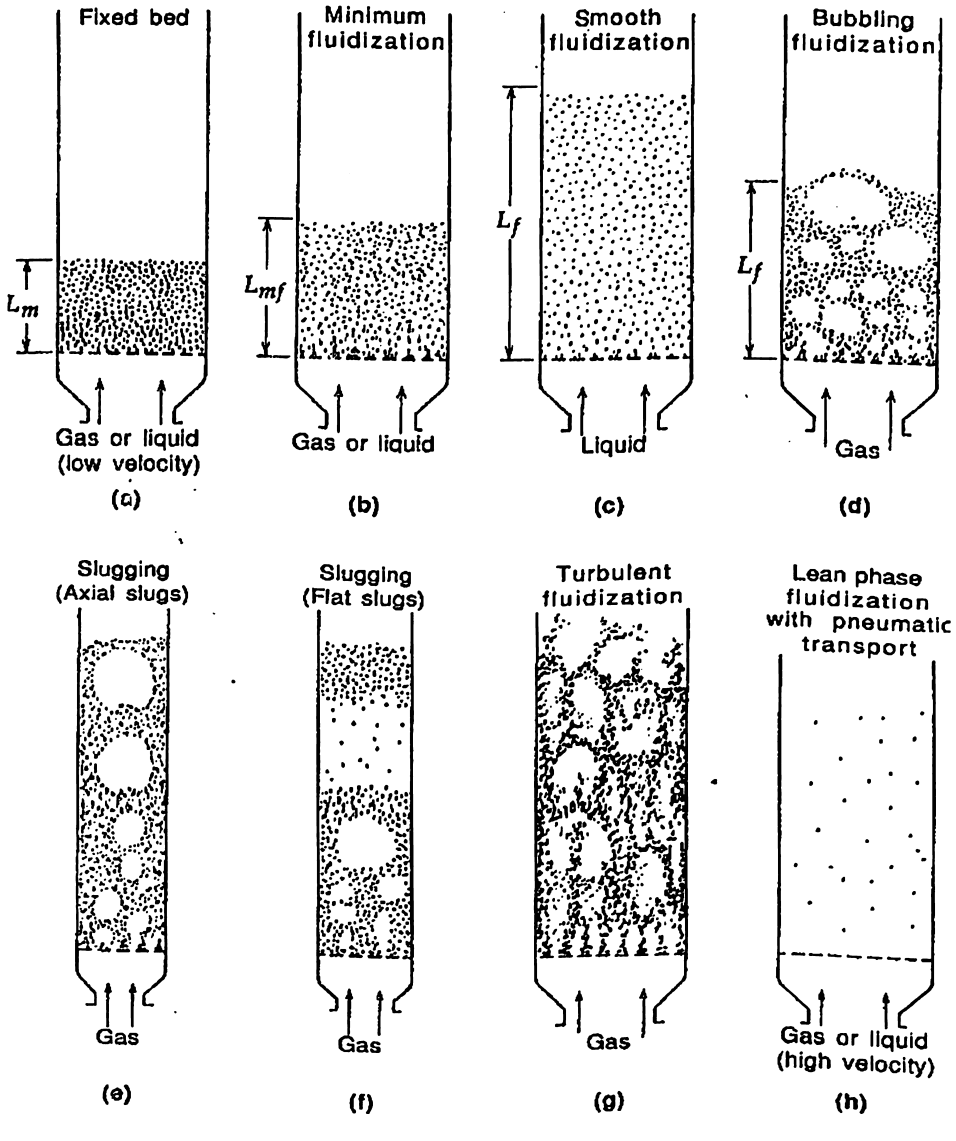

Fig.1.1 Regimes of Fluidization (Kunii and Levenspiel, 1991)

2) Expanded Bed: Particles move apart and a few of them start vibrating with further increase of the flow velocity. However, the movement of particles is in a restricted region. This regime is termed as the expanded bed.

3) Minimum Fluidization: At a still higher gas velocity, a point is reached when all the particles are just suspended by the upward flowing fluid. This is referred as minimum fluidized bed as shown in Fig. 1.1(b). This condition is achieved by counterbalancing of the frictional force between particle and fluid by the weight of the particles.

TH-1848_Shankarrao

In solid – liquid system, increase in flow rate above minimum fluidization results in smooth or progressive expansion of bed. Gross flow instabilities remain small, and heterogeneity or large-scale voids of liquids are not observed. Such a fluidized bed is called either homogeneously or smoothly fluidized bed as shown in Fig. 1.1(c). For gas - solid systems, homogeneous fluidization is observed under special conditions of fine light particles with dense gas at high pressure.

4) Bubbling Fluidization: Increasing flow rate beyond minimum fluidization, void regions form near distributor plate and grow as they rise in the upward direction in the bed. Gas-solid systems show large instabilities with bubbling and gas channeling with rise in flow rate beyond minimum fluidization. At high flow rate, vigorous agitation of particles is seen. Such a bed is called aggregative or heterogeneous or bubbling fluidized bed as shown in Fig. 1.1(d).

5) Slugging Fluidization: The gas bubbles formed above the distributor plate coalescent and grow as they rise, they may eventually become large enough to spread across the vessel. In case of fine particles, their flow is smoothly down by the wall around the rising void of gas. This is called as slugging with axial slugs shown in Fig. 1.1(e). For coarse particles, the portion of the bed above the bubble is pushed upwards as in the case of a piston. Particles rain down from the slug which finally disintegrates. At about this time another slug forms and this unstable oscillatory motion is repeated. This is called flat slugging as shown in Fig. 1.1(f).

6) Turbulent Fluidization: At sufficiently high gas flow rate, the terminal velocity of solids is exceeded, the upper surface of bed disappears, entrainment becomes appreciable and, instead of bubbles, turbulent motion of solid cluster and void of gas of various size and shapes can be observed. This is the turbulent fluidized bed as shown in Fig. 1.1(g).

7) Fast Fluidization: With further increase in gas velocity, solids are carried out of the bed along with the gas-making a lean phase fluidized bed as shown in Fig. 1.1 (h). In lean phase fluidization the rate of entrainment of particles is very high, necessitating the use of an outside cyclone separator to recirculate the entrained particles back to the bed. This system is called fast fluidized bed. Behaviour of fluidized bed varies significantly

TH-1848_Shankarrao

with superficial air velocity. Hydrodynamic characteristics and heat transfer characteristics in CFB are explained in subsequent sections.

1.3 Hydrodynamic Characteristics

Various regimes of fluidization have been explained in the earlier section. It is observed that depending on the air velocity, there may be different type of fluidization regimes. Hydrodynamic properties like pressure, suspension density, voidage also changes along the height of the riser with the change in velocity of air. Figure 1.2 explains the variation of pressure drop with velocity.

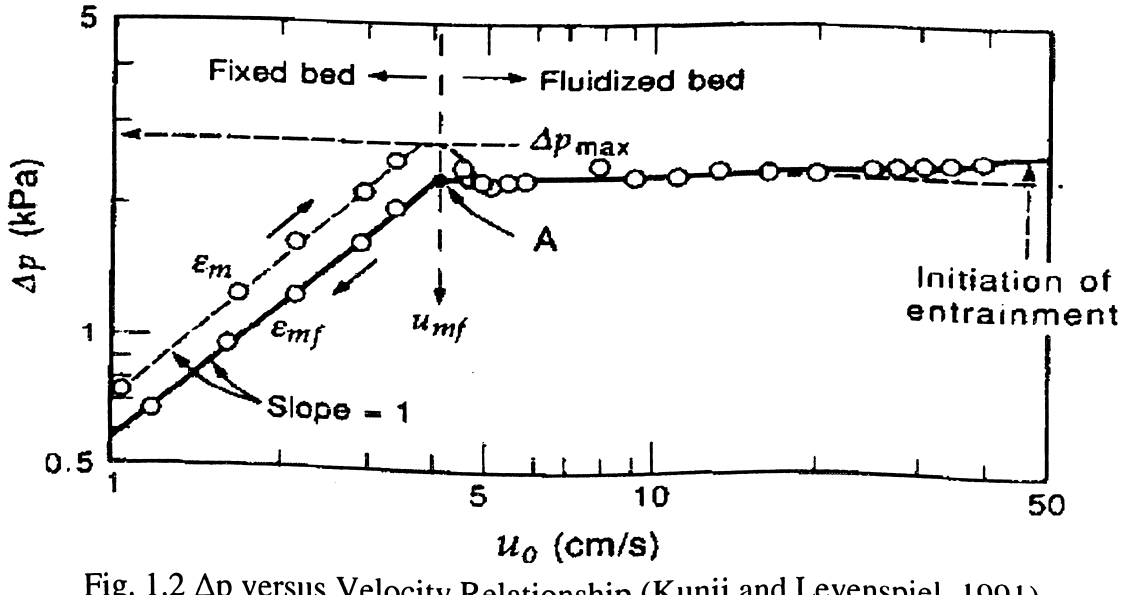

Fig. 1.2 Δp versus Velocity Relationship (Kunii and Levenspiel, 1991)

Pressure drop versus velocity relationship is an indication of quality of fluidization. The pressure drop is approximately proportional to gas velocity. With further increase in velocity, the voidage in the fixed bed increases from ε_m to ε_{mf}. This results in a decrease in pressure drop. With further rise in velocity, bed expands with appearance of bubbles, which create non-homogeneity. Interestingly, despite rise in velocity, the pressure drop remains unchanged. The reasoning for this effect is given in terms of well aeration of dense gas solid phase that deforms easily without appreciable resistance a characteristic liquid behavior. With decrease in gas velocity, fluidized particles settle to form a loose bed (fixed bed) of voidage ε_m.

1.4 Heat Transfer Characteristics

Heat transfer study within the circulating fluidized beds has been a subject of detailed investigations since 1980 onwards. CFB is an intermediate phase between turbulent fluidized bed and dilute pneumatic conveying. Heat transfer characteristics are strongly dependent on hydrodynamic characteristics of CFB unit. As noted in the earlier section, distribution of particles in the riser column varies in the axial and off axial direction with change in velocity of air. Heat transfer to the walls of a CFB is due to conduction from clusters of particles falling along the walls. The heat transfer coefficient plays a major role for designing a fluidized bed boiler. Following section presents the need of present study.

1.5 Major Objectives of the Study

CFB technology has been used in power production for last few decades. It is observed from literature that the bed hydrodynamics strongly influences the heat transfer characteristics [Kunni and Levenspiel (1991)] and hydrodynamic characteristics differ significantly with the geometry of the bed cross section [Zhou et al. (1994)]. However, many of the issues related to heat transfer on scale-up of CFB is yet to be explored. Risers of square and rectangular cross-sections are now widely employed in circulating fluidized bed applications [Zhou et al. (1994)]. Hence, there is high demand for scale-up study of CFB on heat transfer characteristics with square cross-sections. Hence, present work is taken up to investigate behavior of CFB in terms of square bed geometry and operating parameters on heat transfer characteristics.

Objectives of present study are explained as follows:

- ✓ To investigate, experimentally and numerically, the effect of various operating parameters like sand inventory, superficial velocity of air, sand particle size on distribution of bed temperature and local heat transfer coefficient.

- ✓ To study, experimentally and numerically, the effect of scale-up (bed cross-section) on wall-to-bed heat transfer characteristics in the CFB risers and to develop empirical correlation.

- ✓ To study experimentally the effect of cyclone barrel diameter and other various operating parameters like sand inventory, superficial velocity of air on bed-to-wall heat transfer characteristics in the cyclone separators of CFBs and to develop empirical correlation.

1.6 Organization of the Thesis

Chapter 2 discusses the literature review on experimental studies on riser, experimental work accomplished to study the effect scale-up on both hydrodynamic and heat transfer characteristics of riser, computational study on riser and experimental studies on cyclone separator.

Chapter 3 deals with description on experimental setup and procedure to be followed. Different subsections of this chapter explains the details about the CFB Setup fabricated at IIT Guwahati, fabrication of heat transfer probe (heater) used in the riser column for wall-to-bed heat transfer study and experimental procedure used while conducting heat transfer study on CFB risers. Arrangement of thermocouples, and the procedure followed to study bed-to-wall heat transfer characteristics in three cyclone separators is also described.

Chapter 4 presents experimental investigations on hydrodynamic and wall-to-bed heat transfer characteristics of CFB risers. Effect of various parameters like superficial velocity of air on variation of pressure drop and suspension density along the riser column is presented. Also effect of superficial velocity of air, sand inventory and bed cross section on off-axial bed temperature distribution and axial distribution of heat transfer coefficient is also explained. Chapter also presents the empirical correlation models on bed Nusselt number as a function of various non-dimensional numbers.

Chapter 5 presents the modeling and simulation of riser using CFD software – Fluent 6.3.26. Results and discussion on effect of particle size, bed cross section, sand inventory and superficial velocity of air on wall-to-bed heat transfer characteristics are explained.

Chapter 6 deals with experimental investigations on bed-to-wall heat transfer study in cyclone separators. Effect of parameters like sand inventory, superficial velocity of air and cyclone separators' barrel diameter on heat transfer characteristics is explained. Chapter also presents the empirical correlation model on Nusselt number as a function of various non-dimensional numbers for the cyclone separators.

Chapter 7 summarizes the present work, states the conclusions drawn from the same, and outlines the scope for future work.

TH-1848_Shankarrao

Chapter 2

Review of Literature and Scope for Present Investigations

TH-1848_Shankarrao

Chapter 2

Review of Literature and Scope for Present Investigations

2.1 Introduction

In the present chapter, review of literature and scope for present investigations are discussed. Sections 2.2 and 2.3 represent the review of experimental and computational studies on CFB risers, respectively. In section 2.2, review on hydrodynamic and heat transfer characteristics associated with risers is reported. In section 2.3, review on numerical studies, modelling and simulation of CFB risers are reported. Section 2.4 reveals the review of experimental studies on cyclone separators. Section 2.5 summaries the chapter and also explains the scope for present investigations.

2.2 Experimental Studies on Riser

In the present section, literature reported on various types of experimental work on CFB riser is discussed. Review includes both hydrodynamic and heat transfer characteristics along the riser column.

Extensive literature is available for heat transfer at the tubes suspended in the core of CFB furnace. Fraley et al. (1983) studied heat transfer from a probe of 9.5 mm OD to a flowing gas-solid mixture through a 75 mm diameter pipe.

Subbarao and Basu (1986) reported the cluster model to predict the heat transfer coefficient in circulating fluidized beds. They have reported heat transfer coefficient is mainly a function of gas and solid flow rates as well as bed density. They have used data of Fraley et al. (1983) to test the validity of model. Only data of Fraley et al. (1983) has been used to test the validity of the model as only they have reported gas and solid flow rates as well as bed densities.

TH-1848_Shankarrao

Basu (1990) has proposed a mechanistic model to explain the interdependence of design and operating parameters. Heat transfer to the wall of a fast fluidized bed has been measured for four different particle sizes, two sizes of heat transfer probes and several temperatures from 30°C to about 900°C.

Kolar and Sundaresan (2002), and Sundaresan and Kolar (2002) reported heat transfer from surface of tubes suspended in core of a CFB furnace to the bed. They have proposed an empirical correlation model to predict the particle Nusselt number.

Masoumifard et al. (2008) conducted experiments on a fluidized bed in order to verify the influence of the axial position, particle diameter and the superficial gas velocity on the heat transfer coefficient from a small horizontal tube of 8 mm diameter, immersed in the fluidized bed. In order to predict the heat transfer coefficient from the fluidized bed to a horizontally immersed tube, a cluster based model has been proposed. The model predictions were compared with the experimental data of this work as well as those from the literature in a wide range of operating conditions. A close agreement was found between the model predictions and the experimental findings.

However, heat transfer data obtained from the tube suspended in the core of CFB is not applicable for water walls in CFB furnace because the flow pattern of the gas-solid mixture is quite different. Extensive literature on hydrodynamic characterisitcs [Arena et al. (1992), Glicksman et al. (1993), Schouten et al. (1999), Noymer et al. (2000), Yan et al. (2005), Kolar and Leckner (2006), Singh and Mittal (2009)] and bed-to-wall (membrane water walls) heat transfer characteristics for hot beds (bed temperature 800-1200 K) and wall-to-bed heat transfer studies in cold CFB units (bed temperature less than 425 K) [Basu and Nag (1987), Wu et al.(1987), Wirth (1995), Basu and Nag (1996), Molerus and Wirth (1997), Shi et al. (1998), Fox et al. (1999), Kolar (2000), Pagliuso et al. (2000), Grulovic et al.(2008), Gungor (2009)] is available.

Arena et al. (1992) reported the hydrodynamics of circulating fluidized beds with risers of different shape and size like as rectangular riser of cross section 0.12 m × 0.012 m and two cylindrical columns having internal diameter 0.12 m and 0.40 m.

Glicksman et al. (1993) reported the simplified scaling relationships for fluidized beds. Schouten et al. (1999) reported that the gas flow pattern in the dense bottom-bed of circulating fluidized beds, operated with Geldart-B type of solids, exhibits three different types of dynamic behavior, dependent on the width of the riser and the aspect ratio of the

TH-1848_Shankarrao

dense bottom of bed. Recent studies on CFBs show that bed-to-wall heat transfer could be correlated with hydrodynamic conditions in the bed [Noymer et al. (2000), Yan et al. (2005)]. Noymer et al. (2000) developed two laboratory scale models to simulate the hydrodynamic behaviour and study the effect of bed diameter on near-wall hydrodynamics. Scaling of CFB boiler hydrodynamics was reported by Kolar and Leckner (2006). Singh and Mittal (2009) conducted experiments on comparative study on hydrodynamic characteristics on two CFB setups of 0.20 m × 0.20 m and 0.25 m × 0.25 m.

Basu and Nag (1987) have proposed a model to predict the heat transfer in a circulating fluidized bed. To verify the model, experiments were conducted in a 102 mm diameter 5.5 m high Plexiglas column, in which the heat transfer coefficient was measured for different superficial velocities, solid circulation rates and at two particle sizes. The wall to bed heat transfer was measured by a probe, flushed with the wall and installed 2.1 m above the distributor plate. It was a 100 mm long 25 mm diameter carbon steel rod with four iron constantan thermocouples located at uniform intervals of 20 mm along its length.

Wirth (1995) reported wall-to-suspension heat transfer in circulating fluidized bed depends on the fluid mechanics immediately near the wall and on the thermal properties of the gas used. Experimental investigations on circulating fluidized bed of low dimensionless pressure gradients with different solid particles like bronze, glass and polystyrene at ambient temperatures show no influence of the conductivity and the heat capacity of the solids on the heat transfer coefficient. A simple correlation is presented for calculating the heat transfer coefficient in circulating fluidized bed. In the correlation, Nusselt number is the function of dimensionless numbers which characterize the gas-solid flow near the wall. These numbers are the Archimedes number and the pressure-drop number. The last number relates the cross-sectional average solids concentration to the solids concentration at minimum fluidization condition.

Shi et al. (1998) performed extensive series of measurements on wall-to-bed heat transfer coefficients, for different solids like FCC, glass beads and solids velocities, in a semi-industrial scale CFB unit running with a variety of solids fractions at ambient temperatures. Their experiments have shown a significant influence of solids concentration and solids movement near the heat transfer surface on the wall-to-bed heat transfer coefficient. They proposed a model to describe the wall-to-bed heat transfer that

TH-1848_Shankarrao

is applicable over the entire range of possible local solids concentrations occurring in CFB systems.

Heat transfer from the wall to the fast bed suspension was investigated for several materials such as sand, FCC, steel by Fox et al. (1999). They have conducted experiments on single circular cross section riser column operated with superficial velocity of air varying from 7.5 – 8.5 m/s at constant particle size of 150 μm.

Meena (2004) has reported wall-to-bed heat transfer characteristics on upper splash region of riser of cross section 0.102 m × 0.102 m and in cyclone separator of same CFB unit of height 2 m.

Grulovic et al. (2008) have reported wall-to-bed heat transfer in hydraulic transport and in particulate fluidized beds of spherical glass particles. They performed experiments in circular riser of 1.36 m long copper tube 27.4/25.4 mm OD/ID as a particulate fluidized beds with Reynolds number varying from 1960 to 7850 (particles of 0.80, 1.10, and 1.94 mm in diameter) and studied the influence of different parameters such as velocity and voidage on heat transfer in fluidized beds.

Singh and Sharma (2008) have conducted experiments for the hydrodynamic and wall-to-bed heat transfer characteristics on 0.15 m × 0.15 m bed cross section. They have conducted experiments in the lower splash region of riser. Effect of superficial velocity of air, effect of sand inventory on heat transfer characteristics was studied.

Praghanmor (2009) has done comparative study on effect of operating parameters like superficial velocity of air (2.8 m/s and 3.5 m/s), sand inventory on wall-to-bed heat transfer characteristics of lower splash region of bed of cross section 0.20 m × 0.20 m and 0.25 m × 0.25 m and also reported simulations on hydrodynamic characteristics of riser of cross section 0.15 m × 0.15 m and height of 2.85 m using Fluent 6.3.26.

Literature on lower and middle splash region reveal that, Schouten et al. (1999) reported hydrodynamics study in the bottom bed. Pagliuso et al. (2000) have reported bed-to-wall heat transfer study in the lower splash region. They reported heat transfer coefficient along the height of the heat exchanger increases with increase in bed density. A simple correlation was proposed to calculate the heat transfer coefficient as a function of particle diameter and suspension density.

Gungor (2009) has reported that in the CFB combustors, amount of bed-to-wall heat transfer and second law efficiency considerably varies between the bottom and the upper zones due to different hydrodynamic characteristics of each zone. He has used 2D

TH-1848_Shankarrao

CFB model which uses the particle-based approach which simultaneously predicts the hydrodynamics and combustion aspects, second law efficiency and entropy generation values which were obtained at different height and volume ratios of the heat transfer surfaces for CFBs. Besides that, the influences of the water flow rates and heat exchanger tube diameters on the second law efficiency are also investigated. Exergy efficiency (also known as the second-law efficiency) computes the efficiency of a process taking the second law of thermodynamics into account.

The energy B balance of a process is given by

$$B_{in} = B_{out} + B_{lost} + B_{destroyed} \tag{2.1}$$

Exergy efficiency is defined as

$$\eta_B = 1 - \frac{(B_{lost} + B_{destroyed})}{B_{in}} \tag{2.2}$$

Table 2.1 shows the comparision of data reported in the litrature on wall-to bed heat transfer studies for variopus parameters. Scale-up studies at laboratory level using multiple CFB risers of different circular cross sections were accomplished and empirical correlations were developed by Mickley and Trilling (1949) and Danziger (1963). Details are as shown in Table 2.2.

Table 2.1 Comparision of Data Reported in Wall-to Bed Heat Trasnfer Studies for Variopus Parameters

Author	U (m/s)	ρ_{sus} (kg/m^3)	Hr (m)	H/B	d_p (μm)
Basu and Nag (1987)	3 – 5	22 – 96.79	5.5	0.98	227
Fox et al (1999)	3.5 – 8.3	30 – 170	5.966	0.69	400
Basu and Nag (1987)	3.7 – 5	21.50 – 58.63	5.5	0.98	87
Nag and Moral (1990)	7.2 – 12.5	25 – 62	5.15	2.55	310
Moral (1990)	7.2 – 12.5	25 – 62	5.15	1.7	310

Table 2.2 Comparisons of Scale-up Studies on Heat Transfer Characteristics

Ref.	CFB Riser Column (m)	Sand Particle Size (mm)	Fluidizing Air Velocity (m/s)	Correlations
Mickely and Trilling (1949)	0.10 0.025 Circular	70 - 452 102 - 285	0.25 - 4.15 2.47 - 4.27	$h = 0.029 (\rho_m \rho_g U / D_P)^{0.263}$
Danziger (1963)	0.038 0.048 Circular	50 FCC Catalyst	0.15 - 6.77 --	$hD_t/k_g = 0.0784 (D_t U_t \rho_g/\mu_g)^{0.66}(W/ \rho_g U)^{0.45}$

Chen et al. (2005) reported mechanistic models, which were based on the surface renewal concept. These models may be used for design heat transfer systems for both bubbling dense beds and fast circulating fluidized beds. Predictions of these models are in good agreement with available heat transfer data, with few points lying outside of ± 25% bands.

2.3 Computational Studies on CFB Riser

Circulating fluidized bed (CFB) is widely used for various industrial applications which include power generation, drying, cracking, and combustion. The increase and diversity in CFB applications demand the need for the development of more efficient experimental techniques, realistic simulations, and other research and design tools.

In spite of many CFB applications, the complexity of the interaction between phases in the risers presents a tangible challenge to the improvement and understanding of these systems. The CFB design is notably complex in terms of scaling-up difficulties, because of the high sensitivity of the flow to scale and operational conditions [Ding and Gidaspow (1990)].

Miller and Gidaspow (1992) reported that dense flow hydrodynamic experiments measure either only the particle velocities or the particle concentrations until 1987. Bader et al. (1988) reported studies on both the particle velocities, particle

TH-1848_Shankarrao

concentrations, which were determined together at first time for the riser flow. Since then, modelers became able to compare and evaluate their theoretical models with experimental studies in detail.

Different drag models, suggested by Syamlal and Obrien (1987), Arastoopour et al. (1990), Gidaspow et al. (1994) were used to predict the most representative gas–solid interphase exchange coefficient.

Gidaspow (1994) reported detailed discussion on the development of granular flow models.

Currently, the Eulerian–Eulerian (two-fluid) model with kinetic theory of granular flow is the most applicable approach to compute gas–solid flow in a CFB [Benyahia et al. (2000), Zheng et al. (2001), Chan et al. (2005)]. This model is particularly appropriate when the particle loading is relatively high. In the two-fluid model, the particles are treated as a continuum as in the gas phase. Thus, there are two interpenetrating phases' gas and particles where each phase is characterized by its own conservation equation of motion. The interactions between the two phases are expressed by additional source terms added to the conservation equations. The kinetic theory of granular flow is used to define the fluid properties of the particle or solid phase through constitutive equations.

Gungor (2008) developed a model using a Particle Based Approach (PBA) to accurately predict the axial pressure profile in CFBs. This simulation model also accounts for the axial and radial distribution of voidage and for the solids volume fraction.

Almuttahar and Taghipour (2008) reported a two-dimensional Eulerian–Eulerian model incorporating the kinetic theory of granular flow which was developed to describe the hydrodynamics of gas–solid flow in the riser section of a high density circulating fluidized bed. A comprehensive numerical model evaluation by comparing experimental results from the literature was done for various operating conditions. It is found that model is capable of predicting the main features of the complex gas-solids flow for different operating conditions within the high density fast fluidization regime. The predicted solid volume fraction and axial particle velocity were reasonably in good agreement with the experimental data. The developed model was capable of predicting the core-annular flow pattern and the cluster formation of the solid phase. The model

TH-1848_Shankarrao

also predicts the coexistence of dense suspension up-flow (DSU) in the lower region and high density fast fluidization in the upper region of the riser for high gas velocity and solid mass flux. However, the model is incapable of accurately predicting the gas-solid flow behavior in low density circulating fluidized bed risers. Hence, more care in setting up the model parameters and applying boundary conditions should be taken to obtain better predictions at varying fluidization regimes.

Zheng et al. (2001) reported three different turbulence models, which were compared with different closures; two models which consider the turbulence effect of the two phases and one which ignores particles turbulence. The model which ignores the particles turbulence, showed the greatest inconsistency predictions with the experimental data. Although the other two models demonstrated better predictions, only one of them showed reasonably good agreement with the experimental data. Therefore, more attention should be given to select the most appropriate turbulence model with the correct empirical constants and closures of the transfer and dissipation of turbulent energy between gas and solids.

Some information on turbulence parameters which hard to obtain in laboratory conditions which can be easily estimated using CFD tools [Ranade (2002), Almuttahar and Taghipour (2008)]. In addition, CFD models provide a more detailed data profile as a function of space and time without interfering or disturbing the flow by internal probes [Ranade (2002), Almuttahar and Taghipour (2008)].

Benyahia et al. (2000) used CFD tool to analyze gas solid flow. Gas / particle flow behavior in the 2D riser section of a CFB, which was simulated using CFD package Fluent to predict velocity, volume fraction, pressure, and turbulence parameters for each phase.

Taghipour et al. (2005) reported a multifluid Eulerian model integrating the kinetic theory for solid particles using Fluent. This CFD software was capable of predicting the gas–solid behavior of a fluidized bed. Comparison of 2D model predictions, using the Syamlal-O'Brien, Gidaspow, and Wen-Yu drag functions, and experimental measurements on the time-average bed pressure drop and gas–solid flow pattern were in reasonable agreement for most of the operating conditions. Almuttahar and Taghipour (2008) also reported the optimum design and scale-up of CFB risers require a fundamental understanding of the mixing patterns of phases including the

TH-1848_Shankarrao

variations on the solid distributions, the continuous formation and dissipation of clusters, and the solid down-flows. They have predicted the gas and solid velocity and volume fraction through 2D simulation on CFB riser. Hartge et al. (2009) predicted solids volume fraction in the riser column of CFB. 3D CFD simulations using Fluent were accomplished. Results obtained using various drag models like Symlal-O'Brien et al, Gidaspow and Yang et al were compared with experimental data.

Behjat et al. (2008) reported the gas volume fraction average error between 2D CFD simulation results and the experimental data for two different drag models, Syamlal-O'Brien and Gidaspow, were 15.4% and 18.1% respectively. It is observed that Syamlal-O'Brien drag model is a better model for predicting the hydrodynamics of gas–solid flow. In this research, unsteady state behavior of gas–solid fluidized beds has been investigated. Preliminary investigation of multiphase flow models revealed that Eulerian-Eulerian model is suitable for modeling of industrial fluidized bed reactors. The model includes continuity equations as well as momentum equations for both phases and the equations for granular temperature of solid particles. A suitable numerical method that employs finite volume method has been applied to discretize the equations. In order to validate the model, predicted time-average bed expansion ratio and cross sectional voidage profiles were compared with corresponding values of experimental data. This comparison showed that the model can predict hydrodynamic behavior of gas solid fluidized bed reasonably well. Simulation results also indicate that small bubbles were produced at the bottom of the bed. These bubbles collide with each other as they move upwards forming larger bobbles. Model predictions of bubble size and gas–solid flow pattern using both Syamlal–O'Brien and Gidaspow drag models were similar.

Bastos et al. (2008) reported the simulations using Ansys CFX software version 10 and reported radial solid velocity profiles, computed on seven axial levels in the circular riser of a high-flux circulating fluidized bed (HFCFB) using a two phase 3D computational fluid dynamics model.

2.4 Experimental Studies on Cyclone Separator

The cyclone separator in the CFB boiler handles a large volume of gas at high temperature. The outer skin temperature of the cyclone separator is relatively high; therefore more heat losses occur by natural convection and radiation. To overcome this

TH-1848_Shankarrao

problem, some cyclone separators are made of water or steam cooled. This heat recovery can enhance the capacity of the boiler. Therefore proper design of cyclone separators of CFBs is essential. Therefore it is important to understand the heat transfer mechanism and the effect of various operating parameters on the heat transfer process in the cyclone separator.

The cyclone separator is an integral part of a CFB. It is a gas cleaning device that utilizes the centrifugal force created by a spinning gas-solid stream to separate particles from a gas. The gas-solid flow enters tangentially to the top of the cyclone. The solid particles are forced to the wall by centrifugal force and then fall down along the wall by gravity. The gas stream executes several complete turns, and it reverses at the bottom of the cyclone to form the inner core that leaves from the top of the unit [Basu and Fraser (1991), Nag (1998)].

Gas-solid flow structure and collection efficiency of the cyclone separator was reported by Dietz (1981), Zhou and Soo (1990), Trefz and Muschelknautz (1993). They reported that the cyclone efficiency decreases with increase in cyclone diameter, gas outlet duct diameter, and gas inlet area.

Avci and Karagoz (2003) developed a mathematical model for calculation of cyclone efficiency, by taking into account, the effects of flow, particle and geometrical parameters, and acceleration assuming that the mixture of fluid and particles is homogenous, and acceleration diminishes depending on the friction and geometry.

Avci and Karagoz (2001) reported the theoretical analysis of pressure losses in cyclone separators under the consideration of geometrical and flow parameters including inlet geometry, surface roughness, velocity and particles concentration, has been performed and a new equation has been developed. The results obtained in this study were compared with experimental values for different type of cyclone separators. It is found that the proposed equation could be used to predict the pressure losses easily and it is worthy especially for industrial applications.

Xiang and Lee (2008) reported the effects of exit tube diameter on the flow field in cyclone separator. Results show that the exit tube diameter influences not only the velocity magnitude, but also the shape of the velocity profiles within cyclones.

TH-1848_Shankarrao

However, no much literature exists on the cyclone separators' heat transfer studies. Orozco and Nguyen (1993) reported an analysis of the heat transfer characteristics of the fin/refractory system in a cyclone furnace. Thermal stresses in the weld joint between the fin and the tubes which contribute to the failure of the fins were estimated. The effect of fins on the average heat transfer coefficient inside the cyclone separator of a CFB for different operating parameters like solid circulation rate, gas superficial velocity and pressure drop were studied by Nag and Gupta (1999).

Some studies on the heat transfer characteristics in a cyclone separator of a CFB were reported by Nag and Singh (1996).

Gupta and Nag (2000) conducted experiments on cyclone separator's wall-to-bed heat transfer and hydrodynamic characteristics in the cold CFB unit of cross section 0.102 m × 0.102 m. It is reported that the cyclone separator is designed according to the high-efficiency Lapple design and made to accommodate two identical heat transfer probes. From the experimental results, the heat transfer coefficient is found to increase with increase in solid circulation rate, as well as gas superficial velocity. The effect of bed inventory and heat flux on heat transfer coefficient has also been investigated. An empirical equation has been developed to predict the heat transfer coefficient in the cyclone separator based on dimensional analysis. The experimental results were compared with the predicted results and a good agreement was observed. The collection efficiency of the cyclone separator was measured for all the operating conditions.

2.5 Summary and Scope for Present Investigations

From the literature review as explained in sections 2.2, it is evident that most of the work is published on hydrodynamic and heat transfer characteristics of single riser column and effect of scale-up on hydrodynamic characteristics of CFB. Few literature is available on wall-to-bed heat transfer characteristics [Mickley and Trilling (1949), Danziger (1963), Basu and Nag (1987), Wirth (1995), Shi et al. (1998), Fox et al. (1999), Grulovic et al. (2008)]. Mickley and Trilling (1949), Danziger (1963) represent correlation on bed Nusselt number developed from the scale-up of two circular risers as shown in Table 2.1. However, it was observed from literature that the hydrodynamics characteristics differ significantly with the geometry of the bed cross section [Zhou et. al (1994)] and bed hydrodynamics strongly influences the heat transfer characteristics [Kunni and

TH-1848_Shankarrao

Levenspiel (1991)]. Risers of square and rectangular cross-sections are now widely employed in circulating fluidized bed applications [Zhou et. al (1994)]. Also scale-up is important for design point of view. Hence, there is high demand for scale-up study of CFB on heat transfer characteristics with square cross-sections. Therefore present work involves parametric study and effect of scale-up on wall-to-bed heat transfer characteristics using three CFB units of different square cross section riser.

Based on the available literature on simulation, it is found that most of the works reported for the CFB hydrodynamic and heat transfer by Eulerian model with good degree of accuracy (Section 2.3). Experimental findings of the present study will be validated using Fluent 6.3.26 with Eulerian model.

It is evident from section 2.4 that most of the investigations were reported on hydrodynamic characteristics of cyclone separators. Wall-to-bed heat transfer characteristics of single cyclone separator are reported only by Gupta and Nag (2000). Therefore present work involves parametric study and effect of scale-up on bed-to-wall heat transfer characteristics using three cyclone separators of different diameters.

TH-1848_Shankarrao

Chapter 3

Experimental Setup and Procedure

TH-1848_Shankarrao

Chapter 3

Experimental Setup and Procedure

3.1 Introduction

In the present chapter experimental setup and procedure are described. Section 3.2 represents the details about the CFB Setup fabricated at IIT Guwahati. Fabrication of heat transfer probe (heater) used in the riser column for wall-to-bed heat transfer study is also explained in this section. Experimental procedure used for the heat transfer study in the riser column is described in section 3.3. Similarly experimental setup and procedure used for conducting heat transfer study in the cyclone separators is described in section 3.4, followed by summary in section 3.5.

3.2 Experimental Setup

CFB setups were designed and fabricated at IIT Guwahati (Gavali, 2005). Figure 3.1 presents three CFB units with bed cross sections of 0.15 m × 0.15 m, 0.20 m × 0.20 m, and 0.25 m × 0.25 m. All the CFB units are constructed with same riser height of 2.85 m. Both the riser and downcomer are of same cross-section area and made of Plexiglass. All sections were interchangeable with one another. Hence, the set-ups were useful enough for studying the different aspects of heat transfer along the bed height. Experiments were conducted on the three CFB units with sand as the bed material and air as the fluidizing medium. Air was supplied by a high-pressure high discharge blower, and the air flow rate, controlled by main line bypass valve, was measured by a standard designed orifice plate. A butterfly valve is located in the return leg of each unit to measure the solid circulation rate in the column by closing the valve and measuring the volume of solids collected above it over a certain period of time. Each CFB unit contains a cyclone separator and a bag filter. Entrained solids will be recovered in a cyclone separator and returned to the bottom of the riser column. Static pressure will be measured along the riser height at suitable intervals and along the cyclone height. Fine wire mesh (BS 400)

TH-1848_Shankarrao

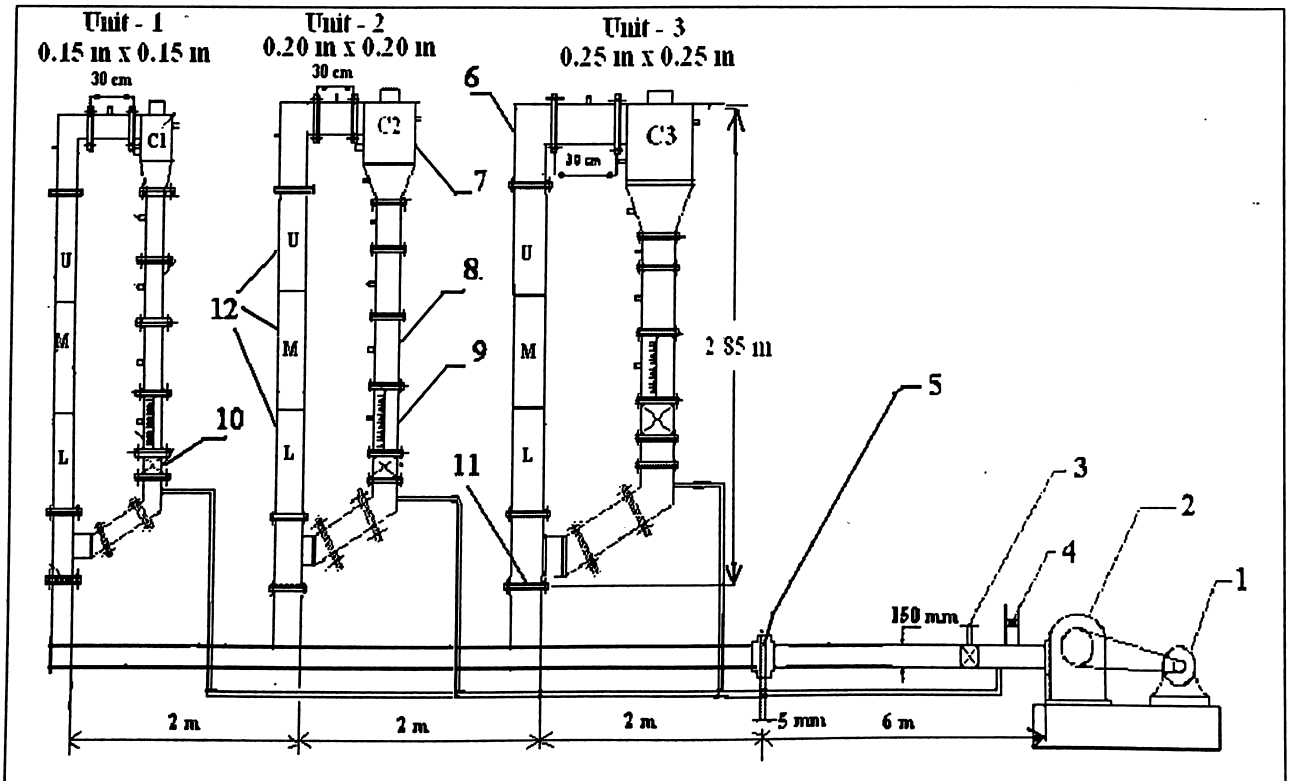

1. Motor
2. Blower
3. Bypass Valve
4. Safety Valve
5. Orifice Plate
6. Riser Column
7. Cyclone Separator
8. Downcomer
9. Sand Measuring Section
10. Butterfly Valve
11. Distributor Plate
12. Heater Section

Fig. 3.1 Schematic of Experimental Setup

and cigarette filters were used at pressure tapping ends to minimize pressure fluctuations in the water filled U-tube manometer.

Heat transfer probes (heater section) of suitable design have been used to investigate the local heat transfer coefficient along the riser. Heater can be placed at any appropriate height above the distributor plate for one set of experiments and then positions can be changed for next set of experiments by keeping the same set of operating parameters fixed as in the first set. Electrical energy input to the heaters will be controlled by variac and measured with Wattmeter. The constructional feature of the heater is as shown in Fig. 3.2. The heater section was fabricated with MS sheet of 2 mm thickness with a height of 0.6 m (Fig. 3.2). Nichrome wire as a heater coil of 2 kW capacities was wound over the mica sheet of 1.5 mm thickness which covers the MS wall of the heater section. Another mica sheet, which acts as an electric insulator, was wrapped over the Nichrome wire. To avoid the heat losses by radiation, ceramic wool and asbestos sheets were wrapped over the assembly.

TH-1848_Shankarrao

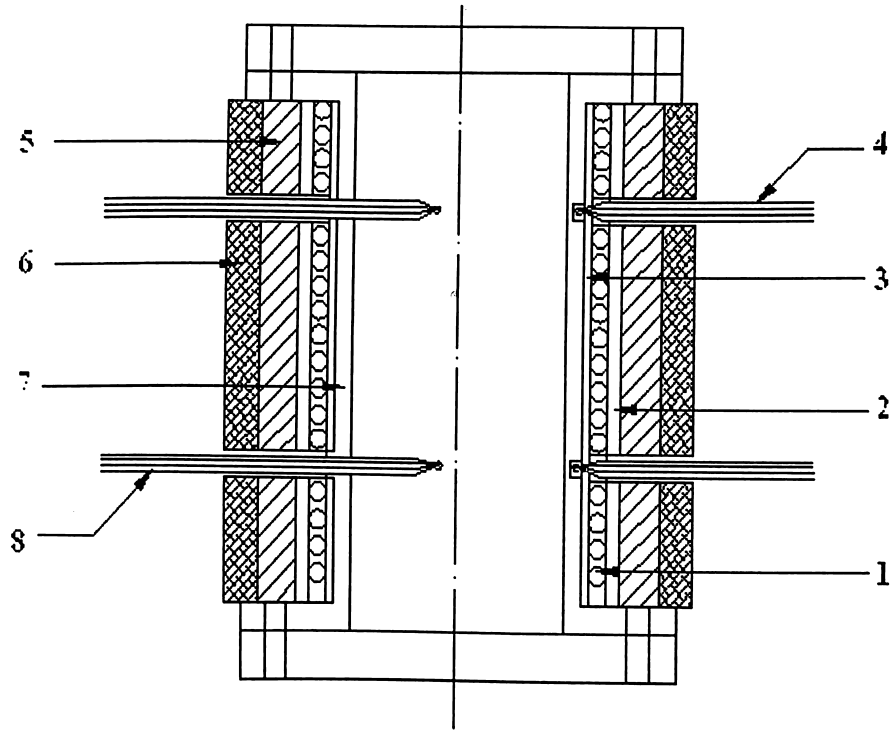

1	Nichrome Wire	2	Mica
3	Mica	4	Wall Temperature Thermocouple
5	Asbestos Sheet	6	Ceramic Wool
7	MS Sheet Probe Wall	8	Bed Temperature Thermocouple

Fig. 3.2 Schematic of Heater

Heat was supplied to the heater section with electric supply through variac. To measure the temperature of the surface of the heater section and the bed, calibrated T-type thermocouples were installed on the wall as well as inside the heater section respectively in the same height as shown in Fig. 3.3.

Ten set of thermocouples with equal spacing of 0.055 m along the height of the heater section were used to measure the bed temperature and surface temperature of the heater section, as shown in Fig. 3.3. A section was taken in the lateral direction at 0.44 m above the inlet of the heater. Five thermocouples were placed along the horizontal direction in this section with equal spacing at the non-dimensional distance [X/b] of 0.1, 0.3, 0.5, 0.7 and 0.9, respectively (Fig. 3.3). Fabrications of all heaters for three different CFB units were done in a similar way. Here the non-dimensional distance [X/b] is the distance (X) measured from the left hand side wall of the heater to the thermocouple end, normalized with respect to the width (b) of the heater.

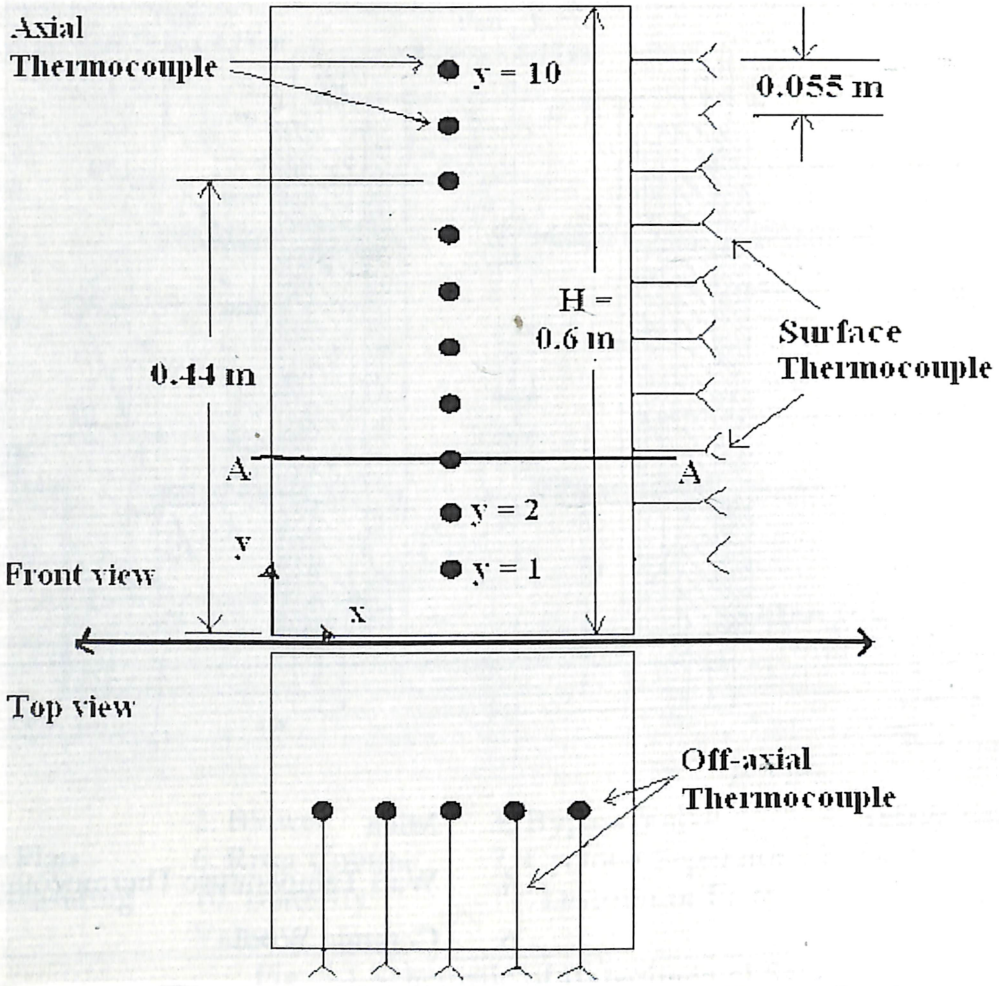

Fig. 3.3 Positions of Thermocouples in Heater Section

Experiments were conducted on each CFB unit keeping other two CFB units in off position. Experiments were conducted under similar operating conditions on three CFB units when heater section (as shown in Fig. 3.1) was placed at upper (U), middle (M) and lower (L) position i.e at a height of 0.6 m, 1.2 m and 1.8 m above the distributor plate respectively.

Snaps 1-3 show the experimental facility, data acquisition system and electrical instrumentation. Specifications used for the present study are given in Appendix A.

TH-1848_Shankarrao

Snap 1 CFB Setups

TH-1848_Shankarrao

Snap 2 Data Acquisition System

Snap 3 Electrical Instruments

TH-1848_Shankarrao

3.3 Experimental Procedure for Riser

Experiments were conducted under steady state condition on the three CFB units to examine the effect of bed cross section on heat transfer characteristics under similar operating conditions. To maintain the similar operating conditions in each CFB unit, weight of static sand inventory per unit area of distributor plate (P) was maintained same. Also, experiments on each CFB unit were carried out at five superficial velocities of air (U = 2.5 m/s, 2.75 m/s, 3 m/s, 3.3 m/s, and 4 m/s). Non-dimensional form for superficial velocity of air (U*) is given by

$$U^* = \frac{U'}{U_{mf}} \tag{3.1}$$

Where (U') and (U_{mf}) are superficial air velocity and minimum fluidizing air velocity, respectively. All experiments were conducted with mean particle size of 460 μm (Appendix B) and input heat flux at the wall of each heater was maintained at 1000 W/m^2 (Appendix C). Input heat flux was restricted to 1000 W/m^2 to prevent damage of plexiglass column of riser and to avoid breakage of Nichrome wire. Experiments were conducted with two different sand inventories so that weight per unit area of distributor plate of each CFB setup was maintained either 3050 N/m^2 or 1750 N/m^2 (Appendix C). The range of the weight of sand inventory per unit area of the distributor plate 1750-3050 N/m^2 was selected because beyond this limit of inventory, fast fluidization was not achievable. This is because there would be insufficient amount of sand inventory on the distributor plate to achieve fast fluidization if it was less than 1750 N/m^2. Experiments could not be conducted for the value of weight of the sand inventory per unit area of the distributor plate (P) more than 3050 N/m^2 because of constraint of maximum capacity of experimental setup (blower) to push the maximum weight of inventory of sand per unit area of distributor plate into the fast fluidization above the distributor plate in 0.25 m × 0.25 m CFB setup.

At particular weight of sand on distributor plate of a CFB setup, effect of velocity of air on off-axial bed temperature distribution and axial distribution of heat transfer coefficient in the heater section was studied by varying non-dimensional velocity parameter (U*) from 5 to 8 (Appendix C). U* was varying from 5 to 8, because, at U* < 5, fast fluidization was not achievable and U* > 8 was limited by the capacity of the blower.

TH-1848_Shankarrao

The suspension density of the bed (ρ_{sus}) can be evaluated (Appendix C) by the equation (Kunni and Levenspiel, 1991)

$$\rho_{sus} = \rho_s (1-\varepsilon) + \varepsilon \rho_g \tag{3.2}$$

where voidage (ϵ) is defined as the volume fraction of the bed by occupied by air bubbles. The bed voidage (ϵ) at any cross-section of riser has been estimated from the measured pressure drop (ΔP_b) from a differential water filled U-tube manometer connected across two pressure taps separated by a distance 0.6 m along the height of the riser. ρ_g is the density of air in kg/m^3.

Voidage (ϵ) is given by

$$\varepsilon = 1 - \frac{10\Delta h}{\rho_s L_m} \tag{3.3}$$

where Δh is difference of height in manometric fluid, measured in cm of water, L_m is the distance between two consecutive pressure taps (0.6 m approx. for all CFB units) across which pressure drop, hence voidage has to be determined, ρ_s is the density of sand (2600 kg/m^3).

Solid circulation rate (G_s) i.e (solid mass flux) (Appendix C) is given by

$$G_s = \frac{\rho_s L_a A_D (1-\varepsilon_{mf})}{A_B . t} \tag{3.4}$$

where L_a is accumulation height in m, t is the time elapsed in *s* after closing the butterfly valve to gain L_a in graduated column of down-comer, ρ_s is the density of sand in kg/m^3, A_B and A_D are cross sectional area of riser column and graduated column or sand height measuring section in m^2, respectively, as shown in Fig. 3.1, ε_{mf} is the voidage at minimum fluidization. In the present study, $A_B = A_D$ in each CFB unit.

The local heat transfer coefficient (h) is calculated (Appendix C) by

$$h = \frac{Q}{A_S (T_S - T_B)} \tag{3.5}$$

where Q is rate of heat supplied to the heater measured using calibrated wattmeter. T-type calibrated thermocouples (Appendix D) and data acquisition system with Easy Lab software version 1.0 were used to measure the surface temperature (T_S) and (bulk mean) bed temperature (T_B), A_S is the surface area of the heater.

Average heat transfer coefficient (h_{avg}) along the heater section at its any particular location above the distributor plate is calculated by

TH-1848_Shankarrao

$$h_{avg} = \frac{1}{H}\int_0^H h_y .dy \tag{3.6}$$

where H is the height of the heater (0.6 m), h_y is the local heat transfer coefficient. Local heat transfer coefficient (h_y) is calculated at 10 different points (y = 1, 2.....10 as shown in Fig. 3.3) along the height of heater section.

3.4 Experimental Procedure for Cyclone Separator

Parametric Studies were done on cyclone separators of three CFB setups with riser of cross sections 0.15 m × 0.15 m, 0.20 m × 0.20 m and 0.25 m × 0.25 m, respectively as shown in Fig. 3.1. Cyclone separators (C1, C2, and C3) as shown in Fig. 3.1 with barrel diameter (D_c) 0.27 m, 0.36 m, and 0.45 m were used in the present study. Cyclone separators were fabricated with mild steel and design was made based on the procedure given by (Stairmand 1951). Various geometrical ratios of cyclone separator components were chosen based on (Stairmand 1951); details of the same are enlisted in Fig. 3.4.

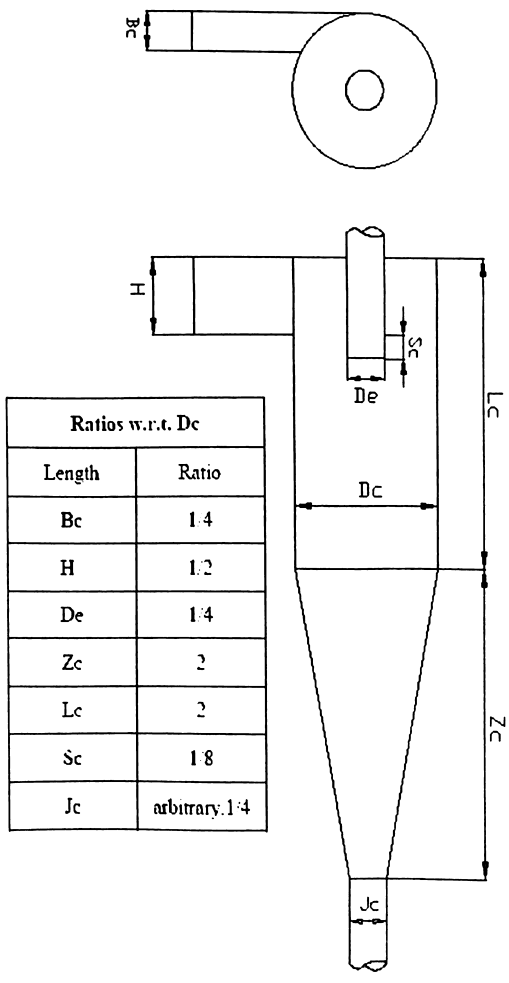

Ratios w.r.t. Dc	
Length	Ratio
Bc	1/4
H	1/2
De	1/4
Zc	2
Lc	2
Sc	1/8
Jc	arbitrary.1/4

Fig. 3.4 Cyclone Separator

In the present study, heat was provided at the riser column with the help of a heater of height 0.6 m which is located at a height of 0.6 m above the distributor plate (portion L of Fig. 3.1). Heat is carried by bed (sand and air mixture) to the cyclone separator enabling the investigators to study the bed-to-cyclone wall heat transfer. Local heat transfer coefficient (h_c) in the cylindrical portion along the length (Lc) (refer Figs. 3.4 and 3.5)

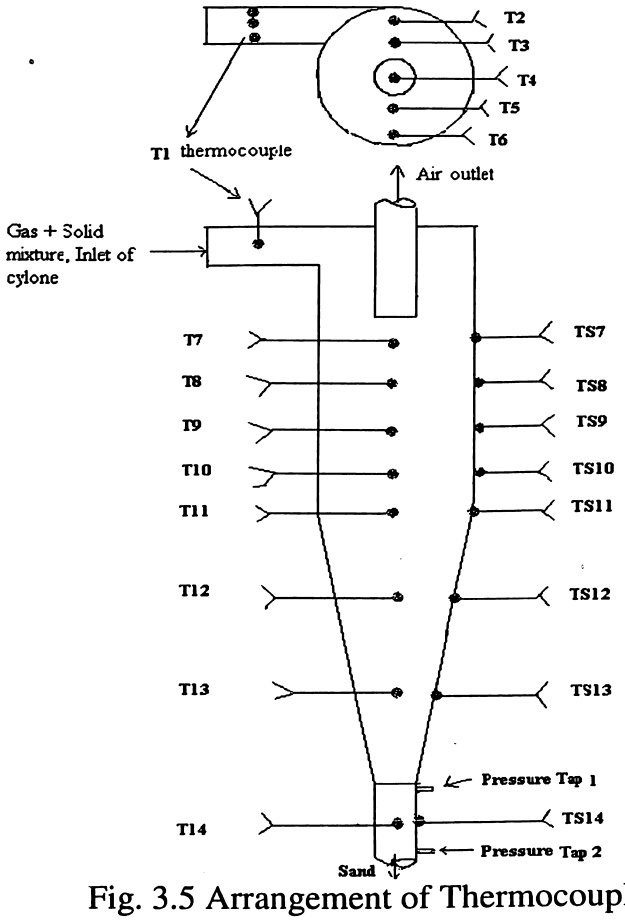

Fig. 3.5 Arrangement of Thermocouples

of each cyclone was evaluated at the non-dimensional distance (Y/H_C) of 0.1, 0.2, 0.3, 0.4, 0.5 with respect to (T7-T11) respectively. Where the non-dimensional distance (Y/H_C) is the ratio of distance (Y) of the thermocouple location with respect to (T7-T11) as shown in Fig. 3.5, measured from the inlet of the cyclone, normalized with respect to the total height of the cyclone ($H_C = L_C + Z_C$). Also, bed (sand and air mixture) temperature distribution in the radial direction of each cyclone was measured at five different locations at (T7-T11) as shown in Fig. 3.5. Variations of temperature in the radial direction of the cyclones were measured at (T7-T11) in terms of non-dimensional distance (r/R), where $R = D_C / 2$ is the radius of the cyclone cylindrical barrel and r is the location of the thermocouple from the centre of the barrel. Five T-type calibrated

TH-1848_Shankarrao

thermocouples (T2), (T3), (T4), (T5) and (T6) were used in the radial direction with non-dimensional distance (r/R) -0.9, -0.5, 0.0, 0.5, 0.9 respectively. Temperature measured using these five thermocouples placed in the radial direction at locations (T7-T11) is used to evaluate the bulk mean temperature (T_{Bc}) at particular location in cyclone separator. This helps in the evaluation of local heat transfer coefficient (h_c) along the height of the cyclone. Thermocouples (TS7), (TS8), (TS9), (TS10) and (TS11) were used to measure the outer wall skin temperature of each cyclone separator as in Fig. 3.5.

Local heat transfer coefficient (h_c) along the cyclone separator's height is calculated (Appendix C) by

$$h_c = q'' / (T_{Bc} - T_{Sc}) \tag{3.7}$$

where T_{Bc} and T_{Sc} represent the bed (air + sand mixture) and wall temperature of cyclone separator, respectively.

Mean heat flux (q") in each cyclone separator is calculated by

$$q'' = (q_1 - (q_2 + q_3) / As_c \tag{3.8}$$

where q_1 is the amount heat carried by air + sand mixture which was calculated at the inlet of cyclone separator, As_c is the surface area of cyclone separator in m^2, q_2 and q_3 is the heat carried by air and sand in W, measured at the two outlets of cyclone separator - chimney and bottom outlet of cyclone (portion between pressure tap1 and tap2), respectively, as shown in Fig. 3.5. Speed and temperature of air at outlet of cyclone was measured using anemometer. The speed at outlet of cyclone was measured using the anemometer, just holding the anemometer at the top of the outlet. Then the speed in m/s indicated on the screen of the anemometer was noted.

3.5 Summary

A CFB test facility comprising three CFB units of 2.85 m height and cross-sections 0.15 m × 0.15 m, 0.20 m × 0.20 m, and 0.25 m × 0.25 m has been developed at I.I.T. Guwahati. Measuring instruments and a data acquisition system have also been installed. Three CFB units were fabricated to study the effect of various operating parameters like superficial velocity of air, sand inventory, and bed cross section on wall-to-bed and bed-to-wall heat transfer characteristics in the CFB risers and in the cyclone separators, respectively.

TH-1848_Shankarrao

Chapter 4

Experimental Investigations on CFB Risers

TH-1848_Shankarrao

Chapter 4

Experimental Investigations on CFB Risers

4.1 Introduction

In the present chapter, comparative study on wall-to-bed heat transfer characteristics for three different CFB units of square cross sections 0.15 m × 0.15 m, 0.20 m × 0.20 m, and 0.25 m × 0.25 m has been completed. Risers of all the CFB units were constructed with same height of 2.85 m. A flow regime study was carried out on the CFB riser of cross section 0.15 m × 0.15 m. Effect of superficial velocity of air in each CFB unit and bed cross section on variation of pressure drop and suspension density along the riser column was studied. Effect of superficial air velocity and sand inventory on heat transfer characteristics was also predicted for individual CFB setup. The results obtained were compared with available literatures. Effect of riser cross section on bed temperature distribution as well as on the heat transfer coefficient was compared for the three CFB units. To accomplish the scale-up study, experiments were conducted on three CFB units under similar operating conditions with five different non-dimensional air velocities (U^* = 5, 5.5, 6, 6.6, and 8). At the initiation of two different set of experiments on each CFB unit, weight of two different static sand inventories per unit area of the distributor plate of each CFB unit was maintained to obtain P = 1750 N/m^2 and P = 3050 N/m^2. Sand particles with average size of 460 μm were used in all the experiments. Based on the scale-up study, new correlations were developed relating the bed Nusselt number with various non-dimensional parameters.

4.2 Hydrodynamics Characteristics

A flow regime study was carried out on the CFB riser of cross section 0.15 m × 0.15 m. Sand particles of Geldart B type with average size of 460 μm have been used. Non-dimensional particle size d_p^* and non-dimensional particle velocity u^* were calculated from the following equations (Kunni and Levenspiel, 1991)

TH-1848_Shankarrao

$$d_p^* = d_p\left[\frac{\rho_g(\rho_s-\rho_g)g}{\mu^2}\right]^{1/3} \tag{4.1}$$

$$u_g = u^*\left[\mu\left(\rho_s-\rho_g\right)g/\rho_g{}^2\right]^{1/3} \tag{4.2}$$

where d_p is the mean particle size (460 μm), ρ_g is the density of air (1.2 kg/m^3), ρ_s is the density of sand particle (2600 kg/m^3) and μ_g is the viscosity of air (1.8 x 10^{-5} kg/m.s). The mean particle size was found out experimentally by sieve analysis (Appendix B) Bed inventory (I) of 20 kg was taken for the present analysis. Substituting these values in eq. (4.1) and eq. (4.2), d_p* and u* were found to be 12.34 and 1.464 u_g, respectively. Figure 4.1 indicates that the estimated value of d_p* falls in the range of B type particles.

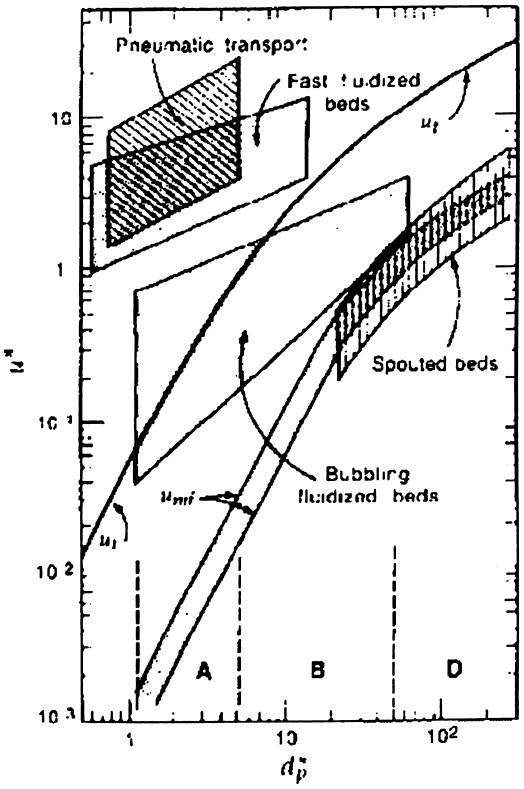

Fig. 4.1 General Flow Regime Curve (Kunni and Levenspiel, 1991)

Experiments were also conducted with same particle size at different air flow rate Q_0. Various flow regimes were observed as shown in Table 4.1. Non-dimensional particle velocity were obtained by using the earlier relationship

$$u^* = 1.464\, u_g$$

Tabulated results are compared with Fig. 4.1 The values of u* given in Table 4.1 are found to be within the ranges according to Fig. 4.1 for the respective flow regimes at

TH-1848_Shankarrao

d_p^* = 12.34. Thus, there is agreement between the flow regime visualization and the general flow regime curve.

Table 4.1 Various Flow Regimes at Different Air Flow Rates

Regime Observed	Manometer Reading, Δh (cm)	Flow Rate, Q_0 (m^3/s),(Appendix C)	Gas Velocity, u_g (m/s)	u*
Bubbling	0.4	0.02218	0.9859	1.443
Slugging	0.7	0.02930	1.3040	1.909
Turbulent	5.0	0.07008	3.1148	4.560
Fast fluidization	11.5	0.10220	4.5440	6.652

4.2.1 Variation of Pressure Drop

Figure 4.2 and Fig. 4.3 presents the variation of pressure drop in terms cm of water Δh along the height of the riser. Figure 4.2 represents the variation of pressure drop for the two superficial velocities of air (2.5 m/s and 4 m/s) along the height of the riser column for the CFB unit B1 (0.15 m × 0.15 m) operated at P = 3050 N/m^2. Pressure taps were provided at 0.62 m (Tap1), 1.18 m (Tap 2), 1.22 m (Tap 3), 1.78 m (Tap 4), 1.82 m (Tap 5) and 2.38 m (Tap 6), respectively above the distributor plate. Pressure drop between Tap 1 and Tap 2, Tap 3 and Tap 4, Tap 5 and Tap 6 was corresponding to the lower (portion L as shown in Fig. 3.1), middle (M) and upper splash region (U), respectively.

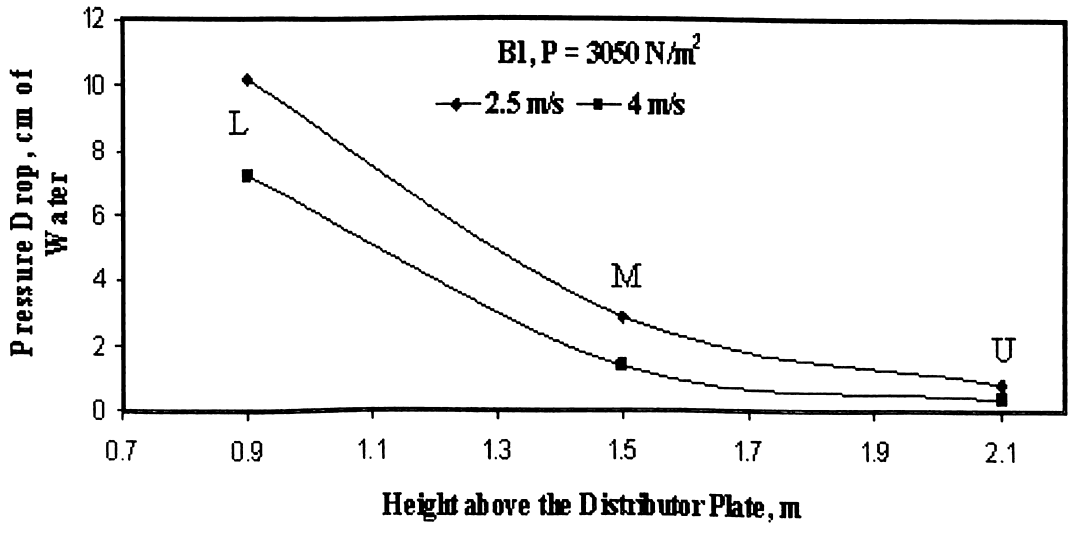

Fig. 4.2 Effect of Superficial Velocity on Variation of Pressure Drop

TH-1848_Shankarrao

Lower portion of riser column was denser, occupying large number of sand particles, while upper splash region had very less number of fine sand particles. Hence average pressure drop along the lower splash region was more than the average pressure drop along the middle and upper splash region. It is observed from Fig. 4.2 that pressure drop decreases with increase in superficial air velocity. This is due to the fact that the sand hold-up along the wall of the riser column decreases with increase in velocity of air, which results in decrease in pressure drop. It is also observed that pressure drop increases with increase in bed cross section area, as shown in Fig. 4.3.

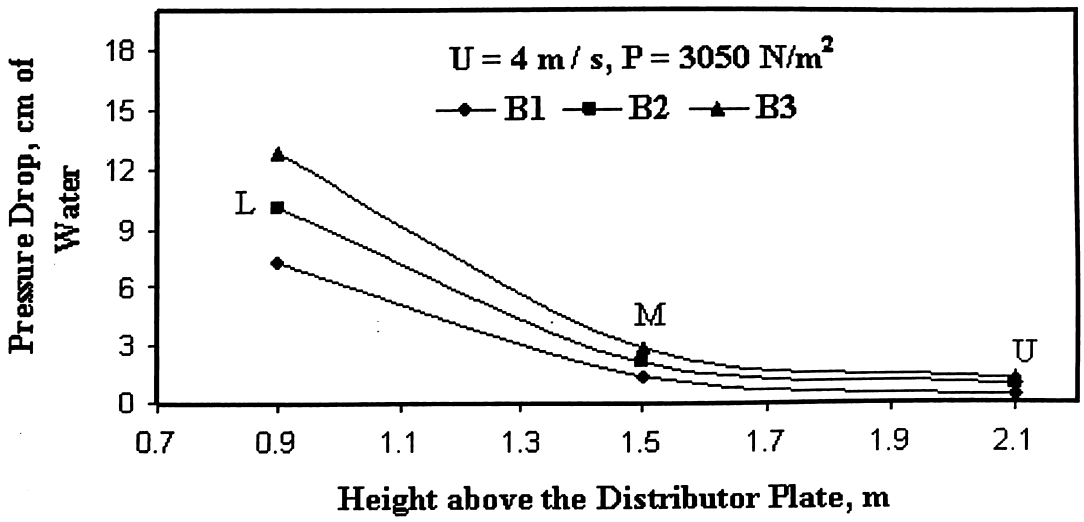

Fig. 4.3 Effect of Bed Cross Section on Variation of Pressure Drop

Figure 4.3 presents the pressure drop variation of three bed cross sections B1, B2 and B3 along the riser height. These results are obtained for non-dimensional superficial velocity $U^* = 8$ and weight of the sand per unit area of the distributor plate (P) = 3050 N/m^2. Thus experiments were performed on all the CFB units B1, B2, and B3 under similar operating conditions. It is observed that the pressure drop along the height of the riser with largest CFB unit (B3) is more than the other two CFB units. This is expected because sand inventory in larger cross section CFB setup was kept proportionately more than the smaller size CFB setups so as to maintain the same weight of sand per unit area of the distributor plate (P = 3050 N/m^2).

4.2.2 Variation of Suspension Density

Variation of suspension density along the height of the riser is as shown in Figs. 4.4 and 4.5. It is observed that suspension density was more at bottom portion of bed and was

TH-1848_Shankarrao

comparatively very less at the upper portion of bed. Fig. 4.4 represents the effect of superficial velocity on suspension density variation along the height of the riser. It is observed that suspension density decreases along the height of the riser with increase in superficial velocity.

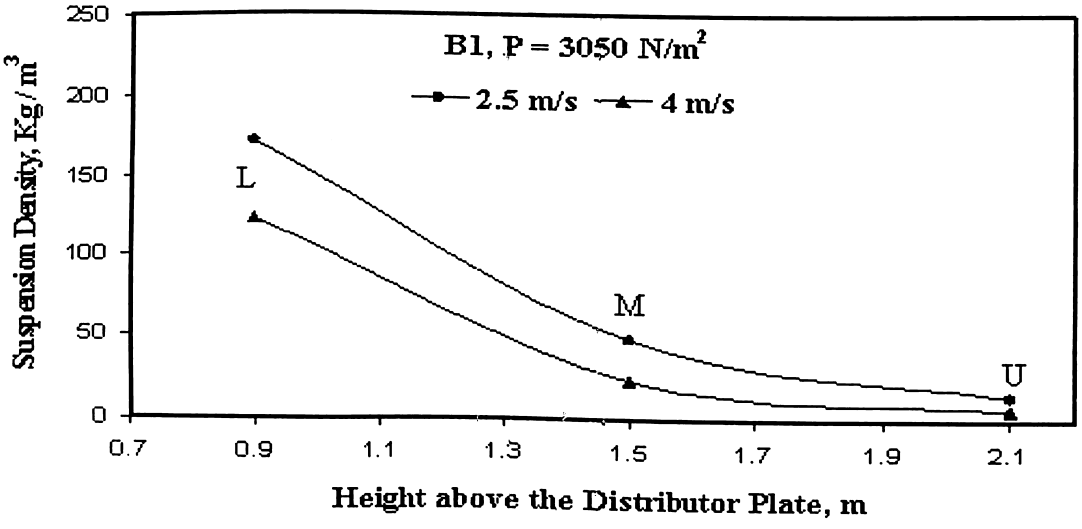

Fig. 4.4 Effect of Superficial Velocity on Variation of Suspension Density

This is because hold-up of sand particles across the riser and near to the wall decreases with increase in velocity of air. It is also observed that suspension density increases with increase in riser cross section of CFB setup as shown in Fig. 4.5 when all the CFB units were operated at similar operating conditions with U* = 8 and P = 3050 N/m^2.

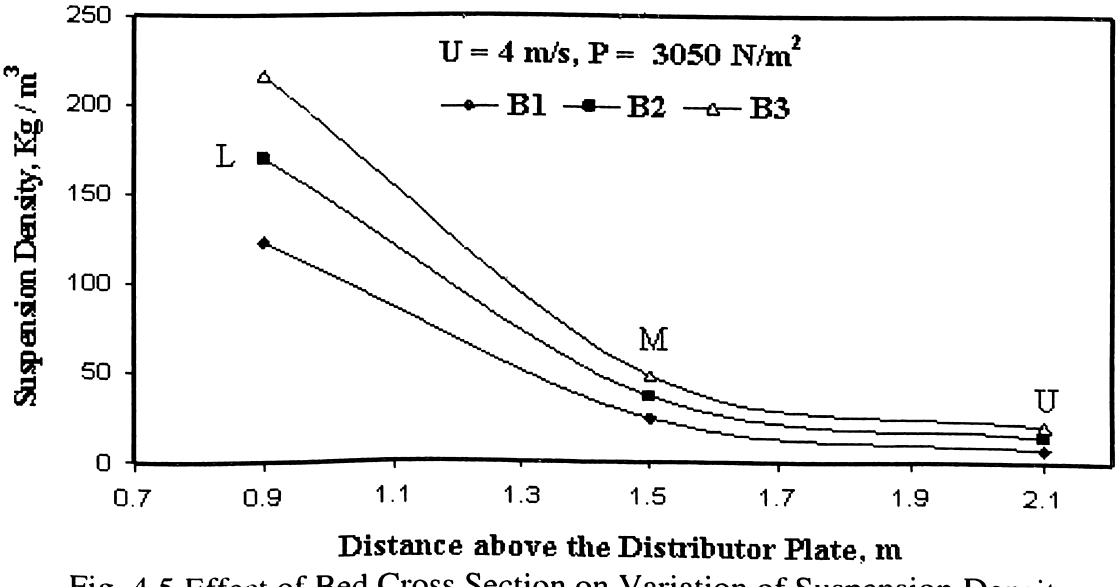

Fig. 4.5 Effect of Bed Cross Section on Variation of Suspension Density

This behaviour is due to the fact that the sand inventory in CFB setup of larger cross section was kept proportionately more than the CFB setup of smaller cross-section so as to maintain the same weight of sand per unit area of the distributor plate (P = 3050 N/m^2). Therefore, weight of sand particles per unit surface area of the larger cross section riser was more than the smaller riser.

4.3 Heat Transfer Characteristics

4.3.1 Bed Temperature Distribution across the Heater

Variations of temperature across the riser cross section are presented in Figs. 4.6-4.10. Fig. 4.6 indicates the variation of bed temperature along the section AA when heater section was placed at 0.6 m, 1.2 m, and 1.8 m above the distributor plate, which means section AA (refer Fig. 3.3 as below) was located at 1.04 m, 1.64 m, and 2.24 m, above the distributor plate, respectively.

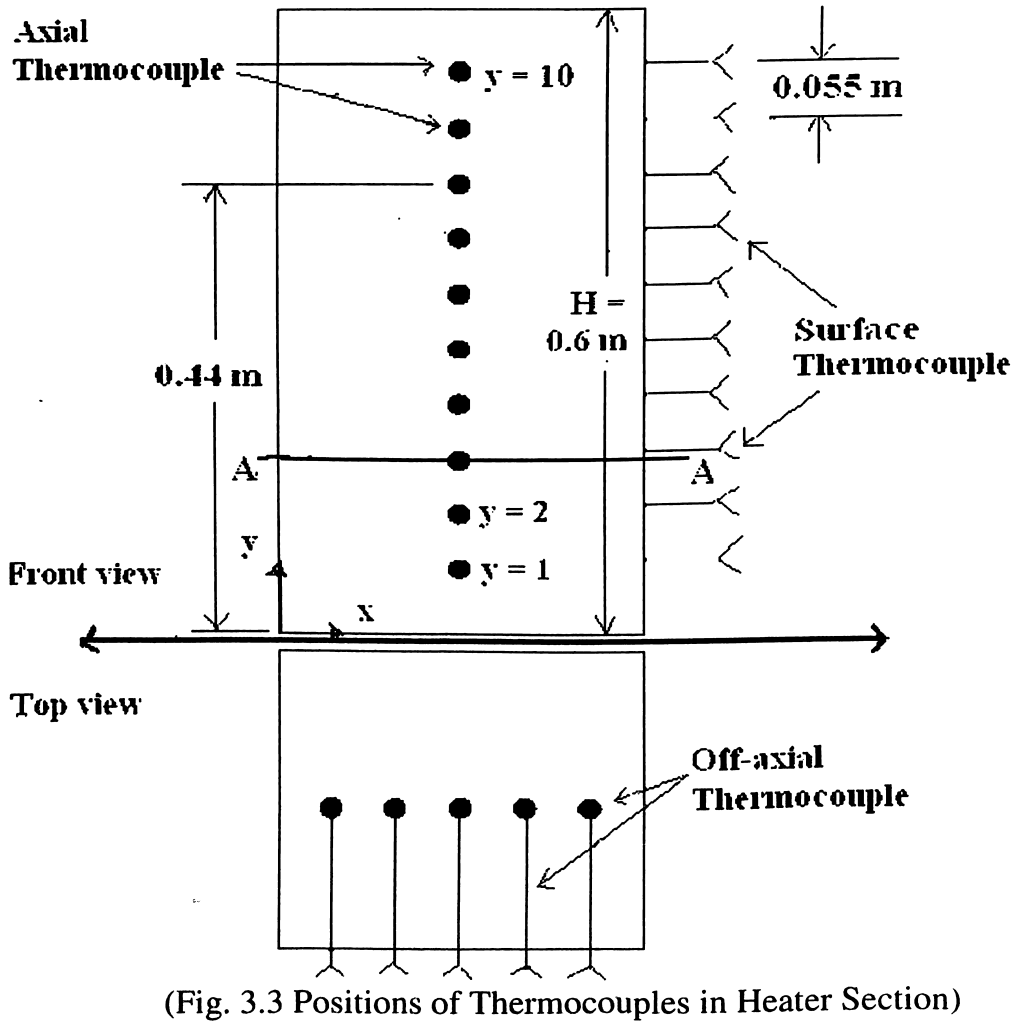

(Fig. 3.3 Positions of Thermocouples in Heater Section)

It is observed that bed temperature was more for the lower position of the heater than its other two positions above the distributor plate. This is because, particle distribution in the riser observed through plexiglass was indicating more sand particles concentration in the lower position (lower splash region) than its other two positions (middle splash and upper splash region) above the distributor plate. Consequently, more quantity of particles in the lower splash region promotes more heat transfer through conduction, because of which bulk mean temperature of bed in this region across a section AA of heater was observed to be higher than that in the other two regions. Thus, sand particles had major role in the heat transfer process from wall-to-bed and the bed temperature distribution. Also thermal conductivity of sand is higher than air, as a result of which more heat conduction takes place thorough sand particles and hence exhibits higher temperature than the portion of heater having lower particle concentration. Therefore Figs. 4.6-4.10 indicate that bed temperature was higher in the portion of higher particle concentration than the portion of heater having lower particle concentration.

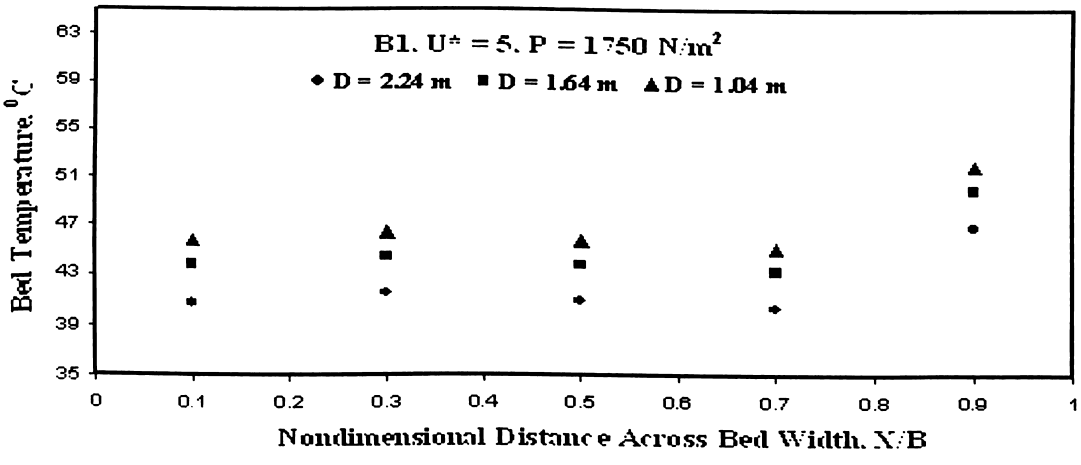

Fig. 4.6 Comparison of Bed Temperature Distribution Across Heater for B1, U* = 5, P = 1750 N/m^2

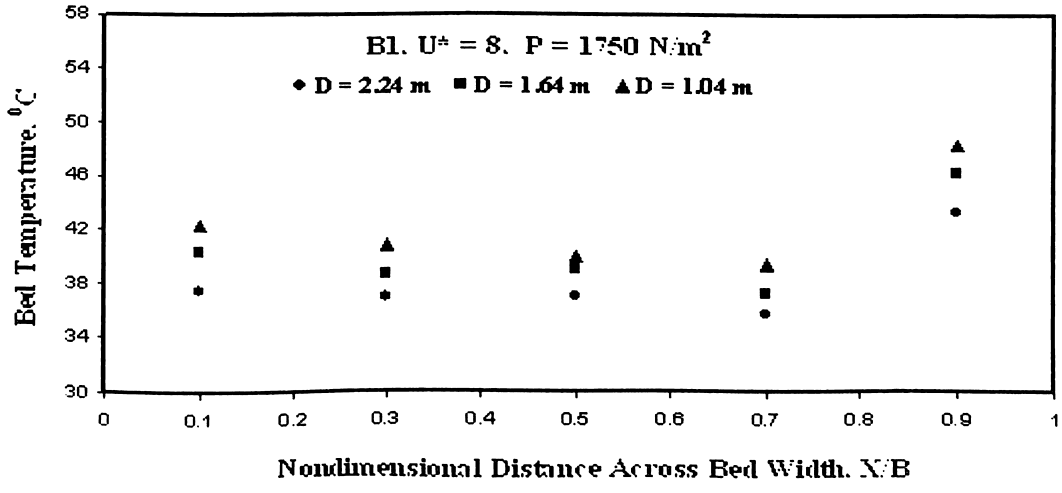

Fig. 4.7 Comparison of Bed Temperature Distribution Across Heater for B1, U* = 8, P = 1750 N/m^2

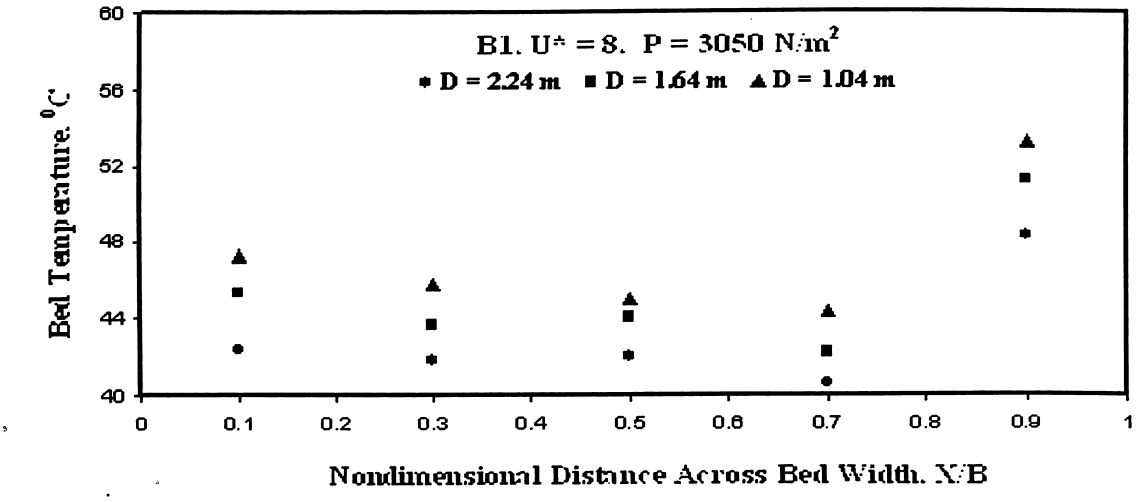

Fig. 4.8 Comparison of Bed Temperature Distribution across Heater for B1, U* = 8, P = 3050 N/m^2

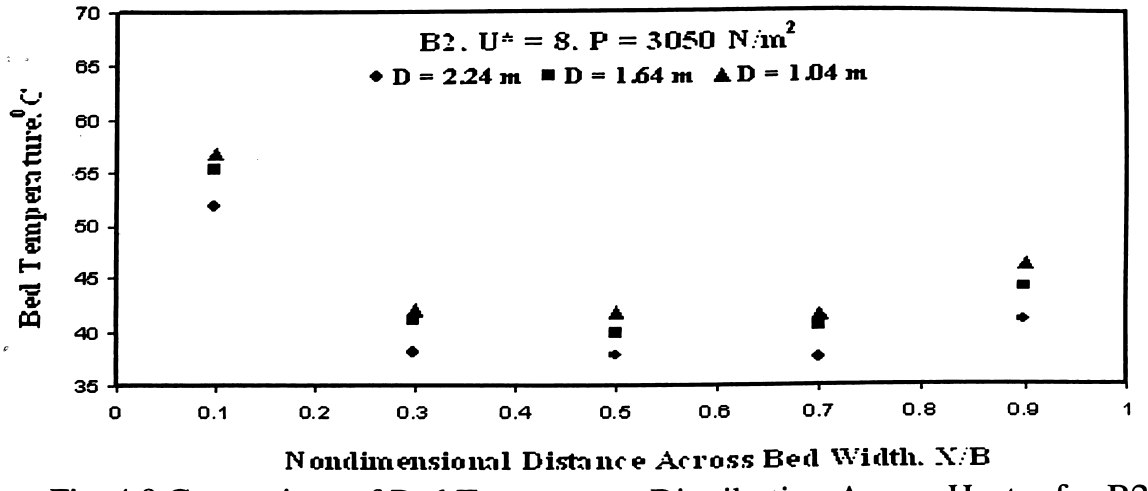

Fig. 4.9 Comparison of Bed Temperature Distribution Across Heater for B2, U* = 8, P = 3050 N/m^2

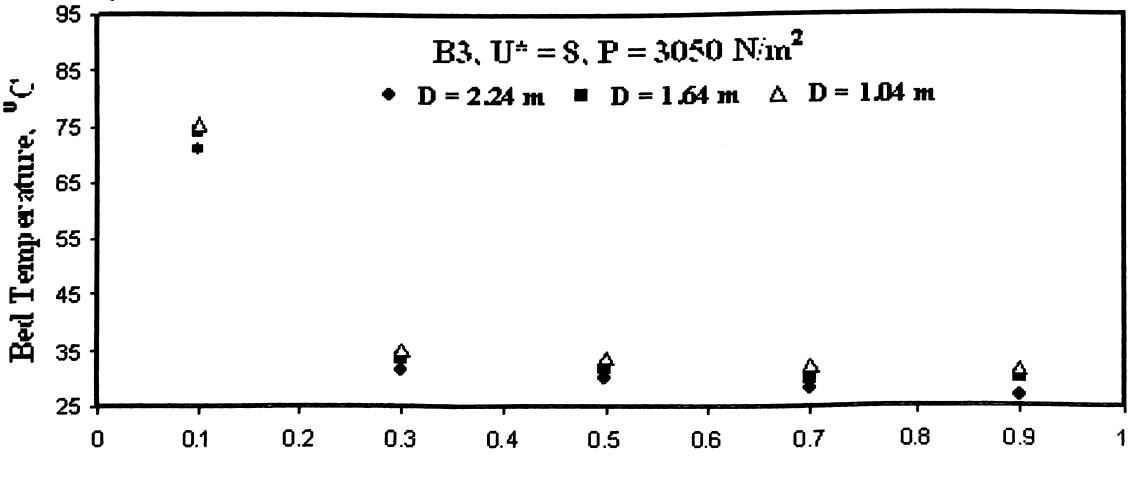

Fig. 4.10 Comparison of Bed Temperature Distribution Across Heater for B3, U* = 8, P = 3050 N/m^2

Figure 4.6 and Fig. 4.7 indicates the effect of non-dimensional velocity parameter (U*) on bed temperature distribution under other similar operating conditions. Figure 4.6 and Fig. 4.7 indicates the bed temperature distribution at nondimensional velocity parameter (U*) = 5 and 8, respectively at a distance above the distributor plate along the riser height (D) = 1.04 m, 1.64 m and 2.24 m. It is observed for any particular value of D that increase in nondimensional velocity parameter (U*) from 5 to 8 resulted in decrease in bed temperature because it is observed through flow visualization that sand concentration decreases in the riser column and also near the wall of the heater with increase in superficial velocity of air, which subsequently decreases the heat transfer from wall-to-bed due to conduction.

Figures 4.8-4.10 present the effect of bed cross section on bed temperature distribution across a heater for the same operating conditions, i.e weight of the sand per unit area of the distributor plate (P) = 3050 N/m^2, heat flux at walls of heater = 1000 W/m^2, nondimensional velocity parameter (U*) = 8, diameter of the sand particle (d_p) = 460 μm. Figures 4.8-4.10 represent the bed temperature distribution for all beds. Let us consider a case if 'D' = 1.04 m. Average bed temperature at lateral section at 1.04 m above the distributor plate was more in smaller cross section heater than larger cross section heater. This is expected because sand inventory in larger cross section CFB setup was kept proportionately more than the smaller size CFB setup so as to maintain the same weight of sand per unit area of the distributor plate. Therefore, weight of sand particles per unit surface area of the larger cross section heater was more than the smaller heater. Therefore at the same value of applied heat flux at heater wall of each CFB setup, distribution of amount heat extracted due to conduction from walls of the heater took place into large number particles, which comparatively more in lager cross section CFB setup, hence average bed temperature was less for larger size heater section than smaller heater.

4.3.2 Axial Distribution of Local and Average Heat Transfer Coefficient

Figures 4.11-4.14 present the axial distribution of local heat transfer coefficient distribution along the height of the heater. Figures 4.11-4.13 present the heat transfer coefficient values for the upper, middle, and lower splash region, respectively for the

TH-1848_Shankarrao

three CFB setups, which were operated at similar operating conditions. Therefore for a specific CFB setup, Figures 4.11-4.13 could be compared to understand the distribution of local heat transfer coefficient in the upper, middle, and lower splash region respectively. The physics or scientific reasoning behind such type of the distribution of local heat transfer coefficient has been explained with respect to Figs. 4.15-4.18. Figure 4.14 presents local heat transfer coefficient for the CFB setup B1. The region 'A' and 'B' as shown in Fig. 4.14 represent the zone of peak which took place at the end of lower and middle splash region. This is because, changes in boundary conditions of heater during its change in position from lower to middle splash region and middle to upper splash region along the riser while conducting the experiments. In real practice if entire riser of a CFB setup gets heated then trend of distribution of local heat transfer coefficient would be similar as shown in Figs. 4.11-4.13, i.e will not be as in Fig. 4.14.

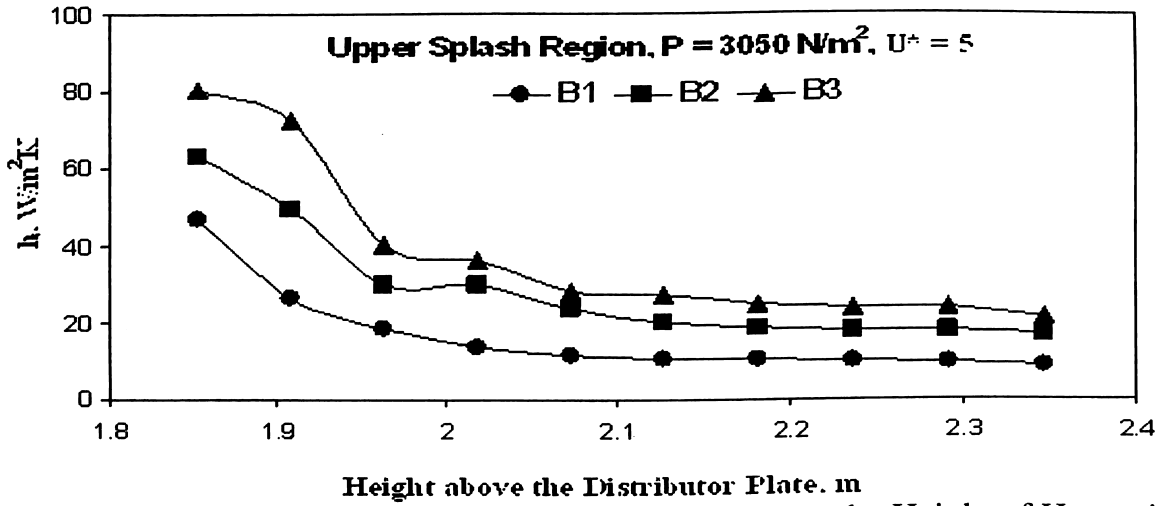

Fig. 4.11 Local Heat Transfer Coefficient Variation along the Height of Heater in Upper Splash Region

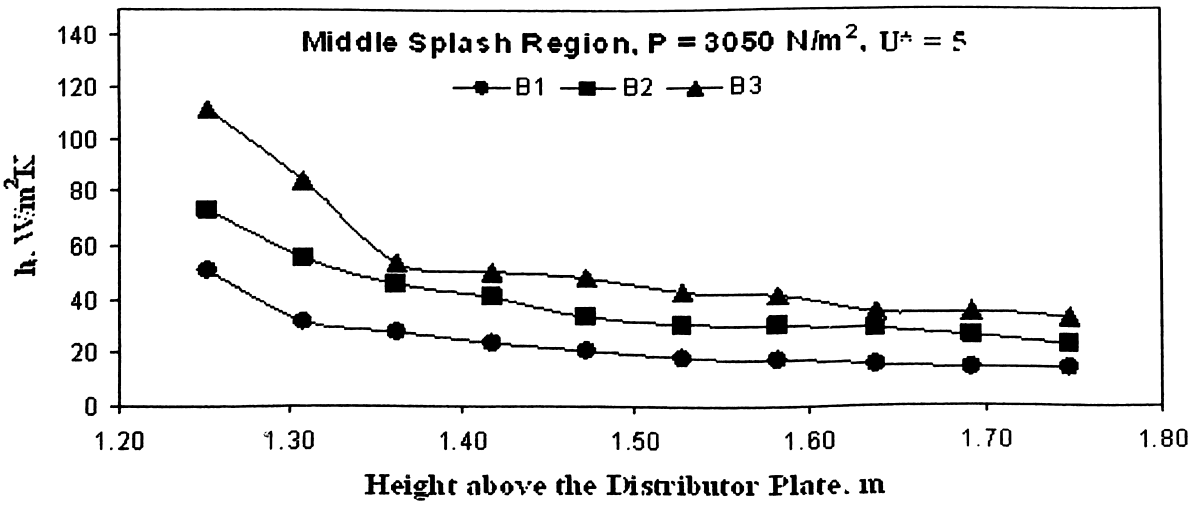

Fig. 4.12 Local Heat Transfer Coefficient Variation along the Height of Heater in Middle Splash Region

TH-1848_Shankarrao

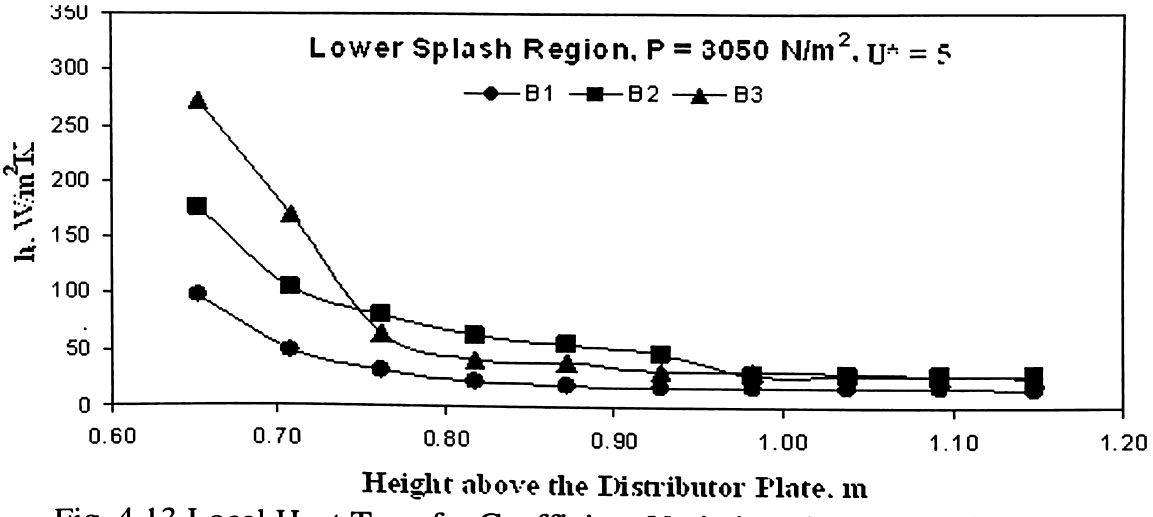

Fig. 4.13 Local Heat Transfer Coefficient Variation along the Height of Heater at Lower Splash Region

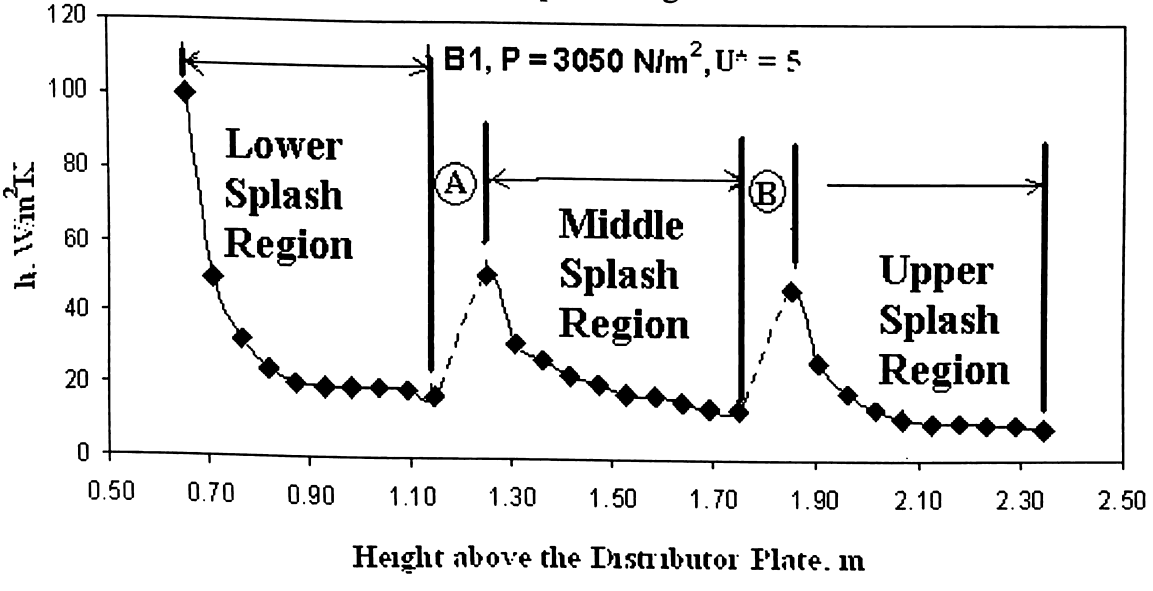

Fig. 4.14 Local Heat Transfer Coefficient Variation along the Height of Heater for B1, P = 3050 N/m^2, U* = 5

Therefore to avoid such peaks, average heat transfer coefficient for upper, middle and lower splash region has been calculated using eq. (3.6). (Refer Figs. 4.15-4.18).

Figures 4.15-4.18 represent the distribution of average heat transfer coefficient along the height of the riser. It can be seen that, for a specific bed, the value of heat transfer coefficient decreases along the height of heater, at upper portion of heater. This is because, as explained earlier (section 4.2.2), the lower splash region contains a denser mixture, having higher concentration of sand particles, than the middle and upper splash regions of the riser. Therefore, due to better heat conduction in the lower splash region, thermal resistance in this region is less than that in the middle and upper splash regions.

TH-1848_Shankarrao

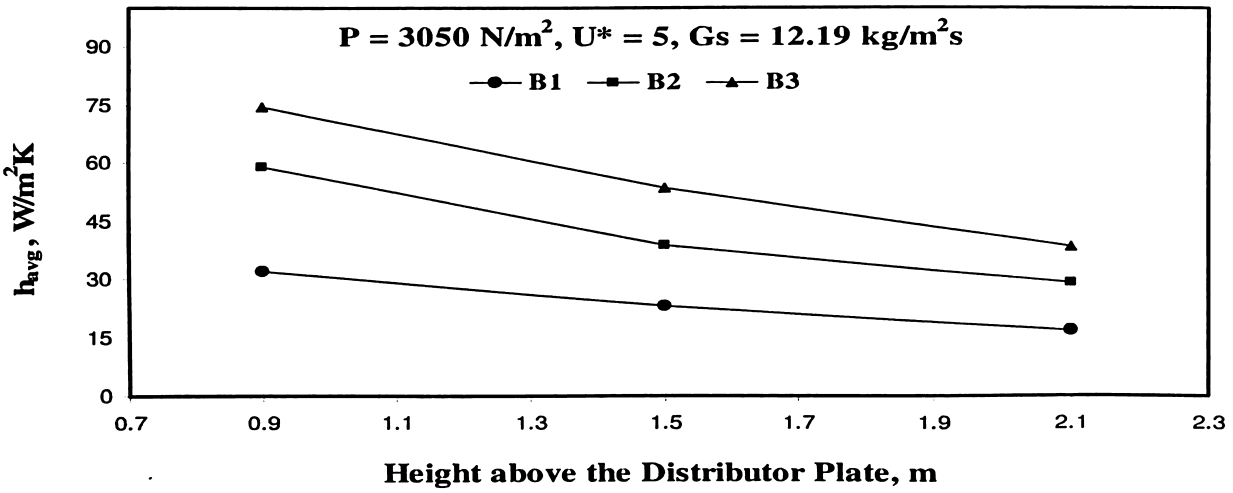

Fig. 4.15 Average Heat Transfer Coefficient along the Height of the Risers at P = 3050 N/m^2, U* = 5

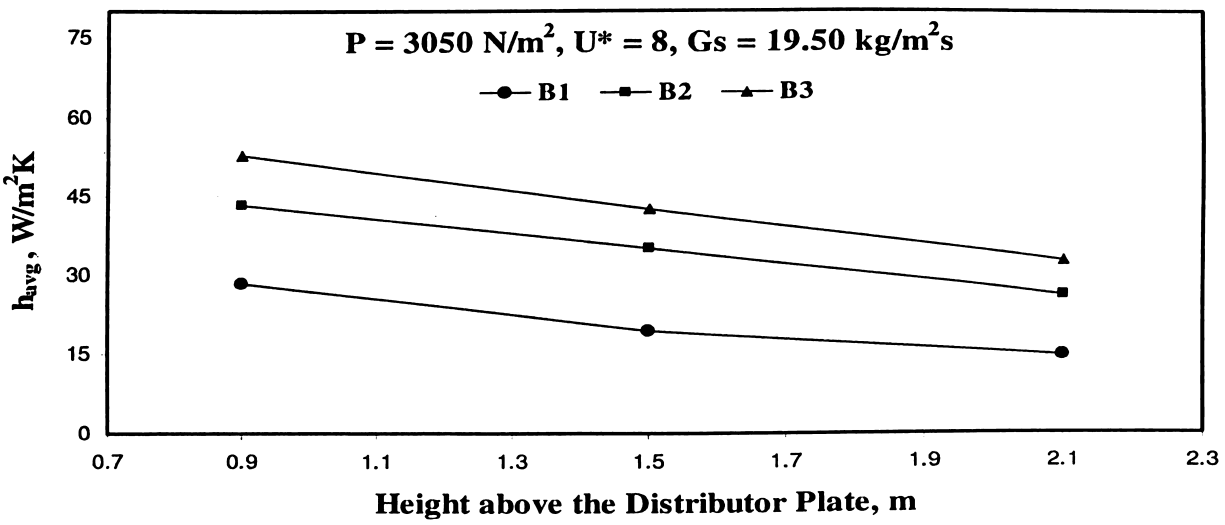

Fig. 4.16 Average Heat Transfer Coefficient along the Height of the Risers at P = 3050 N/m^2, U* = 8

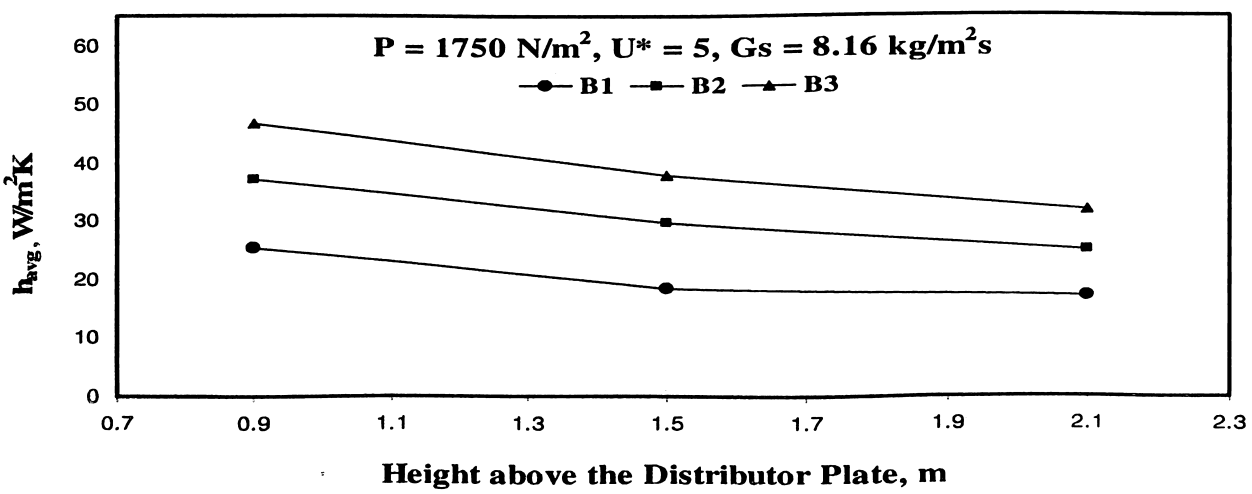

Fig. 4.17 Average Heat Transfer Coefficient along the Height of the Risers at P = 1750 N/m^2, U* = 5

TH-1848_Shankarrao

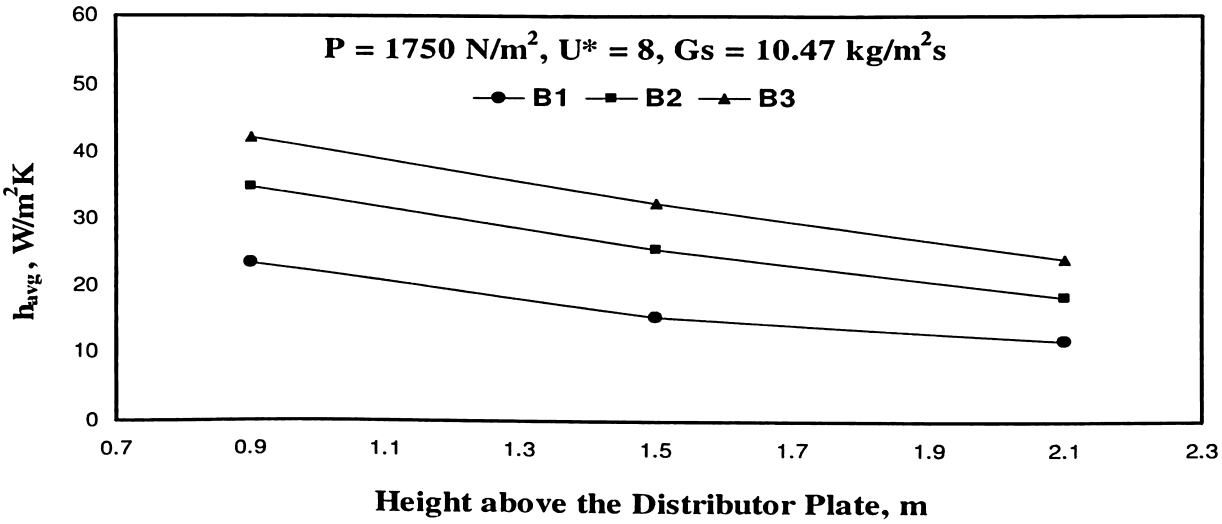

Fig. 4.18 Average Heat Transfer Coefficient along the Height of the Risers at P = 1750 N/m^2, U* = 8

Figures 4.15-4.18 indicate that the average heat transfer coefficient increases considerably with increase in bed cross section. It is observed that the driving temperature difference ($T_S - T_B$) in the larger size bed was lesser than the smaller size beds, while the heat flux was kept fixed. This is because of the higher concentration of solid particles near the wall of the larger heater (as explained in section 4.2.2), and consequently, lower thermal resistance from the bed-to-wall causing better heat conduction.

The effect of non-dimensional velocity on heat transfer coefficient can be observed by comparing Figs. 4.15 and 4.16, and Figs. 4.17 and 4.18, respectively. It is seen that the average heat transfer coefficient decreases with increase in non-dimensional velocity parameter (U*). As explained in the earlier section, bed temperature decreases with increase in non-dimensional velocity parameter (U*) which results in increase in the driving temperature difference ($T_S - T_B$), while the heat flux is constant. This trend is similar to that reported by (Basu and Nag, 1987; Fox et al., 1999; Grulovic et al., 2008) on the axial variation of heat transfer coefficient.

Figures 4.15 and 4.17, and Figs. 4.16 and 4.18, respectively can be compared for the effect of bed inventory on average heat transfer coefficient. It can be observed that, for a specific bed, average heat transfer coefficient increases with increase in sand inventory.

Figure 4.19 and Fig. 4.20 represent the variation of average heat transfer coefficient with respect to average suspension density. Three different trends were observed for CFB units B1, B2, and B3 when these CFB units were operated under

TH-1848_Shankarrao

similar operating conditions (U* = 6 and 8, at P = 3050 N/m^2). Symbol L, M, and U as shown in Figs. 4.19-4.20 represents lower splash, middle splash, and upper splash region respectively.

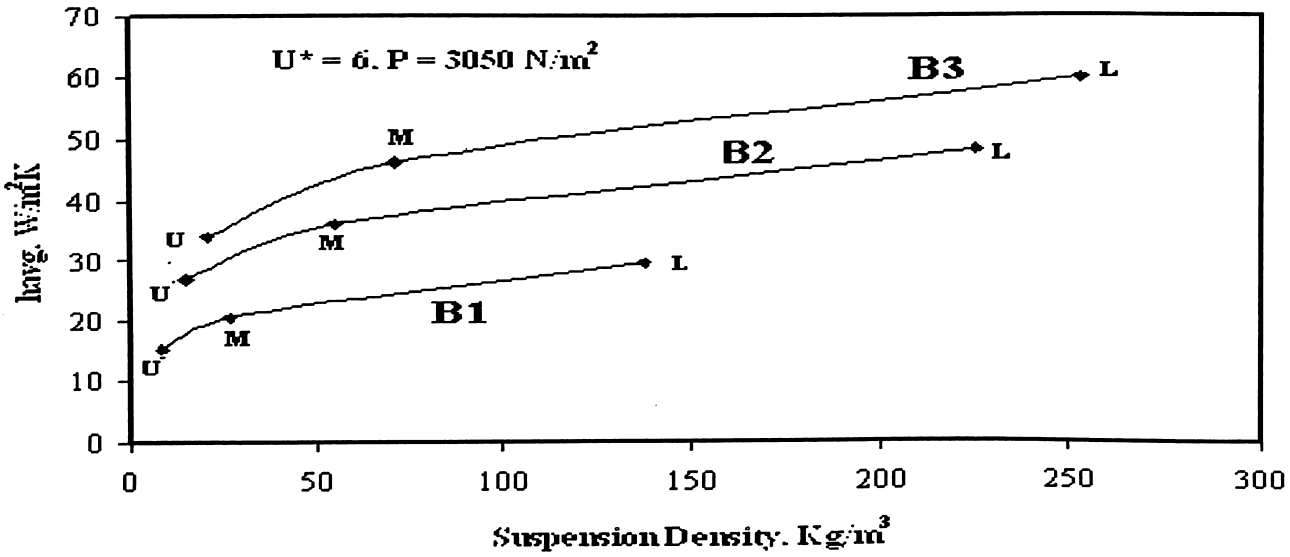

Fig. 4.19 Suspension Density vs Average Heat Transfer Coefficient at U* = 6

It is observed that suspension density for CFB setup B3 was comparatively more than other two CFB units at same respective location in the riser column thus attributing to higher value of heat transfer coefficient. High value of the suspension density is responsible for higher concentration of solid particles near the wall of the larger CFB unit's heater section. As a consequence, lower thermal resistance from the bed-to-wall is developed causing better heat conduction, increasing the heat transfer coefficient, when constant heat flux 1000 W/m^2 was applied at walls of all heaters.

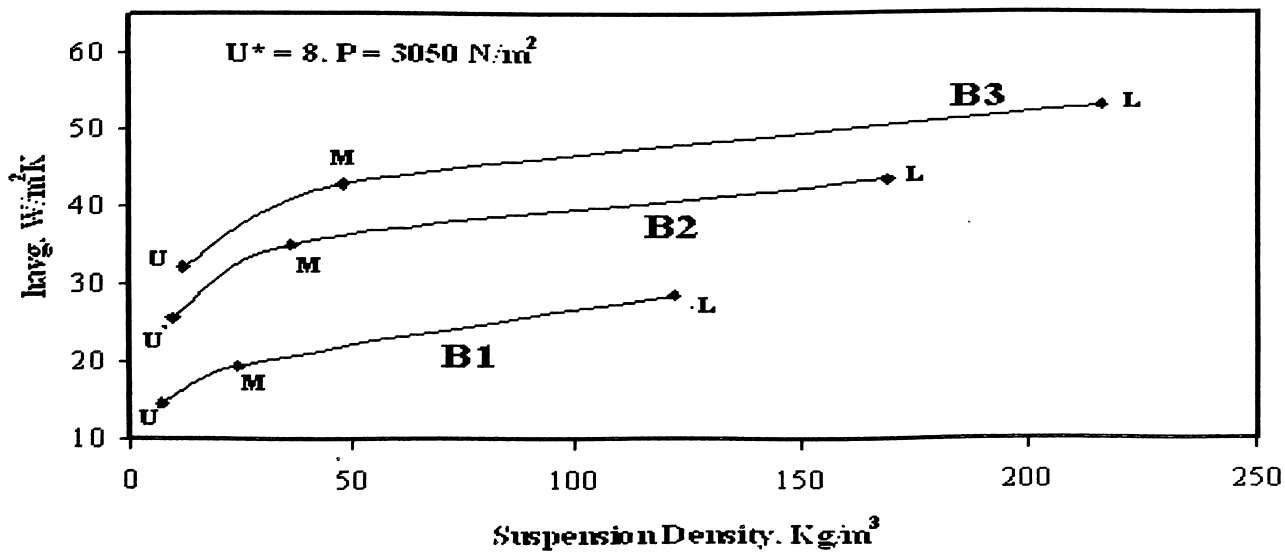

Fig. 4.20 Suspension Density vs Average Heat Transfer Coefficient at U* = 8

TH-1848_Shankarrao

Uncertainty analysis was carried out for the heat transfer coefficient and same is presented in (Appendix E). Factors responsible for the uncertainty in measurement of heat transfer coefficients are the connections of thermocouples, accuracy of T-type thermocouple (±0.5°C), wattmeter accuracy (±5W), and accuracy in length measurement (±1mm), respectively. Uncertainty analyses were done using the method of Kline and McClintok (Kline and McClintok, 1953). Uncertainty in heat transfer coefficients estimation in the present study was calculated to be within ± 4%.

4.4 Development of Heat Transfer Correlations

4.4.1 Correlation for Lower Splash Region

A dimensional analysis is made using Rayleigh's method. 6 (six) non-dimensional numbers were obtained after the analysis. Nusselt number and Reynolds number are the most important and widely used non-dimensional numbers. Based on the literature, three more non-dimensional numbers were included, namely the aspect ratio [H_B/H_D] i.e [ratio of height of the static sand inventory of the fluidized bed (H_B) to the hydraulic diameter of bed (H_D)], non-dimensional velocity parameter U* and non-dimensional height parameter [H_m/H_r] i.e [ratio of height from the distributor plate to location of thermocouple in the heater (H_m) to total height of the riser (H_r)]. In order to facilitate the scale-up of CFB, a new non-dimensional number was introduced, namely, the non-dimensional area parameter [A_B/A_S] i.e [ratio of cross section area of heater (A_B) to surface area of heater (A_S)]. A best-fit equation involving these six non-dimensional numbers fitting 36 experimental data points were obtained with the help of FindFit function of Mathematica version 5.2. The best-fit equation is as follows.

$$Nu_B = 2.721\times10^{-5}[\mathrm{Re}_B]^{1.652}[U^*]^{-0.721}[A_B/A_S]^{2.078}[H_m/H_r]^{-4.354}[H_B/H_D]^{0.169} \qquad (4.3)$$

Correlation presented in eq. (4.3) is valid in the following range of experimental conditions: $23740 < \mathrm{Re}_B < 59517$, $5 < U^* < 8$, $0.0625 < (A_B/A_S) < 0.1041$, $0.22 < (H_m/H_r) < 0.40$, $0.5 < (H_B/H_D) < 1.466$. The bed Nusselt number was in the range of 97.12 to 2813.50. In the present study, Prandtl number (Pr) was not included because the fluidizing medium was air only, and the experiments were conducted on a cold bed, in

which the range of bed temperatures was not large enough to cause significant variation in Pr. Importance of non-dimensional numbers is clearly indicated by their exponent value. Figure 4.21 shows the comparison of the present experimental results with the prediction of the correlation eq. (4.3) showing rms deviation of ±15%.

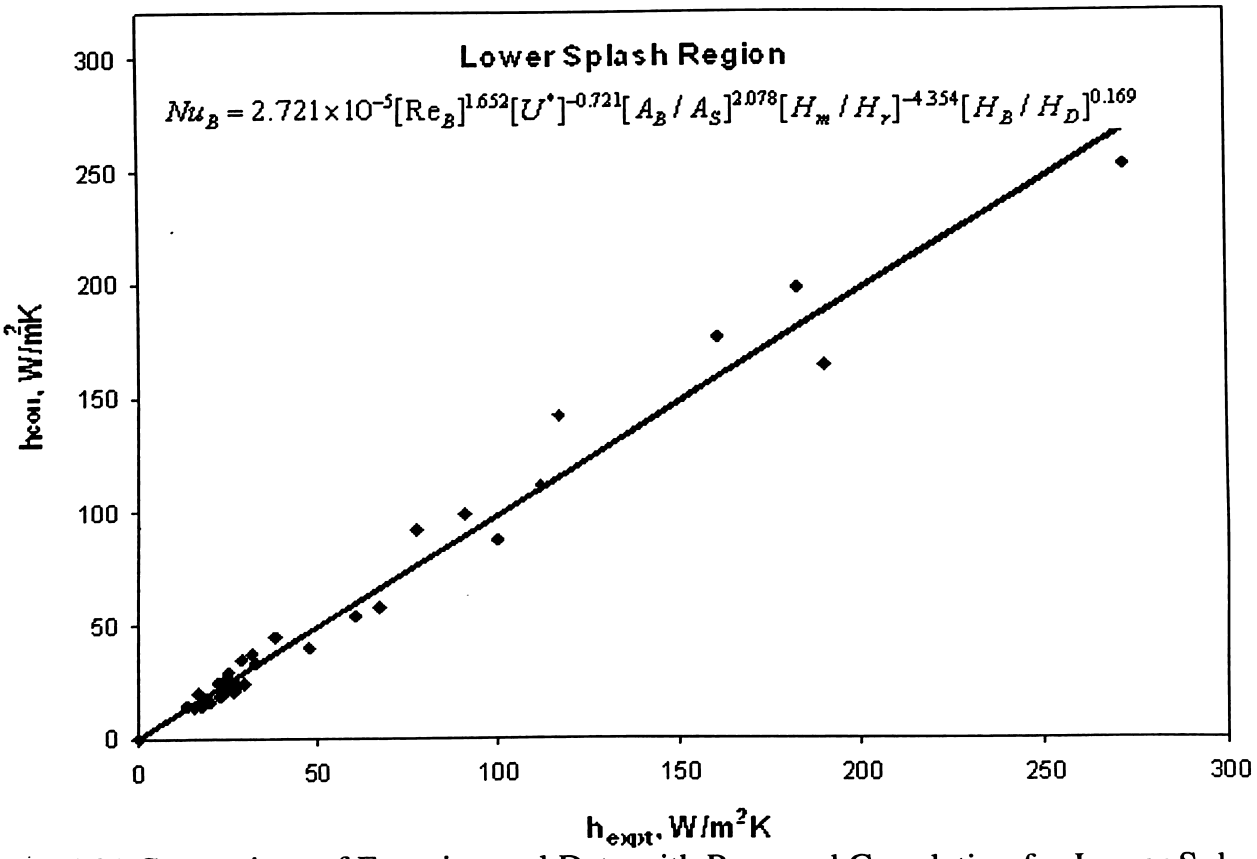

Fig. 4.21 Comparison of Experimental Data with Proposed Correlation for Lower Splash Region

4.4.2 Correlation for Middle Splash Region

Following similar principle as reported in section 4.4.1, a Correlation was developed for the middle splash region (Eq. 4.4)

$$Nu_B = 138.98[\mathrm{Re}_B]^{0.139}[U^*]^{0.264}[A_B / A_S]^{1.864}[H_m / H_r]^{-4.549}[H_B / H_D]^{0.347} \qquad (4.4)$$

This correlation [eq. (4.4)] is valid in the following range of experimental conditions: $23740 < \mathrm{Re}_B < 59517$, $5 < U^* < 8$, $0.0625 < (A_B / A_S) < 0.1041$, $0.5 < (H_B / H_D) < 1.466$. The bed Nusselt number was in the range of 97.12 to 2813.50. Figure 4.22 shows the comparison of the present experimental results with the prediction of the correlation eq. (4.4) showing rms deviation of ±17%.

TH-1848_Shankarrao

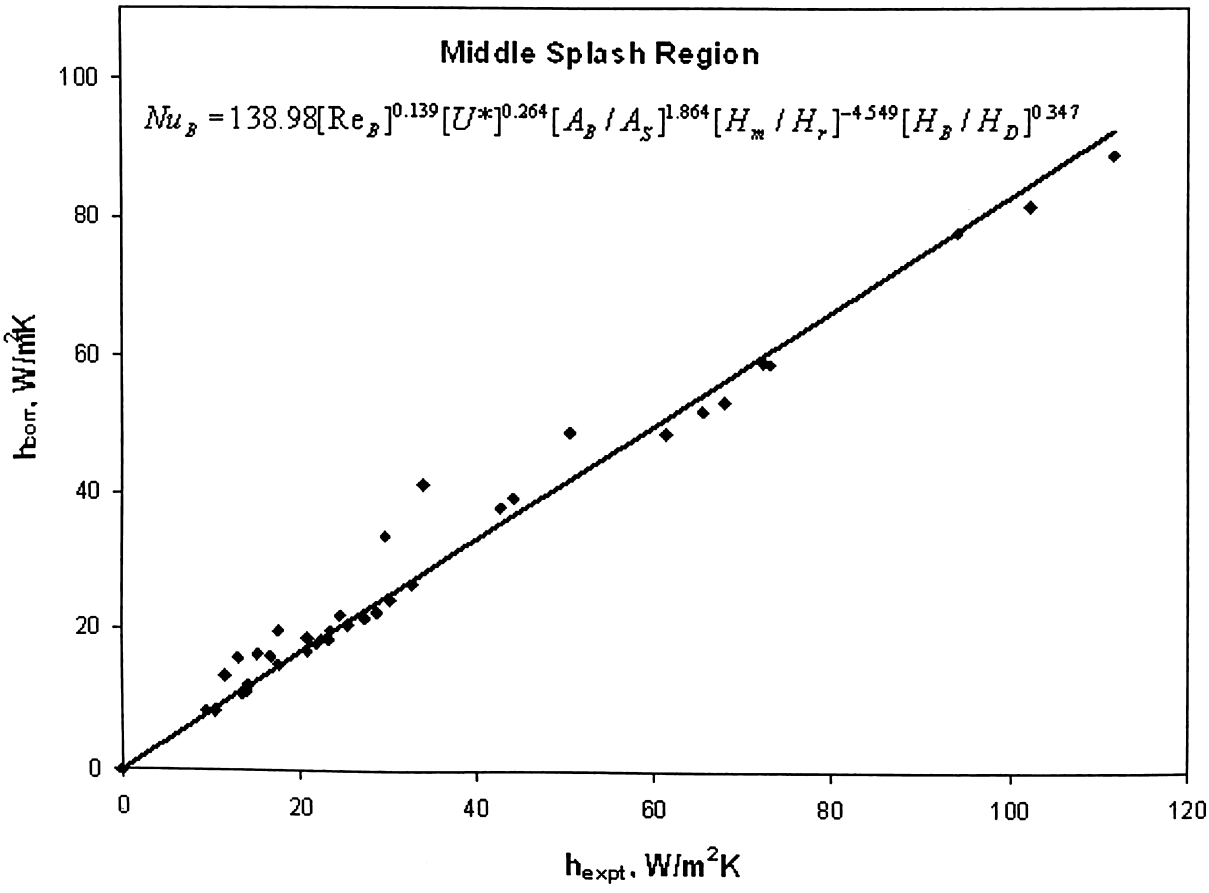

Fig. 4.22 Comparison of Experimental Data with Proposed Correlation for Middle Splash Region

4.4.3 First Correlation for Entire Riser

Dimensional analysis was done similar to that in Section 4.4.1. A best-fit equation involving these six non-dimensional numbers fitting nine hundred experimental data points were obtained with the help of FindFit function of Mathematica. The best-fit equation is as follows.

$$Nu_B = 103.4[R_B]^{0.6}[U^*]^{0.057}[A_B/A_S]^{2.24}[H_m/H_r]^{-0.636}[H_B/H_D]^{0.45} \quad (4.5)$$

Correlation presented in eq. (4.5) is valid in the following range of experimental conditions: $23740 < \mathrm{Re}_B < 59517$, $5 < U^* < 8$, $0.0625 < (A_B/A_S) < 0.1041$, $0.32 < (H_m/H_r) < 0.74$, $0.5 < (H_B/H_D) < 1.466$. The bed Nusselt number was in the range of 73.75 to 774.69. Figure 4.23 show the comparison of the present experimental results with the prediction of the above correlation showing an rms deviation of ±16%.

TH-1848_Shankarrao

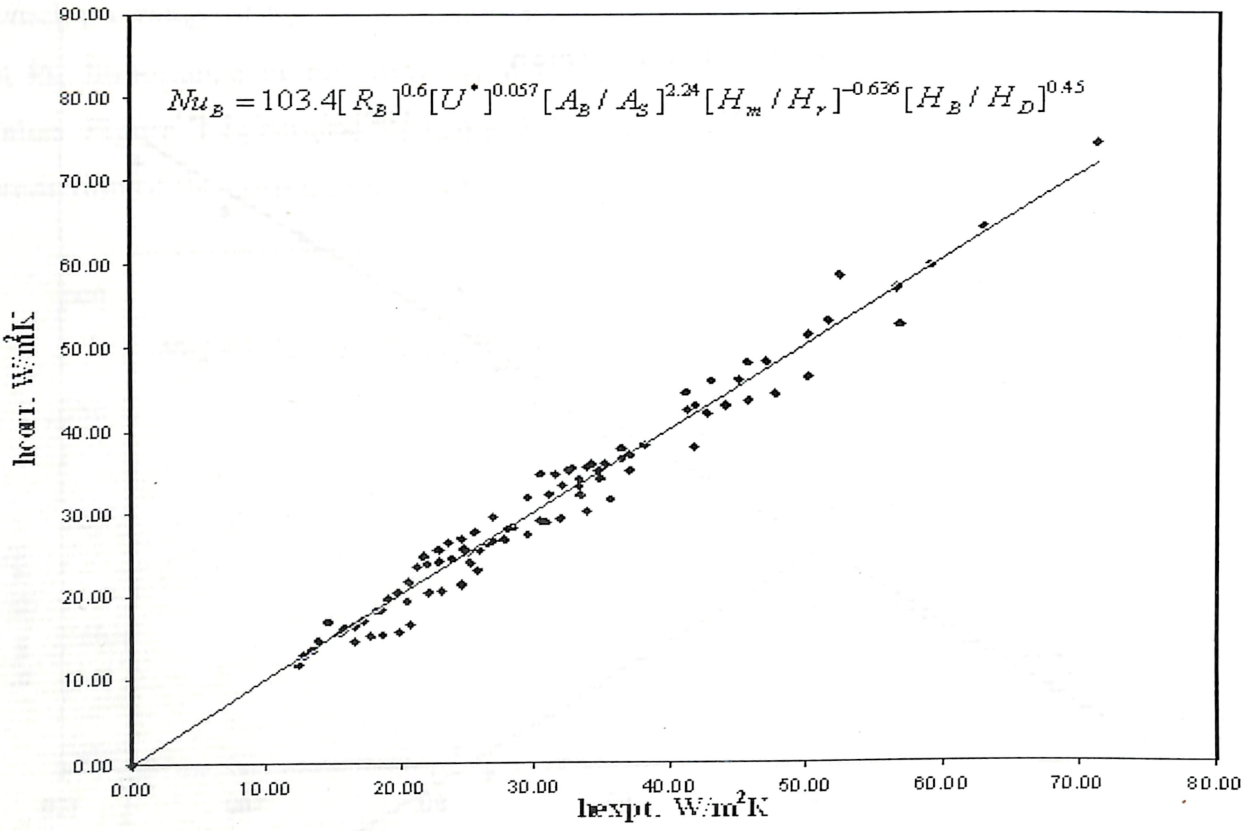

Fig. 4.23 Comparison of Experimental Data with Proposed Correlation for Entire Riser

4.4.4 Second Correlation for Entire Riser

A dimensional analysis was made using Rayleigh's method (Appendix F) and five non-dimensional numbers were obtained. Nusselt number, Reynolds number and Prandtl number are the most important and widely used numbers. Two more non-dimensional numbers were obtained, namely non-dimensional density ratio [ρ_{sus}/ρ_g] i.e [ratio of suspension density (ρ_{sus}) to the density of air (ρ_g)] and new non-dimensional number presenting scale-up i.e non-dimensional geometrical parameter [H/B] i.e [ratio of height of the heater (H) to the hydraulic diameter of the bed (B)]. A best-fit equation involving these non-dimensional numbers (excluding Prandtl number) was obtained using FindFit function of Mathematica 5.2. The best-fit equation is as follows.

$$Nu_B = 59.35\,[Re_B]^{0.22}\,[\rho_{sus}/\rho_g]^{0.24}\,[H/B]^{-1.707} \qquad (4.6)$$

Variation of Prandtl number was not significant enough (Pr = 0.71-0.76) to cause significant variation in the predicted value of heat transfer coefficient. Therefore it has not been included in the empirical correlation. Correlation eq. (4.6) is valid in the following range of experimental conditions: $20629 < Re_B < 84270$, $6 < (\rho_{sus}/\rho_g) < 240$,

TH-1848_Shankarrao

0.69 < (*H/B*) < 4. The bed Nusselt number was in the range of 73.75 to 1547. Prandtl number (Pr) was not included because it was not varying much from bottom of the riser to top of the riser (Pr = 0.71-0.76). Fig. 4.24 shows the comparison of the experimental heat transfer coefficient data of present work plus data obtained from literature with the prediction of the correlation eq. (4.6) showing rms deviation of ± 21.73%. Experiments of other researchers were carried out over a wide range of velocity, bed density particle size, and [H/B] ratio. In order to facilitate the easy comparison of predicted values with experimental values, all data were plotted in Fig. 4.24, with the measured heat transfer coefficient and the theoretical prediction as the coordinates. The middle line (line at 45^0) is the line of prefect agreement, and other two extreme lines show the boundary of ± 21.73%.

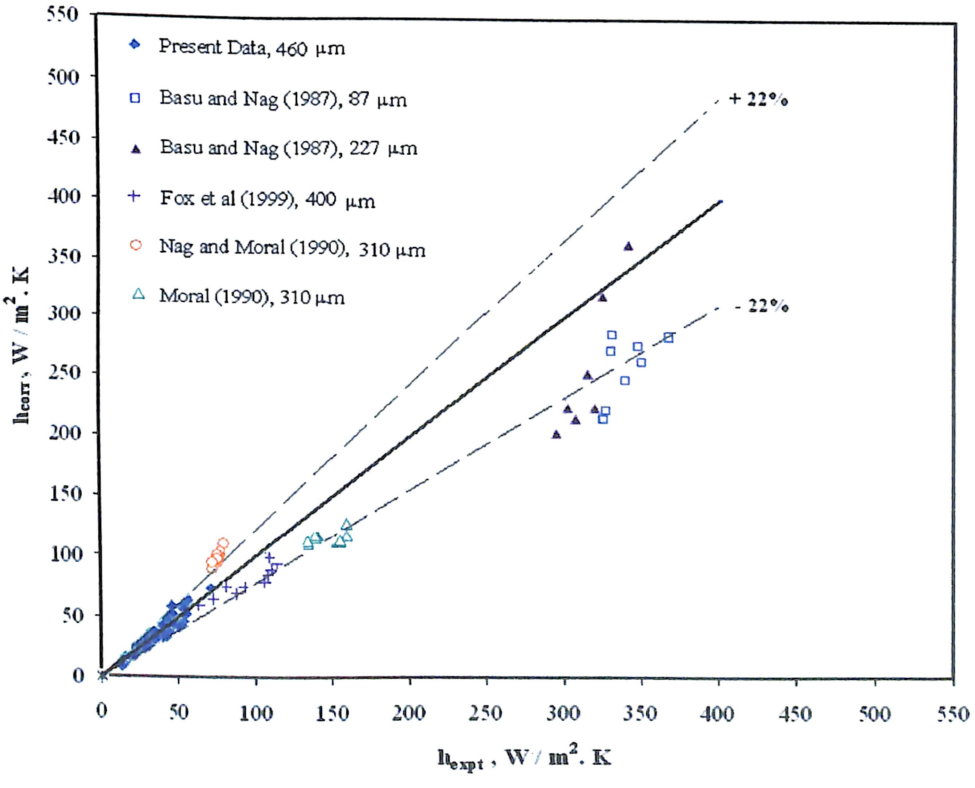

Fig. 4.24 Comparison of Experimental Data with Proposed Correlation

4.4.5 Comparison of Correlations with Experimental Data

Figure 4.25 shows the comparison of correlations, eq. (4.5) and eq. (4.6) with experimental data. Variation of average value of heat transfer coefficient with non-dimensional velocity parameter (U*) is presented in Fig. 4.25 for the upper splash region of CFB bed (B1) of cross section 0.15 m × 0.15 m at P = 3050 N/m^2 (weight of sand inventory per unit area of distributor plate). It is observed that the heat transfer

TH-1848_Shankarrao

coefficient predicted using eq. (4.6) is closer to experimental value than heat transfer coefficient predicted using eq. (4.5). The same may be noted for upper splash region of CFB setup (B2) and (B3) as shown in Figs. 4.26 and 4.27, respectively.

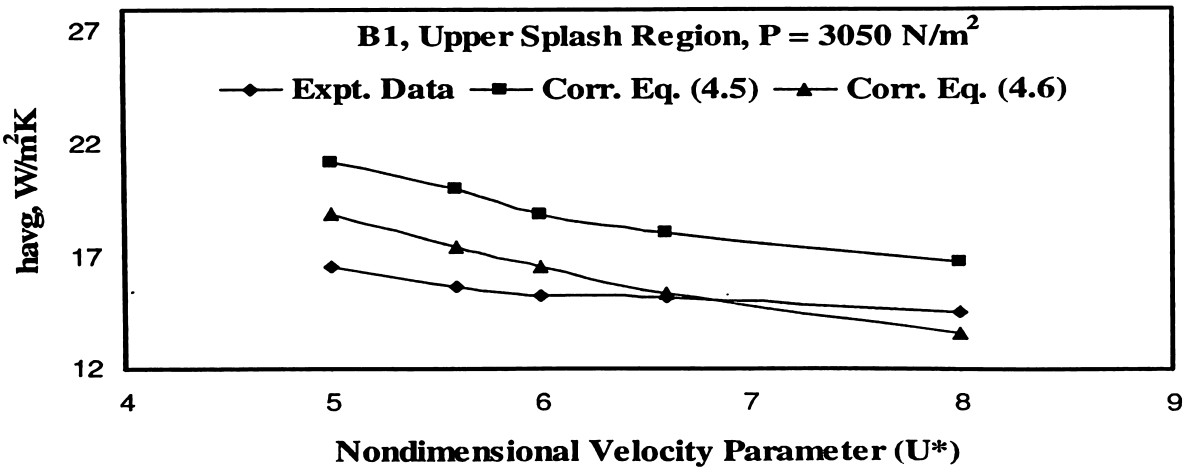

Fig. 4.25 Comparison of Experimental Data with Proposed Correlations for entire Riser for B1, Upper Splash Region, P = 3050 N/m^2

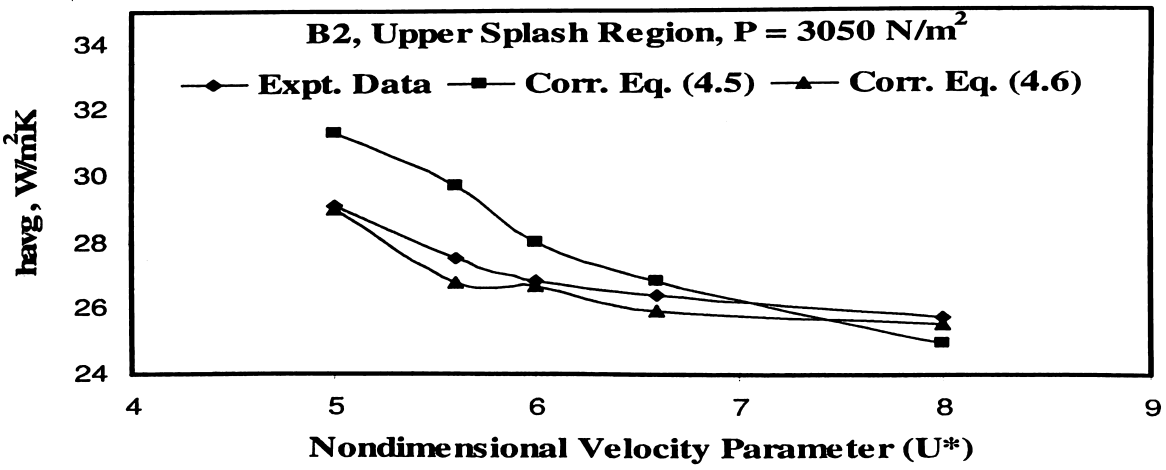

Fig. 4.26 Comparison of Experimental Data with Proposed Correlations for entire Riser for B2, Upper Splash Region, P = 3050 N/m^2

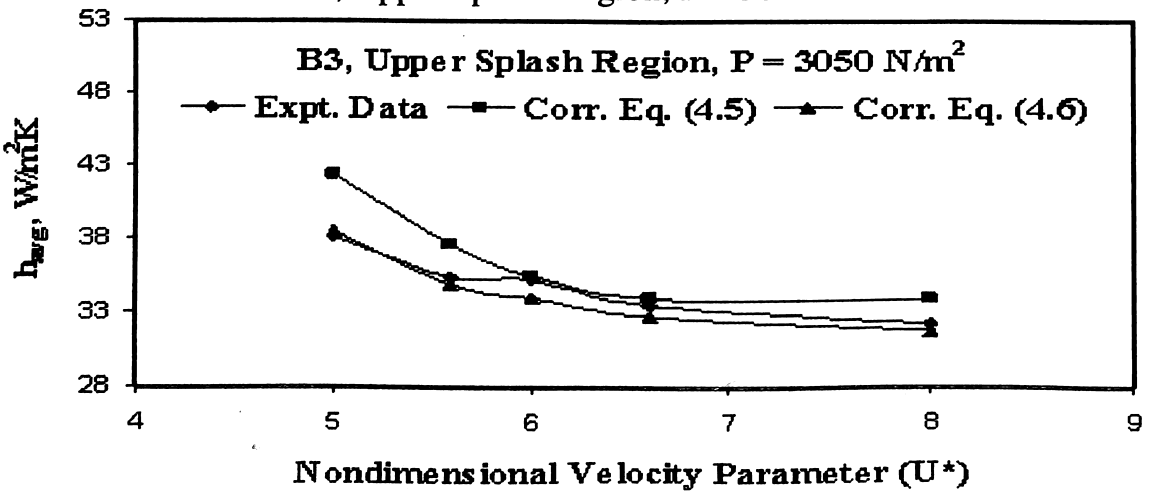

Fig. 4.27 Comparison of Experimental Data with Proposed Correlations for entire Riser for B3, Upper Splash Region, P = 3050 N/m^2

TH-1848_Shankarrao

4.5 Comparison of Non-dimensional Parameters

4.5.1 Bed Nusselt Number (Nu_B) vs Bed Reynolds (Re_B) Number

Figure 4.28 presents the variation of bed Nusselt number with bed Reynolds number for different value of H* [Non-dimensional height parameter, ratio of height from the distributor plate to midpoint of the heater (H_m) to the total height of the riser (H_r)].

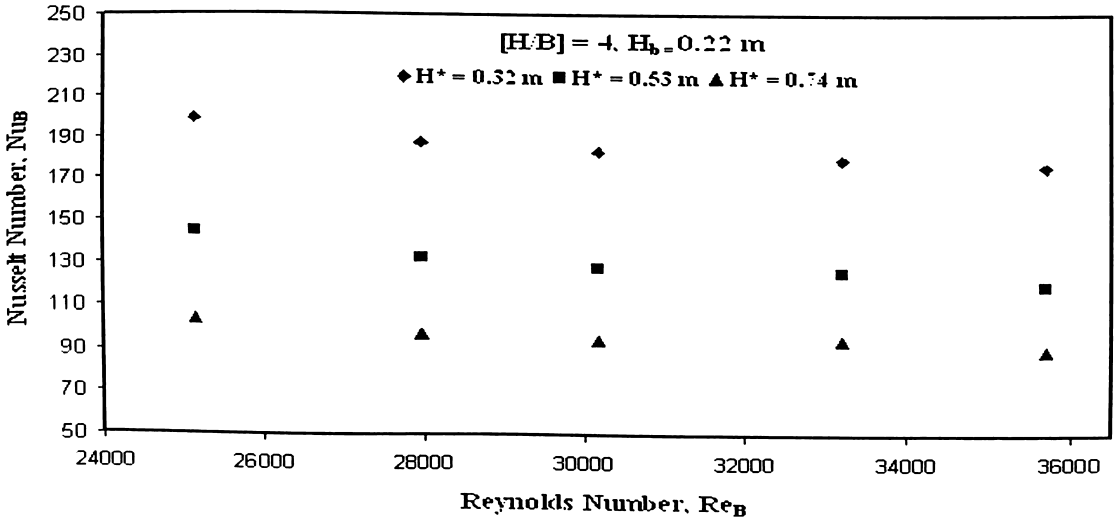

Fig. 4.28 Bed Nusselt Number (Nu_B) vs Bed Reynolds (Re_B) Number

It is observed that the Nusselt number decreases with increase in Reynolds number. This is because increase in superficial velocity decreases heat transfer coefficient as explained in section 4.3.2. At H* = 0.32, variation of Nusselt number was more than at other two values of H*. This is because, at H* = 0.32, bed was denser occupying large number of sand particles while at H* = 0.74, it was more dilute.

4.5.2 Bed Nusselt Number (Nu_B) vs Non-dimensional Geometrical Parameter (H/B)

Figure 4.29 presents the variation of Nusselt number for different value of non-dimensional geometrical parameter (H/B). It is observed that the Bed Nusselt number increases with decrease in non-dimensional geometrical parameter (H/B). This is because, as explained earlier section 4.3.2, heat transfer coefficient increases considerably with increase in bed cross-section (B) and hence decrease in parameter (H/B). Also, bed Nusselt number (Nu_B) was more at the bottom ($H^* = 0.32$) of the riser of each CFB setup due to higher concentration of solid particles. This is because of the

higher concentration of solid particles near the wall of the larger bed, and consequently, lower thermal resistance from the bed-to-wall causing better heat conduction.

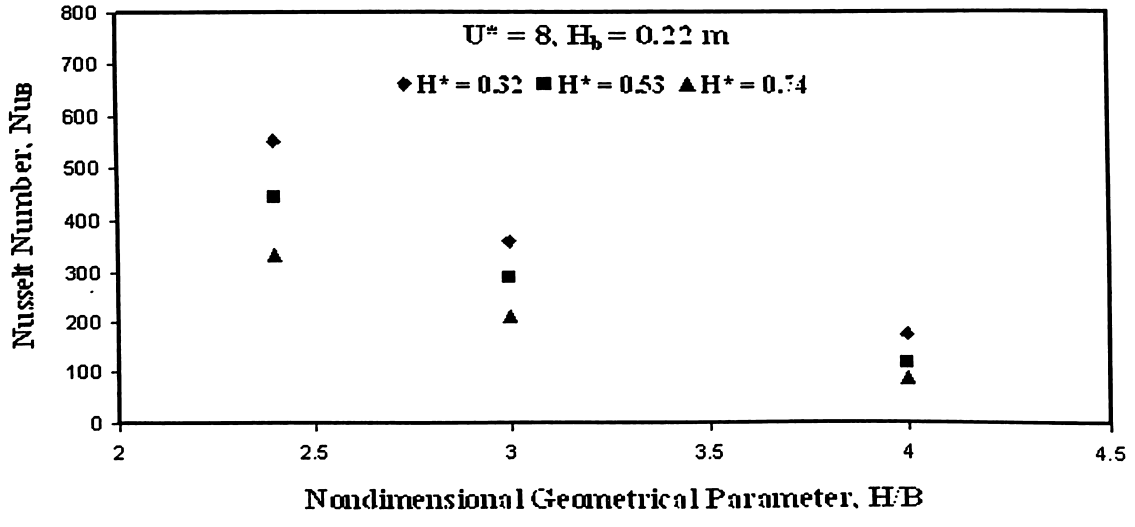

Fig. 4.29 Bed Nusselt Number (Nu_B) vs Non-dimensional Geometrical Parameter (H/B)

4.6 Summary

Experiments were conducted under similar operating conditions on three CFB setups. Effect of superficial velocity of air, sand inventory, and bed cross section on heat transfer coefficient and bed temperature distribution was predicted and results were compared with available literatures. In all the setups, it is observed that pressure drop and suspension density increases wih increase in riser cross section area, decreases with increase in superficial velocity of the air. In all the setups, it is observed that the bed temperature decreases with increase in cross section area of the riser, superficial velocity of air and increases with increases in sand inventory. Heat transfer coefficient increases with increase in cross section of the riser, sand inventory and decreases with increase in superficial velocity of air. Empirical correlations on lower splash region, middle splash region, and on entire riser were developed using Rayleigh's method (to obtain the non-dimensional numbers) and FindFit function (to obtain the constants of the correlations / exponents of the non-dimensional numbers) of Mathematica version 5.2.

TH-1848_Shankarrao

Chapter 5

Computational Study on CFB Risers

TH-1848_Shankarrao

Chapter 5

Computational Study on CFB Risers

5.1 Introduction

In the present chapter, CFD simulations using Fluent 6.3.26 were accomplished to study the effect of superficial velocity of air, particle size, sand inventory, and bed cross section on heat transfer characteristics. 3D CFD simulations were performed on steady state wall-to-bed heat transfer characteristics on CFB riser of cross section 0.15 m × 0.15 m and height 2.85 m for its heated portion (heater) of same cross section and height of 0.6 m, located at 0.6 m and 1.8 m above the distributor plate which is the lower splash and upper splash region of CFB, respectively. To study the effect of bed cross section on heat transfer characteristics, further simulations on upper splash region of height 0.6 m, located at 1.8 m above the distributor plate were accomplished for riser of cross section 0.30 m × 0.30 m. Modelling and meshing were done with Gambit software – version 2.4.6. The wall of heater was maintained at the constant heat flux q" = 1000 W/m^2. RNG k-ε model was used for turbulence modelling. Eulerian model with Gidaspow phase interaction scheme is used to simulate the two phase flow (air + sand mixture flow).

Effect of superficial velocity of air and sand inventory on heat transfer characteristics is predicted with respect to lower splash region of riser of cross section 0.15 m × 0.15 m for two superficial velocities of air (2.5 m/s and 4 m/s) and two sand inventories (4 kg and 7 kg) for particle size of 460 μm. Effect of particle size on heat transfer characteristics of lower splash region is predicted using six particle sizes falling in the range of Geldart *B* type particles (60 μm, 100 μm, 160 μm, 260 μm, 360 μm, 460 μm) at sand inventory of 7 kg and superficial velocity of air 2.5 m/s for the heater of cross section 0.15 m × 0.15 m. Effect of riser cross section on heat transfer characteristics is predicted by comparing the results obtained on heat transfer characteristics with respect to upper splash region of risers of cross section 0.15 m × 0.15 m, 0.30 m × 0.30 m at sand inventory of 7 kg, superficial velocity of air 2.5 m/s and 4 m/s and using particle size of 460 μm.

TH-1848_Shankarrao

5.2 CFD Modeling and Simulation

In Fluent, the governing equations are discretized using the finite volume technique. The discretized equations, along with the initial and boundary conditions, are solved to obtain a numerical solution. Eulerian multiphase model was used for the simulation of air-sand flow. 3-D CFD simulations were done on heater section (portion L, U as shown in Fig.3.1 each of height 0.6 m). Modeling and meshing were done in Gambit 2.4.6. While meshing the heater, cell type selected was tetrahedral/hybrid with T grid meshing scheme. Selected boundary conditions as shown in Fig. 5.1 were air velocity at inlet, bottom of riser = 2.36 m/s - 4 m/s, and volume fraction of sand = 0; volume fraction of sand at inlet at right hand side wall of riser = 1 and sand velocity = 0.00313 m/s - 0.0075 m/s; outlet boundary condition was pressure outlet at top of the riser = 0 Pa gauge pressure of air-sand mixture. While simulating the riser in Fluent 6.3.26, 3D steady state solver was used. Other parameters selected were density of sand = 2600 kg/m^3, mean diameter of sand = 60 - 460 μm, density of air = 1.225 kg/m^3, turbulence model used = RNG k-ε model, numerical method used for pressure velocity coupling = phase coupled SIMPLE, discretization scheme = 1st order upwind, under relaxation parameters for pressure = 0.1, density = 0.1, body forces = 0.1, momentum = 0.1, volume fraction = 0.2, energy = 0.1; convergence criteria = 0.001, solution initialization = from all zones, height of the sand inventory above the distributor plate in the CFB riser = 0.22 m and 0.13 m to obtain the static pressure on distributor plate as 3050 N/m^2 and 1750 N/m^2, respectively.

In the Eulerian multiphase (gas-solid, two fluids) model, conservation equations of mass and momentum for both phases are solved simultaneously. The link between the two phases is through the drag force in the momentum equations.

Continuity equation for kth phase is given by

$$\frac{\partial}{\partial t}(\varepsilon_k \rho_k) + \nabla \cdot (\varepsilon_k \rho_k \vec{u}_k) = \sum_{p=1}^{n} \dot{m}_{pk} \tag{5.1}$$

where $k = f$ *for* *fluid*

$k = s$ *for* *solids*

TH-1848_Shankarrao

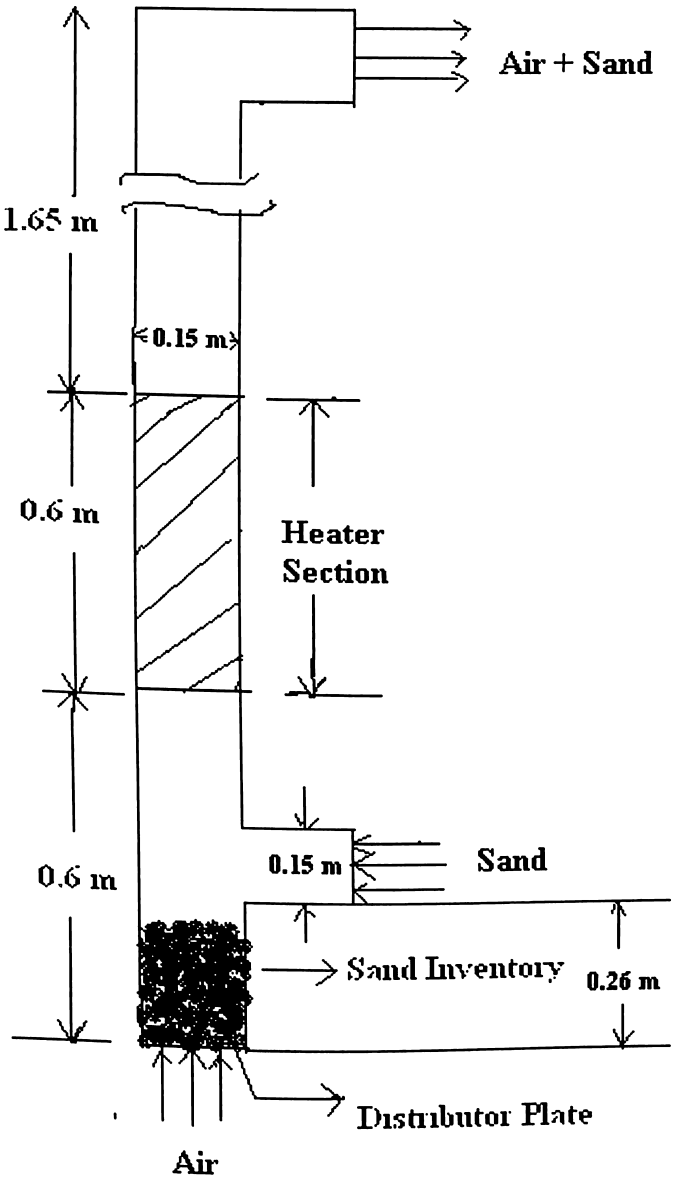

Fig. 5.1 CFB Riser

Momentum equation for the fluid phase is given by

$$\frac{\partial}{\partial t}(\varepsilon_f \rho_f \vec{u}_f) + \nabla \cdot (\varepsilon_f \rho_f \vec{u}_f \otimes \vec{u}_f) = -\varepsilon_f \nabla p + \nabla \cdot \bar{\bar{\tau}}_f + \varepsilon_f \rho_f \vec{g} + K_{sf}\left(\vec{u}_s - \vec{u}_f\right) + \vec{F}_f \tag{5.2}$$

Momentum equation for the solid phase is given by

$$\frac{\partial}{\partial t}(\varepsilon_s \rho_s \vec{u}_s) + \nabla \cdot (\varepsilon_s \rho_s \vec{u}_s \otimes \vec{u}_s) = -\varepsilon_s \nabla p - \nabla p_s + \nabla \cdot \bar{\bar{\tau}}_s + \varepsilon_s \rho_s \vec{g} + K_{sf}\left(\vec{u}_f - \vec{u}_s\right) + \vec{F}_s \tag{5.3}$$

Total volume fraction conservation

$$\varepsilon_s + \varepsilon_f = 1 \tag{5.4}$$

Equation (5.1) represents the mass balance of each phase with temporal and spatial gradients on the left hand side and mass creation ($\dot{m}$) of the p_{th} species (in this case, zero) by reaction or phase change. Equations (5.2) and (5.3) are momentum conservation equations for the fluid (air in this case) and solid phase, respectively. The left side represents temporal and spatial transport terms whereas the right hand side has terms for the various interaction forces involved. Note that the hydrodynamic pressure is shared by both phases and hence, the gradient of pressure (p) is multiplied by the respective volume fractions (ε) in both equations. (ρ), ($\vec{u}$) and ($\vec{g}$) represent to density, velocity and acceleration due to gravity, respectively. The stress term (τ_f) represents the shear stress in gas phase in eq. (5.2). Equation (5.3) represents the solids phase equation, where (τ_s) represents the shear stress term due to collision among particles.

Terms $K_{sf}\left(\overrightarrow{u_f}-\overrightarrow{u_s}\right)$ and $K_{sf}\left(\overrightarrow{u_s}-\overrightarrow{u_f}\right)$

represent the momentum exchange or drag between the two phases in eqs. (5.2) and (5.3), respectively. These terms are equal in magnitude and opposite in sign and account for the friction at the interface between the phases. The terms ($\overline{F_f}$) in eq. (5.2) and ($\overline{F_s}$) in eq. (5.3) represent all other forces that may affect the flow, such as electrical, magnetic and other effects.

$$
\begin{aligned}
&For \\
&\varepsilon_g > 0.8, \\
&K_{s,f} = \frac{3\varepsilon_s \varepsilon_g \rho_g}{4 d_s} C_{d,s}\left(\varepsilon_g^{-2.65}\right)\left|\overline{u_s}-\overline{u_g}\right| \\
&C_{d,s} = \frac{24}{\varepsilon_g.\mathrm{Re}_s}.[1+0.15.(\varepsilon_g.\mathrm{Re}_s)^{0.687}] \\
&For \\
&\varepsilon_g \le 0.8, \\
&K_{s,f} = 150.\frac{\varepsilon_s^{\,2}.\mu_g}{\varepsilon_g.d_s^{\,2}} + 1.75.\frac{\varepsilon_s.\rho_g}{d_s}.\left|\overline{u_s}-\overline{u_g}\right|
\end{aligned}
\qquad (5.5)
$$

The drag is an effective way of representing the surface integral of all the forces that exist at the interface between the phases. Inter-phase momentum exchange factor of Gidaspow's drag closure as presented in eq. (5.5). In eq. (5.5), Re_s and d_s are the Reynolds number and diameter of the solid particles, respectively and other symbols have their standard meaning. Energy equation (5.6) was applied during 3D heat transfer simulations for heater section.

TH-1848_Shankarrao

$$\frac{\partial}{\partial t}(\rho E)+\nabla.(\vec{u}(\rho E+p))=\nabla.(k_{eff}\nabla T-\sum_{j}h_j j_j+(\bar{\bar{\tau}}_{eff}.\vec{u}))+S_{hj} \quad (5.6)$$

where k_{eff} is the effective conductivity and j_j is the diffusion flux of species *j*.

The four terms of the right hand side in eq. (5.6) represents energy transfer due to conduction, species diffusion, viscous dissipation and volumetric heat sources (S_{hj}). Now, heat transfer simulations (by enabling energy equation) for the heater section were carried using to obtain the (bulk mean) bed temperature (T_B) and wall temperature (T_S), for a constant heat flux q" = 1000 (W/m^2) applied at the walls of heater. Local convective heat transfer coefficient (h) was calculated by using eq. (3.5).

5.3 Grid Independence Test

Grid independence test has been performed on the CFB riser of cross section 0.15 m × 0.15 cm and 2.85 m in height. Heater section of 0.6 m height and placed 0.6 m above the distributor plate represents the lower splash region as shown in Figs. 5.1 and 5.2. Modelling and meshing has been done in the Gambit software. Size function option was used with start size (spacing near to the wall) 0.006 – growth factor 1.2 – maximum size limit 0.02. Hexahedral cells near to wall and tetrahedral cells in the core region of riser were used for the meshing. Heat flux of 1000 W/m^2 has been applied to the wall of heater section only and grid independence test have been preformed 125608, 230982, 438866 cells. Remaining boundary conditions were air velocity at inlet of riser 2.5 m/s and pressure outlet – 0 Pa and speed of sand at return leg – 0.00468 m/s. Initial inventory of sand on the distributor plate was 7 kg with sand particle size of 460 μm. Remaining details were as explained in section 5.2. Grid independence test shows (Fig. 5.3) that the meshes with 230982 and 438866 cells give results close to the experimental values, and the difference between them is acceptable, while the mesh with 125608 cells differs significantly from the experimental values. The time required to obtain the results using 438866 cells will be approximately twice the time required for simulating the 230982 cells on computer facility (server for Fluent simulation) with 3 GHz processor, 4 GB ram and 4 hardisks each of 146 GB capacity. Therefore on the basis of time required to simulate and to get reasonable accuracy of results, 230982 cells were used to simulate the CFB riser of 0.15 m × 0.15 m and 2.85 m in height. Figure 5.3 represents the axial distribution of local heat transfer coefficient along the height of the heater.

TH-1848_Shankarrao

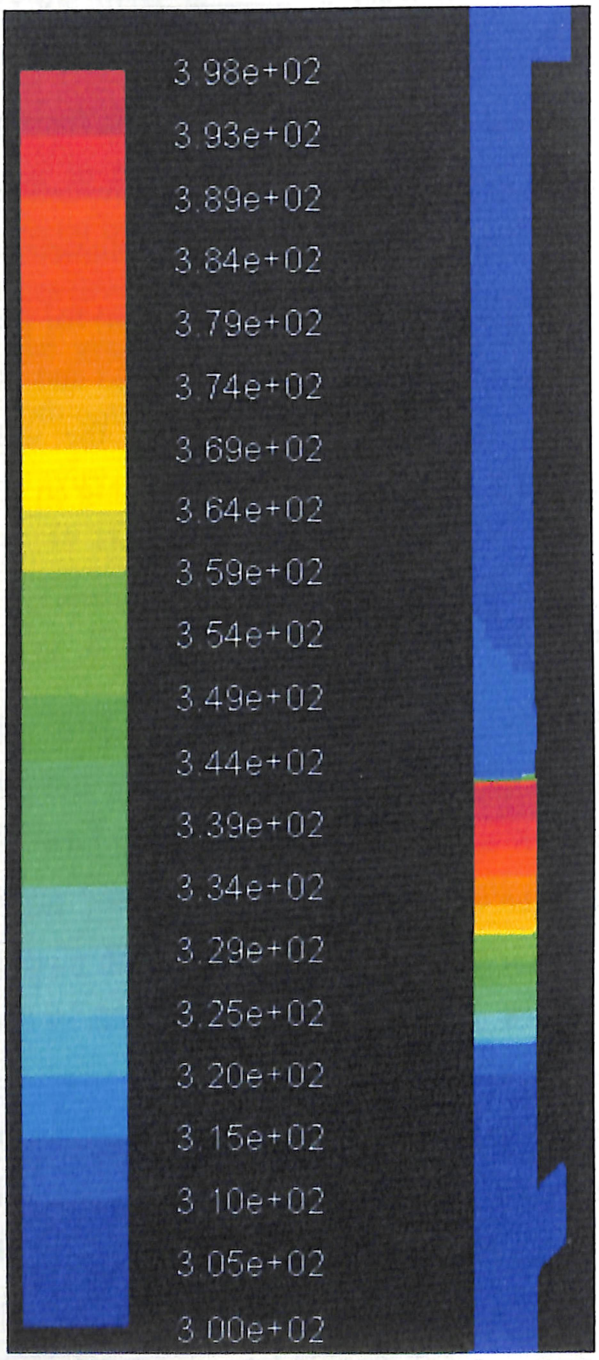

Fig. 5.2 Temperature (K) Contour for 0.15 m × 0.15 m CFB Riser at U = 2.5 m/s, P = 3050 N/m^2

TH-1848_Shankarrao

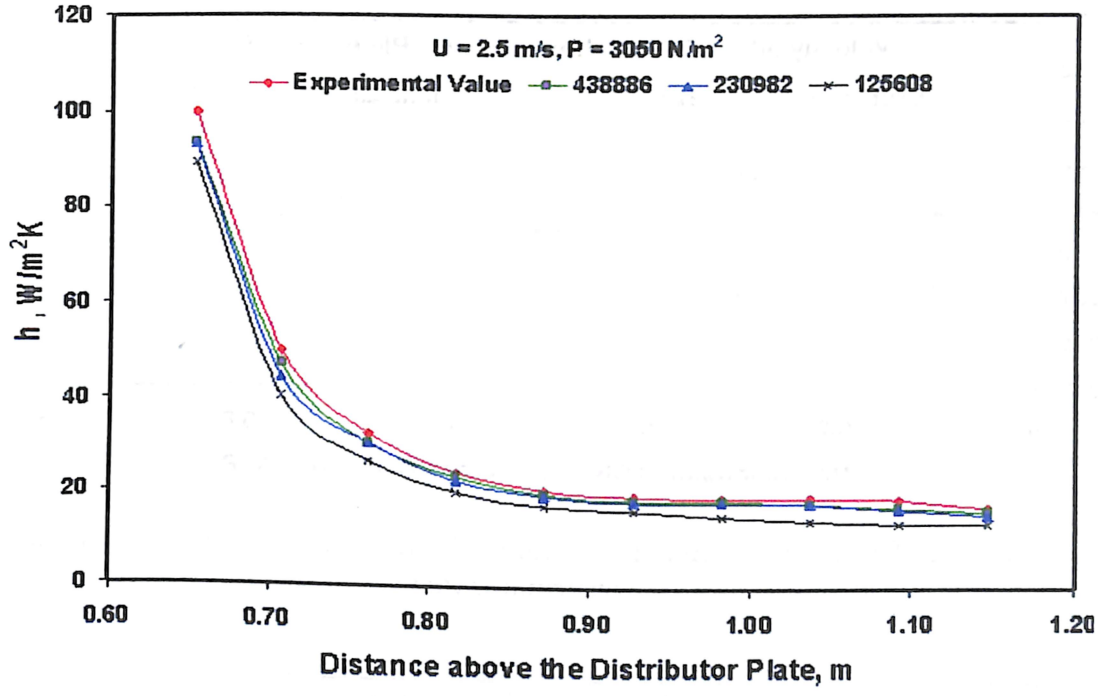

Fig. 5.3 Grid Independence Test

5.4 Effect of Velocity on Heat Transfer Characteristics

Effect of superficial velocities of air on heat transfer characteristics is presented in Figs. 5.4-5.6. Results were compared with available experimental data. Simulations were done

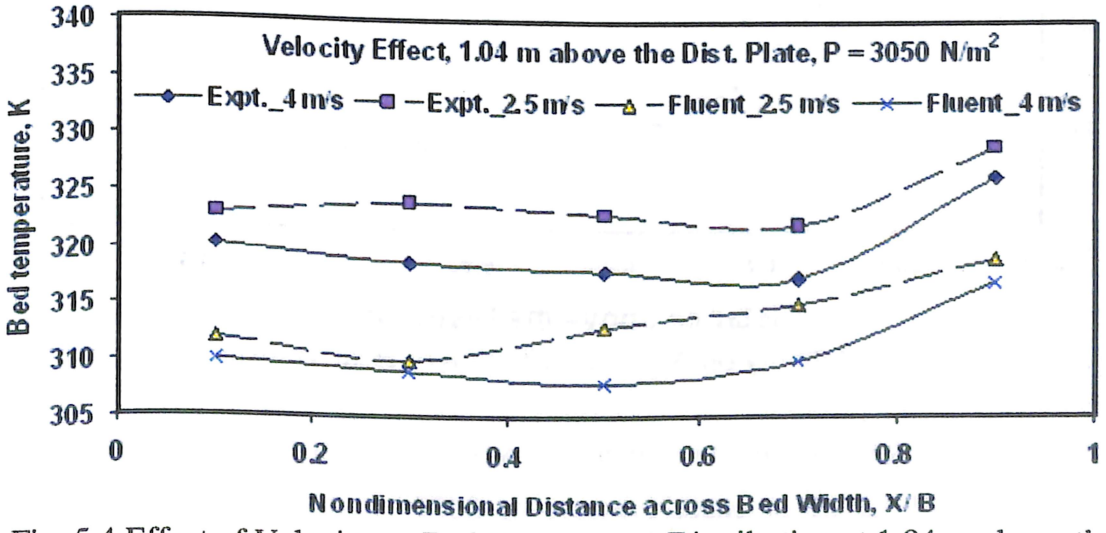

Fig. 5.4 Effect of Velocity on Bed Temperature Distribution at 1.04 m above the Distributor Plate

TH-1848_Shankarrao

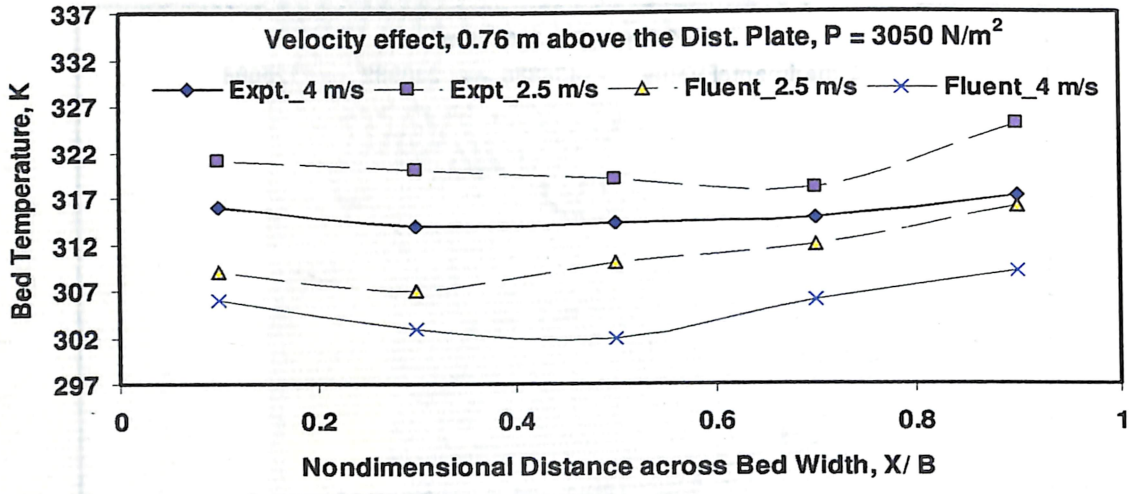

Fig. 5.5 Effect of Velocity on Bed Temperature Distribution at 0.76 m above the Distributor Plate

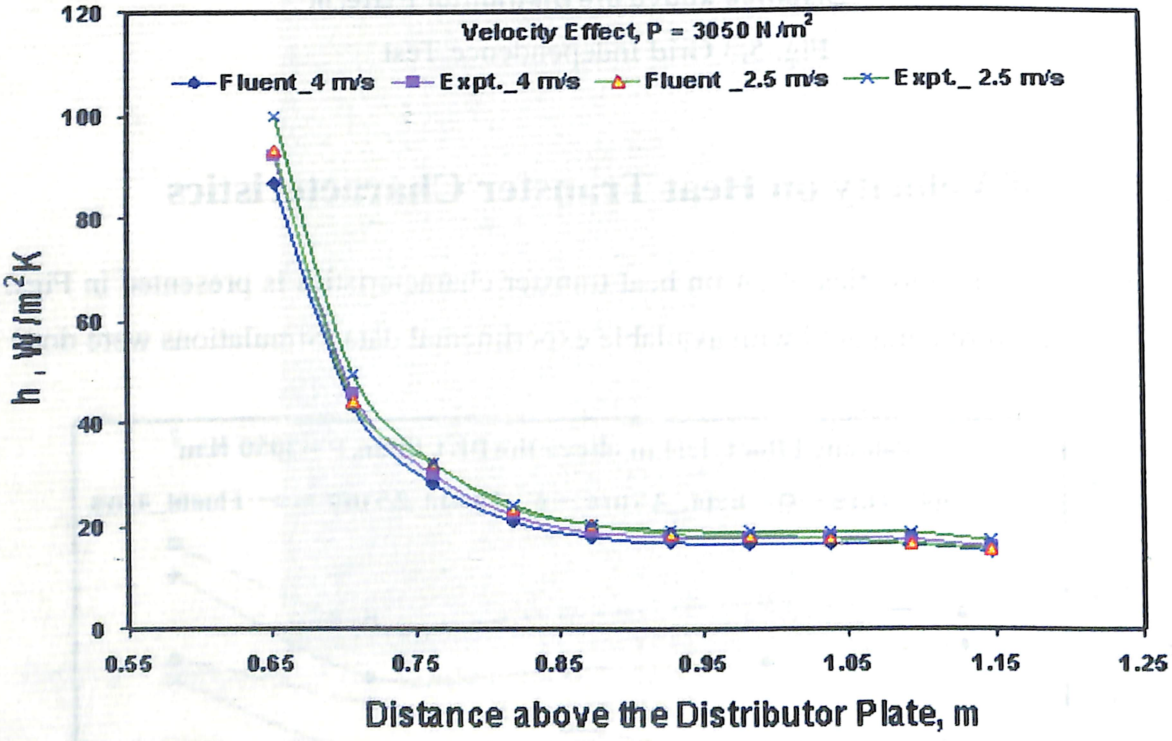

Fig. 5.6 Effect of Velocity on Axial Distribution of Heat Transfer Coefficient

in the lower splash region for the two superficial velocities of air – 2.5 m/s and 4 m/s at sand inventory of 7 kg i.e at static pressure of 3050 N/m^2 due to weight of sand inventory per unit area of distributor plate. Temperature counters is presented in Fig. 5.2. Remaining details are mentioned in sections 5.2 and 5.3. Sand velocity at inlet at right hand side wall of riser was 0.00468 m/s and 0.0075 m/s at U* = 5 and U* = 8 for CFB unit B1 and CFB unit of cross section 0.30 m × 0.30 m. It is observed that bed temperature and heat transfer coefficient decreases with increase in superficial velocity

TH-1848_Shankarrao

of air. This is because as explained in section 4.3, sand concentration decreases across the section of the riser column and also near the wall of the heater with increase in superficial velocity of air which reduces the heat transfer from wall-to-bed due to conduction. Therefore bed temperature decreases with increase in superficial velocity of air, which results in increase in the driving temperature difference ($T_S - T_B$) and decrease in heat transfer coefficient, while the heat flux was held constant. The percentage difference between predicted values and experimental values was varying from 2% to 18% for bed temperature distribution and hence also for axial distribution of heat transfer coefficient, because heat flux was held same (eq. 3.5).

5.5 Effect of Particle Size on Heat Transfer Characteristics

Effect of particle size on heat transfer characteristics has been completed for the Geldart *B* type of the particles. The experiments have been completed on the available CFB set-up B1 using particles of average size of 460 μm. Fluent provides more flexibility to complete this study for other particle average sizes of 60 μm, 100 μm, 160 μm, 260 μm, 360 μm, and 460 μm. Eulerian multiphase model with Gidaspow phase interaction scheme have been used to simulate the two phase flow. Simulations were performed

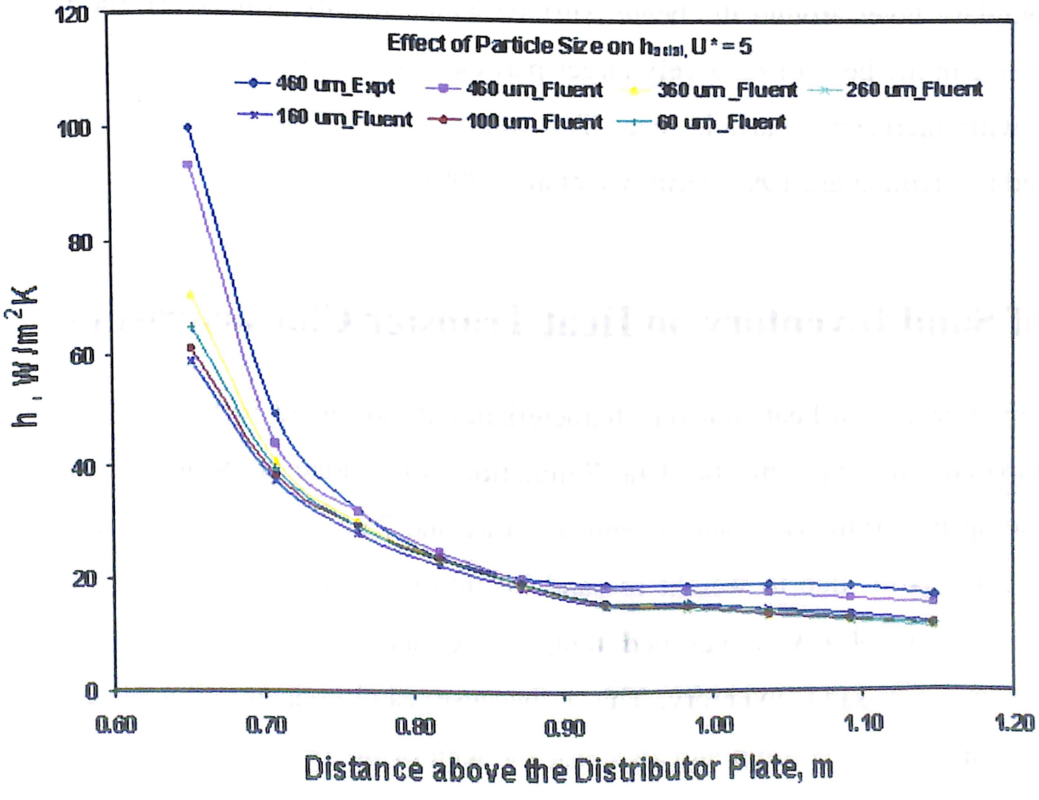

Fig. 5.7 Effect of Sand Particle Size on Axial Distribution of Local Heat Transfer Coefficient

TH-1848_Shankarrao

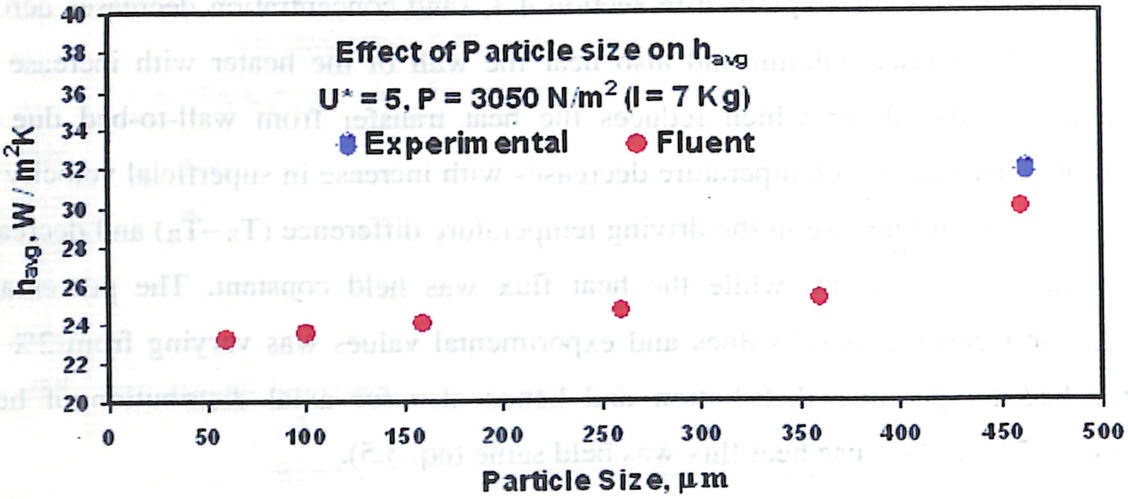

Fig. 5.8 Effect of Sand Particle Size on Average Value of Heat Transfer Coefficient

using 2.5 m/s superficial velocity of air and selected initial bed inventory above the distributor plate was 7 kg. Walls of the heater placed 0.6 m above the distributor plate section was kept with constant heat flux of 1000 W/m^2; it has been observed that heat transfer coefficient increases with increase in particle size as shown in Figs. 5.7-5.8. Figure 5.7 shows axial distribution of local heat transfer coefficient and under similar operating conditions, Fig. 5.8 represents variation of average value of heat transfer coefficient against various particle sizes. The physics or reason behind this was effective erosion of boundary layer around the heater surface which results in decrease the heat transfer resistance in the beds of relatively larger particles, with a consequent increase in heat transfer with increasing particle size. The trends obtained were comparable to results reported by (Kim et al., 1999; Grulovic et al., 2008).

5.6 Effect of Sand Inventory on Heat Transfer Characteristics

Effect of sand inventories on heat transfer characteristics is presented in Figs. 5.9-5.10. Results are compared with experimental data. Simulations were done in the lower splash region of CFB setup B1 for the two sand inventories 4 kg and 7 kg i.e at static pressure of 1750 N/m^2 and 3050 N/m^2 due to weight of sand inventory per unit area of distributor plate, respectively. It is observed that bed temperature and heat transfer coefficient increases with increase in sand inventory. This is because, sand concentration increases across the section of the riser column and also near the wall of the heater with increase in sand inventory which increases the heat transfer from wall-to-bed due to conduction.

TH-1848_Shankarrao

Therefore bed temperature increases with increase in sand inventory, which results in decrease in the driving temperature difference ($T_S - T_B$) and hence increase in heat transfer coefficient, while the heat flux was held constant.

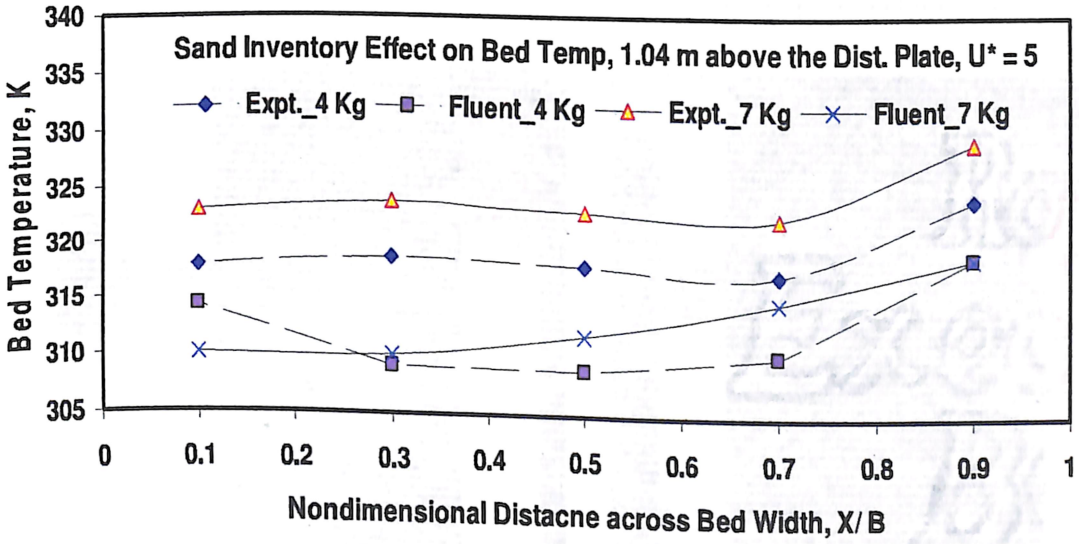

Fig. 5.9 Effect of Sand Inventory on Bed Temperature Distribution at 1.04 m above the Distributor Plate

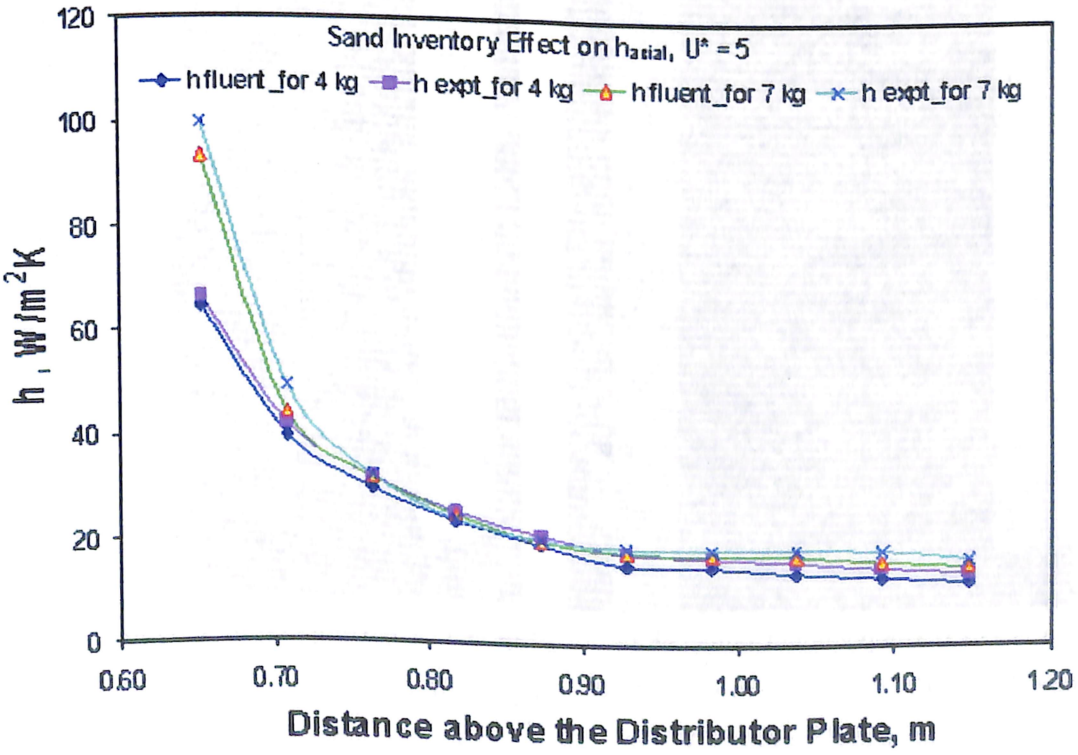

Fig. 5.10 Effect of Sand Inventory on Axial Distribution of Heat Transfer Coefficient

TH-1848_Shankarrao

5.7 Effect of Bed Cross Section on Heat Transfer Characteristics

Effect of bed cross section on heat transfer characteristics has been investigated. Riser of bed cross section 0.30 m × 0.30 m has been modelled and simulated using Fluent 6.3.26. Results obtained on bed temperature distribution and heat transfer coefficient have

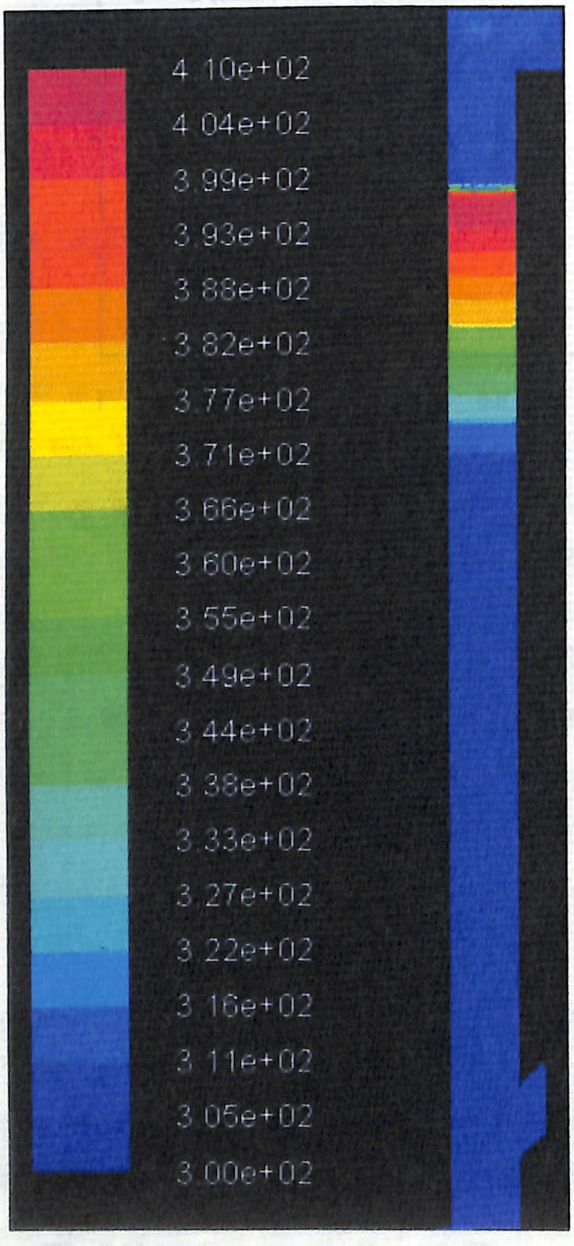

Fig. 5.11 (a) Temperature Counter (K) – Upper Splash Region of 0.15 m × 0.15 m at U = 4 m/s and P = 3050 N/m^2

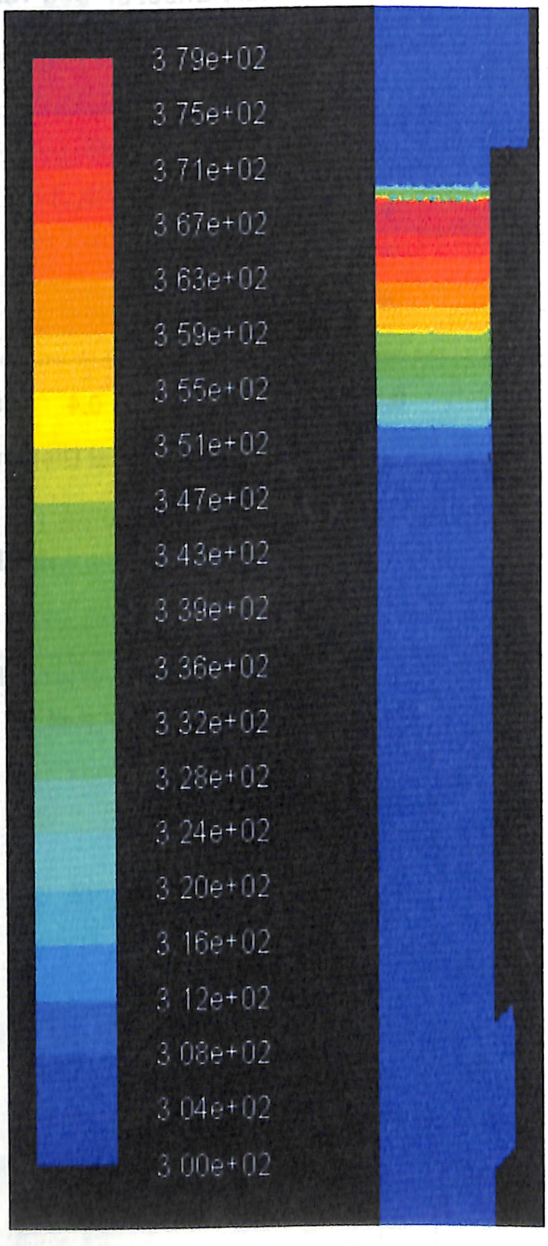

Fig. 5.11 (b) Temperature Counter (K) – Upper Splash Region of 0.30 m × 0.30 m at U = 4 m/s and P = 3050 N/m^2

TH-1848_Shankarrao

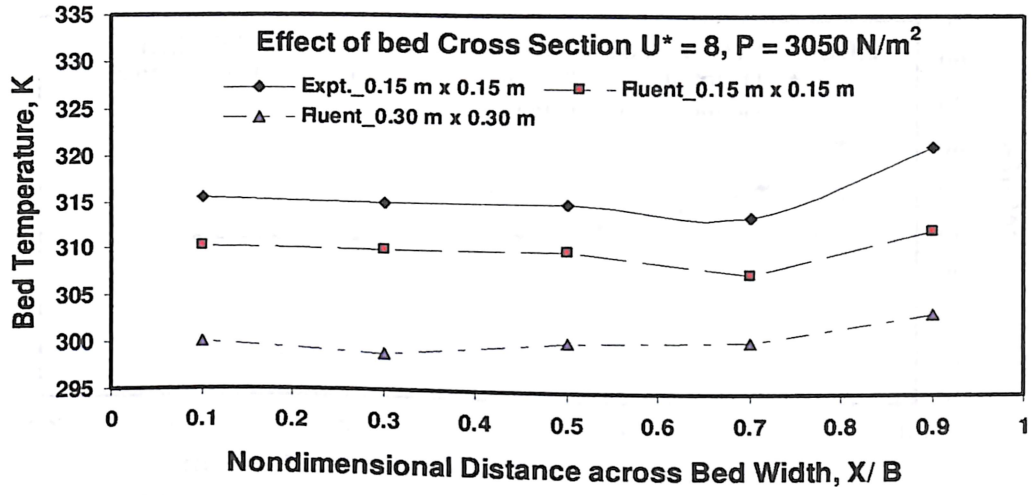

Fig. 5.12 Effect of Bed Cross Section on Bed Temperature Distribution at a Section 2.24 m above the Distributor Plate at U* = 8, P = 3050 N/m^2

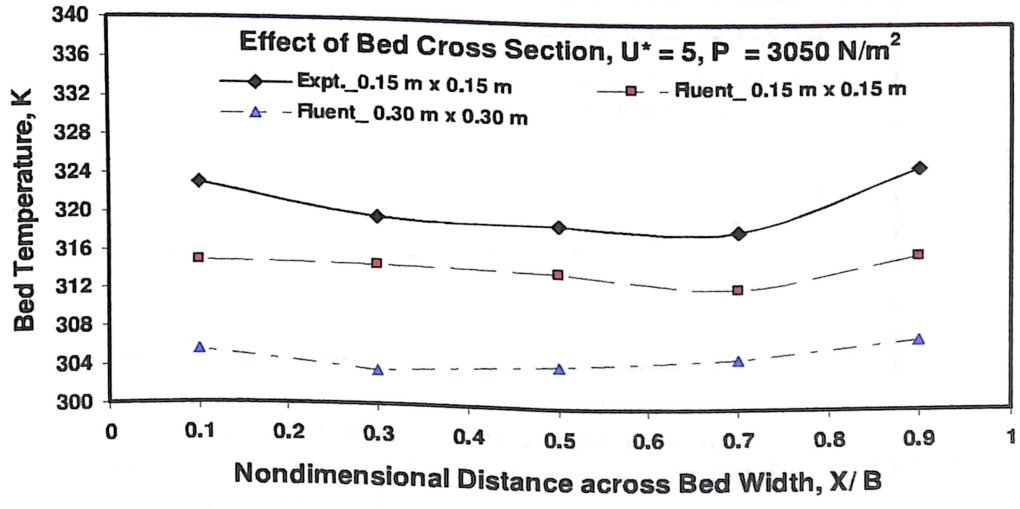

Fig. 5.13 Effect of Bed Cross Section on Bed Temperature Distribution at a Section 2.24 m above the Distributor Plate at U* = 5, P = 3050 N/m^2

been compared with results obtained 0.15 m × 0.15 m CFB bed. Simulations have been completed for the upper splash region for both the beds with superficial velocity 2.5 m/s and 4 m/s, and maintaining the pressure 3050 N/m^2 due to weight of sand inventory per unit area of the distributor plate. Eulerian multiphase model with Gidaspow phase interaction scheme was used to simulate the two phase flow. Particle size used was 460 μm and heat flux of 1000 W/m^2 was applied at the walls of heater. Remaining details are mentioned in sections 5.2 and 5.3. Sand velocity at inlet at right hand side wall of riser was 0.00468 m/s and 0.0075 m/s at U* = 5 and U* = 8 for CFB unit B1 and CFB unit of cross section 0.30 m × 0.30 m. Temperature counters are presented in Fig. 5.11 at

TH-1848_Shankarrao

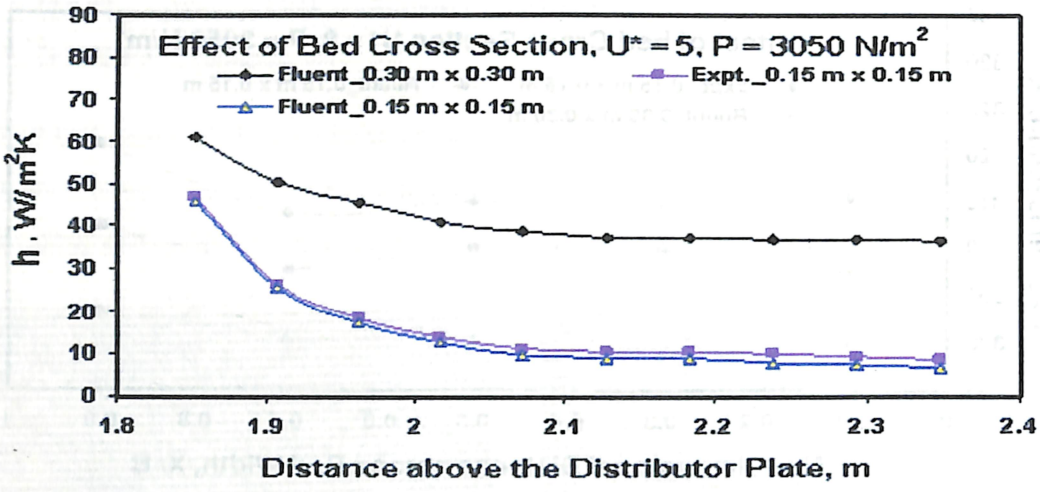

Fig. 5.14 Effect of Bed Cross Section on Axial Distribution of Local Heat Transfer Coefficient at U* = 5, P = 3050 N/m^2

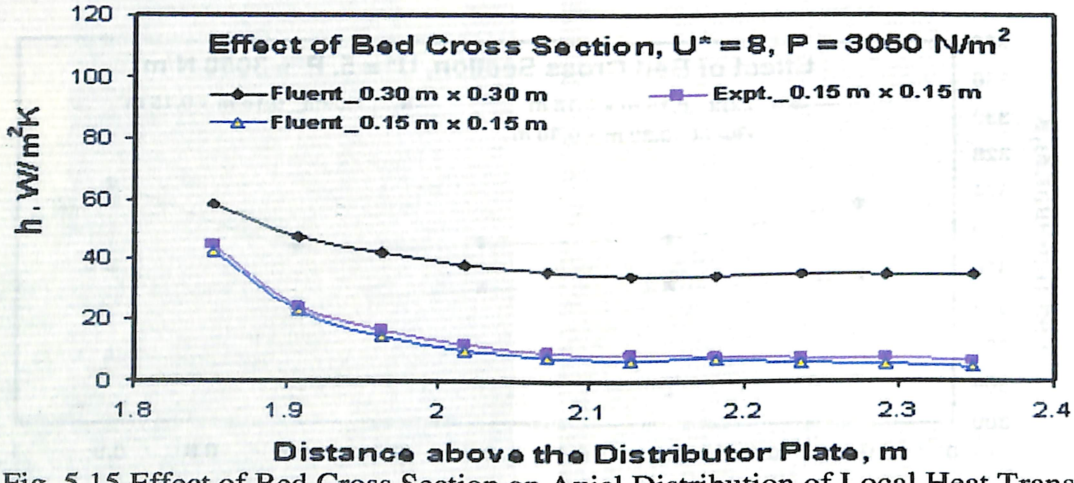

Fig. 5.15 Effect of Bed Cross Section on Axial Distribution of Local Heat Transfer Coefficient at U* = 8, P = 3050 N/m^2

operating conditions of U* = 8 and P = 3050 N/m^2. Figures 5.12-5.13 and Figs. 5.14-5.15 represent the bed temperature distribution across a bed cross section at 2.24 m above the distributor plate and axial variation of local heat transfer coefficient, respectively. Average bed temperature at lateral section at 2.24 m above the distributor plate was more in smaller cross section heater than larger cross section heater. This is expected because sand inventory in larger cross section CFB setup was kept proportionately more than the smaller size CFB setup so as to maintain the same weight of sand per unit area of the distributor plate. Therefore, weight of sand particles per unit surface area of the larger cross section heater was more than the smaller heater. Therefore at same heat flux applied at heater wall of each CFB setup, distribution of

TH-1848_Shankarrao

amount heat extracted due to conduction from wall of the heater took place into large number particles, which were comparatively more in larger cross section CFB setup, hence average bed temperature was less for lager size heater than smaller heater. It is observed that in the wall-to-bed heat transfer study, heat transfer coefficient increases with increase in bed size. This is because the driving temperature difference ($T_S - T_B$) in the larger size bed was lesser than the smaller size beds, while the heat flux was held fixed. This is because of the higher concentration of solid particles near the wall of the larger bed, and consequently, lower thermal resistance from the bed-to-wall causing better heat conduction.

5.8 Summary

In the present study, simulations using Fluent 6.3.26 were completed to study the effect of parameters like superficial velocity of air, sand inventory, sand particle size, and bed cross section on wall-to-bed heat transfer characteristics. Simulations were completed under same operating conditions, those used while conducting the experiments on available CFB setups. Results obtained were compared with available experimental data. After validation of results, further simulations were completed to study the effect of particle sizes (60 μm - 360 μm) and bed cross section of 0.30 m × 0.30 m. It is observed that bed temperature increases with increase in sand inventory and decreases with increase in superficial velocity of air and bed cross section. Local heat transfer coefficient decreases with increase in superficial velocity of air. It increases with increase in sand inventory, particle size and bed cross section.

TH-1848_Shankarrao

Chapter 6

Experimental Investigations on Cyclone Separators

TH-1848_Shankarrao

Chapter 6

Experimental Investigations on Cyclone Separators

6.1 Introduction

In the present chapter, study has been completed on heat transfer behavior in the cyclone separators of different cross sections of three different cold Circulating Fluidized Beds (CFBs). Steady state experiments were carried out by providing heat in the riser of a CFB and consequently examining bed-to-wall heat transfer in the cyclone separator. To study the effect of scale-up (increase in barrel diameter of cyclones) on heat transfer characteristics, experiments were conducted under similar operating conditions on three CFB setups. Cyclone design ratios i.e ratios of various dimensions of cyclone with respect to cyclone barrel diameter were maintained same for each cyclone separator. Experiments were conducted on each CFB setup for same value of five non-dimensional air velocities (U^* = 5, 5.5, 6, 6.6, and 8) at two different weights of sand inventory per unit area of the distributor plate (i.e. P = 1750 N/m^2 and 3050 N/m^2). Average sand particle size was 460 μm for all the set of the experiments. Effect of parameters such as superficial velocity of air and sand inventory on heat transfer characteristics was predicted for individual cyclone separator. Local heat transfer coefficient along the height of cylindrical portion of cyclone separators were evaluated and compared. Also, temperature across the barrel diameter of all cyclone separators were measured and compared. Empirical correlation was developed. Prediction of this correlation was in agreement (± 14.31%) with experimental data.

6.2 Temperature Distribution

Figure 6.1 presents the effect of cyclone barrel diameter (D_C) on temperature distribution across a section located at non-dimensional distance 0.1 below the inlet of

TH-1848_Shankarrao

each cyclone separator of the different CFBs for the operating conditions: weight of sand per unit area of distributor plate (P) = 3050 N/m^2, heat flux at the wall of the heater placed in the riser column of each CFB setup = 1000 W/m^2, non-dimensional velocity parameter (U*) = 5, particle size (d_p) = 460 μm. Figure 6.1 presents that temperature across the section was less for larger size cyclone separator (C3) compare to smaller size cyclone separator (C1). This is because of bed temperature across the heater section located in the CFB riser was less for larger size heater than smaller size heater. This is expected because sand inventory in larger cross section CFB setup was kept proportionately more than the smaller size CFB setup so as to maintain the same weight of sand per unit area of the distributor plate. Therefore, weight of sand particles per unit surface area of the larger cross section heater was more than the smaller heater. Therefore at same heat flux applied at heater wall of each CFB setup, distribution of amount heat extracted due to conduction from wall of the heater took place into large number particles, which were comparatively more in lager cross section CFB setup, hence bed temperature was less for lager size heater than smaller heater. Later same sand + air mixture enters the cyclone separator after its exit from riser outlet of each CFB setup. Therefore bed temperature across the section was less for larger size cyclone (C3) than smaller size cyclone (C1).

Figure 6.1 may be compared with Fig. 6.2 to examine the effect of velocity on temperature distribution across the section of specific cyclone separator. It is observed that increase in non-dimensional velocity parameter (U*) from 5 to 8 resulted in decrease in temperature across the heater section of riser because, while the heat flux (hence the heat transfer rate) remains the same, the energy balance for the heated section implies less enthalpy gain for the fluid. Same sand + air mixture with specific temperature enters the cyclone separator after its exit from riser outlet. Therefore temperature across the section found to be decreased with increase in non-dimensional velocity parameter (U*) in each cyclone separator.

Figure 6.2 may be compared with Fig. 6.3 to examine the effect of sand inventory on temperature distribution across the section of specific cyclone separator. It is observed that temperature distribution across any heater section placed in the riser increases with increase in sand inventory from P = 1750 N/m^2 to P = 3050 N/m^2. This is because, while the heat flux (hence the heat transfer rate) remains the same, higher fraction of the energy is stored in the solids, which are recirculated in the bed.

TH-1848_Shankarrao

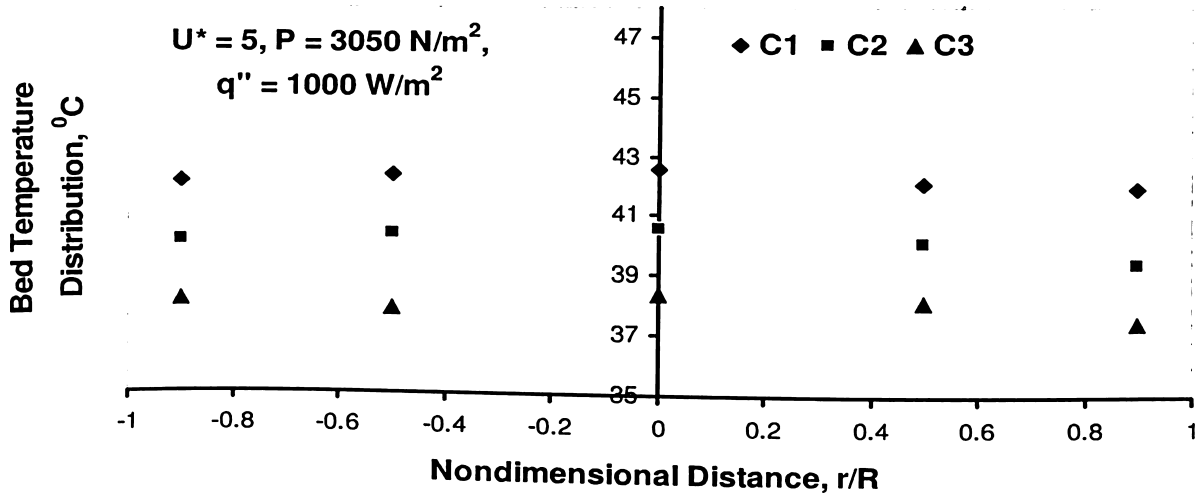

Fig. 6.1 Temperature Distribution at U* = 5, P = 3050 N/m^2

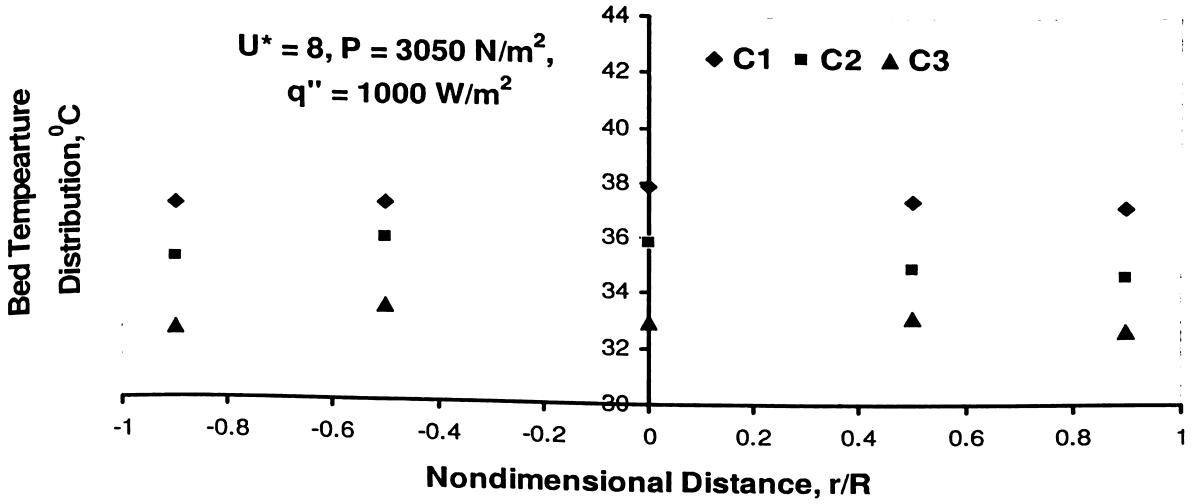

Fig. 6.2 Temperature Distribution at U* = 8, P = 3050 N/m^2

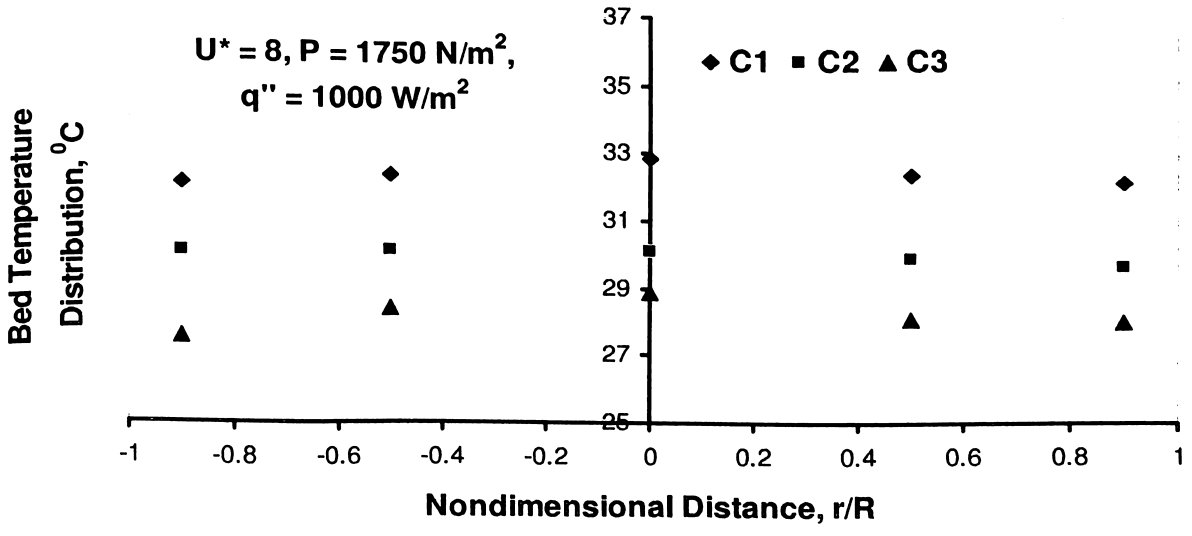

Fig. 6.3 Temperature Distribution at U* = 8, P = 1750 N/m^2

TH-1848_Shankarrao

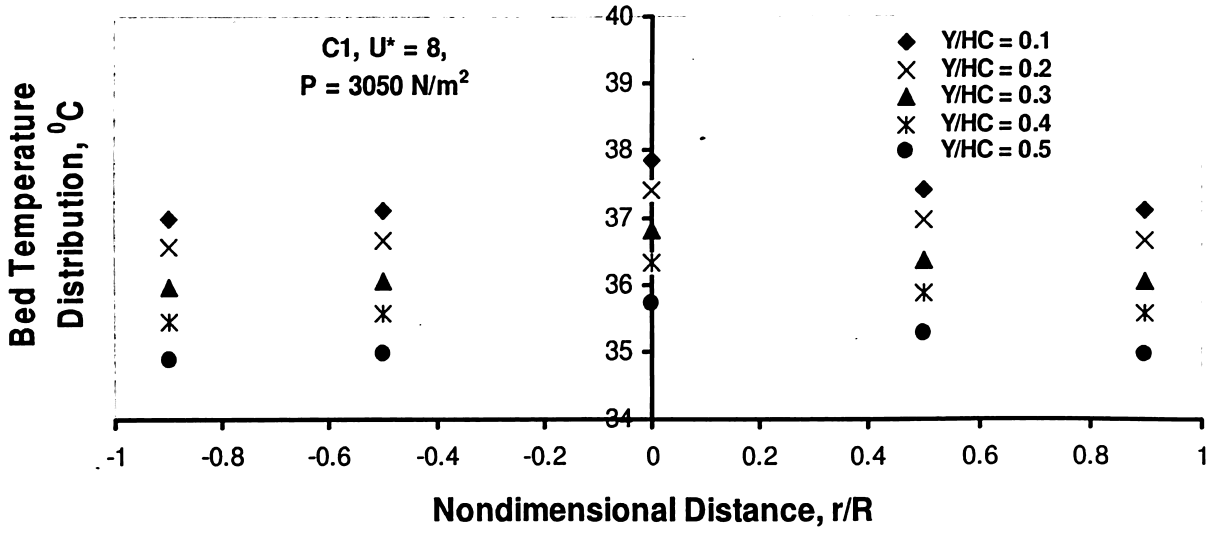

Fig. 6.4 Temperature Distribution in C1, at U* = 8, P = 3050 N/m^2

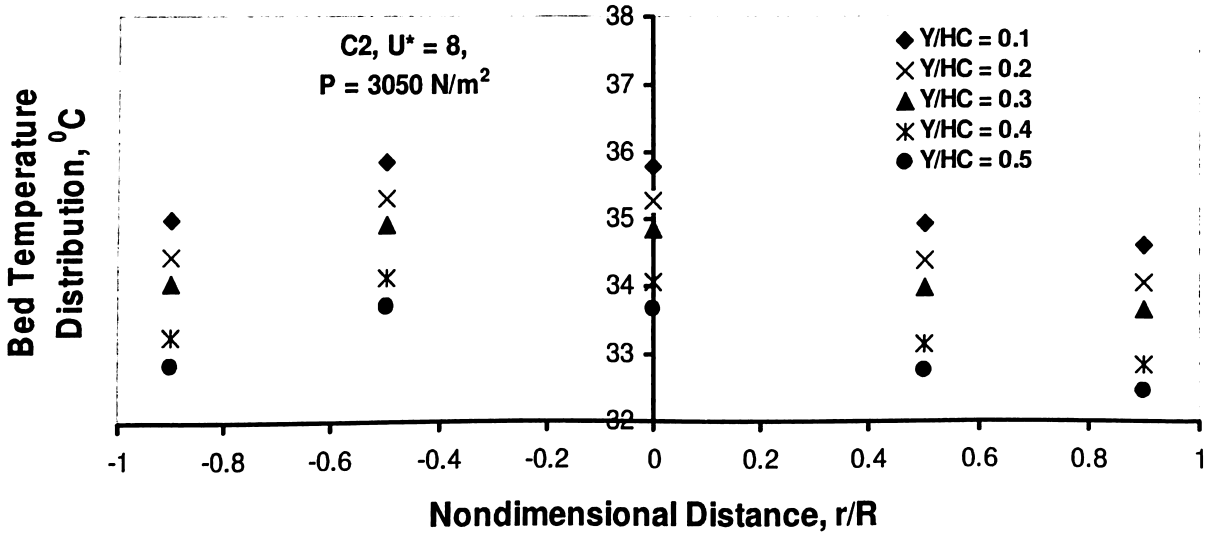

Fig. 6.5 Temperature Distribution in C2, at U* = 8, P = 3050 N/m^2

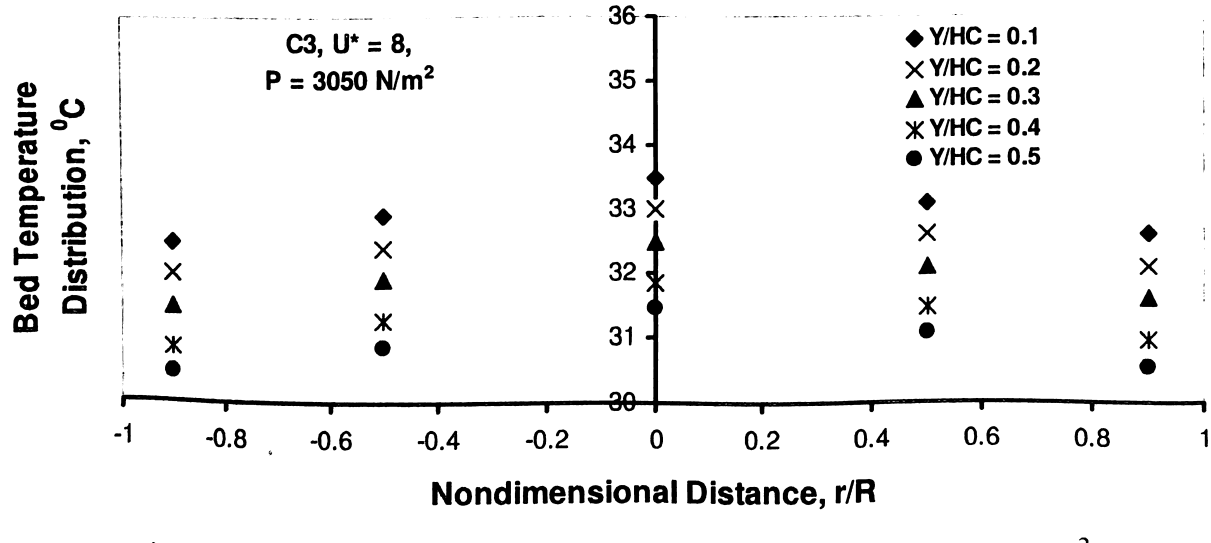

Fig. 6.6 Temperature Distribution in C3, at U* = 8, P = 3050 N/m^2

TH-1848_Shankarrao

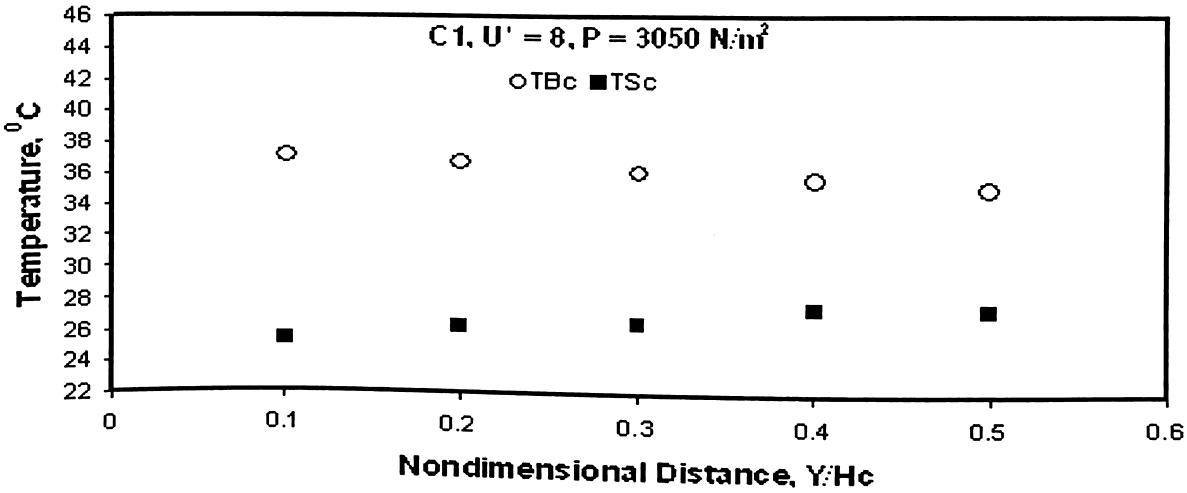

Fig. 6.7 Bulk Mean Bed Temperature Distribution and Wall temperature Distribution in C1, at U* = 8, P = 3050 N/m^2

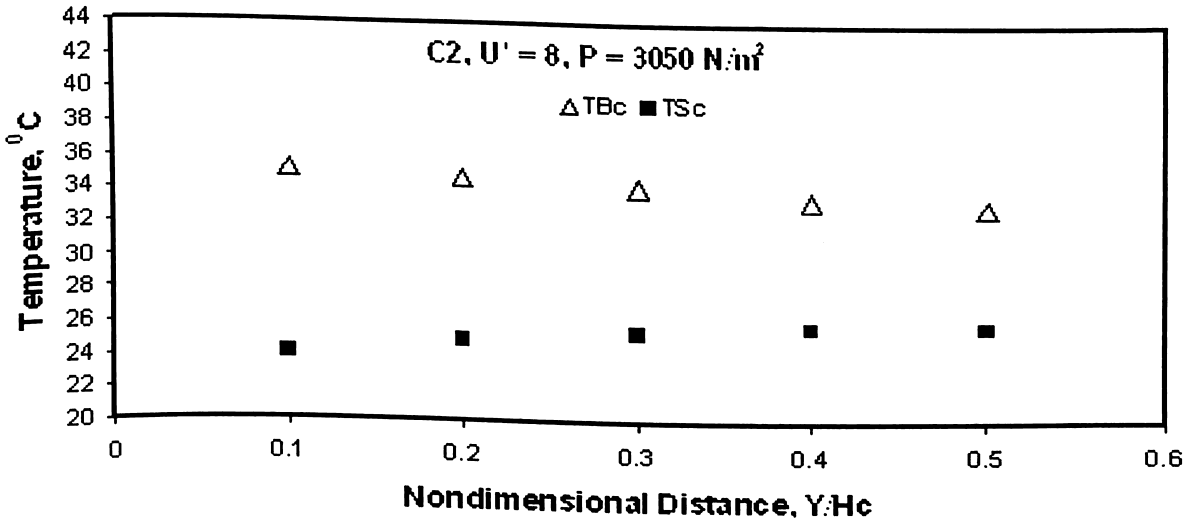

Fig. 6.8 Bulk Mean Bed Temperature Distribution and Wall temperature Distribution in C2, at U* = 8, P = 3050 N/m^2

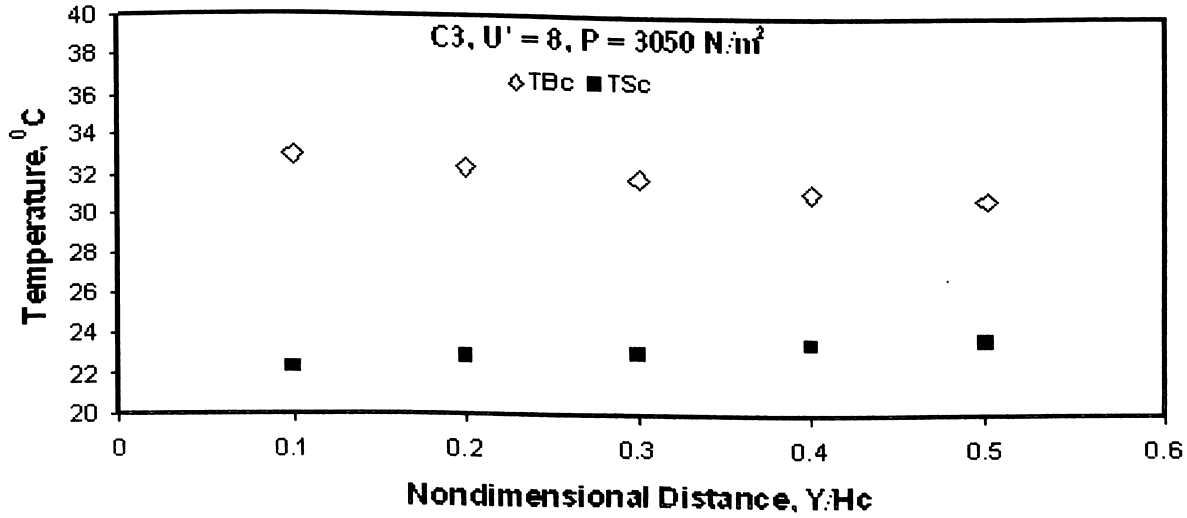

Fig. 6.9 Bulk Mean Bed Temperature Distribution and Wall temperature Distribution in C2, at U* = 8, P = 3050 N/m^2

TH-1848_Shankarrao

Therefore bed temperature found to increase in any cyclone separator with increase in sand inventory.

Figures 6.1-6.3 show the temperature was more at the core and less towards the wall of cyclone. This is because of the heat transfer from the cyclone wall to the surrounding air.

Figures 6.4-6.6 show the bed temperature distribution across the cyclone separator's cylindrical barrel (r/R varying from -1 to 1 as presented in Figs. 6.4-6.6) for the cyclone separators (C1, C2, and C3), respectively. These temperature values with respect to different non-dimensional distance (Y/H_C) of 0.1, 0.2, 0.3, 0.4, and 0.5 were used further to evaluate bulk mean temperature values as presented in Figs. 6.7-6.9. Figures 6.7-6.9 show the comparison of bulk mean temperature and wall temperature for the cyclone separators (C1, C2, and C3), respectively. For each cyclone separator, temperature distribution at a non-dimensional distance (Y/H_C) of 0.1, 0.2, 0.3, 0.4, and 0.5 is presented at the operating condition U* = 8, P = 3050 N/m^2. It may observe that for each cyclone separator, the bulk mean temperature decreases while local wall temperature increases with increase in non-dimensional distance Y/H_C. This is because, heat transfer from air + sand mixture to the wall of the cyclone separator resulted in decrease in temperature of air + sand mixture with increase in value of non-dimensional parameter (Y/H_C) from 0.1 to 0.5. The temperature values presented in the Figures 6.7-6.9 were used further to obtain the temperature difference (T_{Bc} - T_{Sc}) in eq. (3.7) and hence to obtain the local heat transfer coefficient values, for example, as presented in Fig. 6.11 in the following section 6.3.

6.3 Axial Distribution of Local Heat Transfer Coefficient

Figures 6.10-6.13 show the axial distribution of local heat transfer coefficient along the height of each cyclone separator when three CFB setups were operated at same operating conditions. Figure 6.10 shows the axial distribution of local heat transfer coefficient along the cyclone height when three CFB setups were operated at same operating conditions i.e at P = 3050 N/m^2, heat flux at the wall of the heater placed in the riser column = 1000 W/m^2, nondimensional velocity parameter (U*) = 5, particle size (d_p) = 460 μm. Local heat transfer coefficient for the larger cyclone separator

TH-1848_Shankarrao

(C3) was found to be more than other two smaller size cyclone separators (C2 and C3). This is because of driving temperature difference ($T_{Bc} - T_{Sc}$) was found to be lesser for the larger cyclone separator (C3) than cyclones separators (C1) and (C2). Also amount of heated sand particles suspended per unit surface area of cylindrical portion of larger cyclone separator were comparatively more, resulted in lower thermal resistance from the bed-to-wall causing better heat conduction. (Note: While conducting the experiments, pressure taps were provided on the wall of the cyclone separator at locations T7 and T11 as shown in Fig. 3.5. Using these pressure taps, pressure drop was obtained. Observed pressure drop in terms of (Δh) cm of water is used to calculate the voidage across the cyclone barrel diameter. Subsequently estimated voidage was used to calculate suspension density (solid holdup) of sand particles in the cylindrical portion of cyclone separator.)

Heat transfer coefficient value was less at the top of the any cyclone at the non-dimensional distance of 0.1 because the temperature difference between sand + air mixture and wall of the cyclone separator was more compare to respective temperature difference at the non-dimensional distance of 0.5, as shown in Figs. 6.10-6.13. This is because due to heat transfer from air + sand mixture to wall of cyclone separators, temperature of air + sand mixture decreases (as shown in Figs. 6.4 - 6.6) from inlet of the cyclone (at $Y/H_C = 0.1$) towards (at $Y/H_C = 0.5$) and therefore surface temperature of wall increases at respective value of Y/H_C.

Figure 6.10 may be compared with Fig. 6.11 to study the effect of velocity on the axial distribution of local heat transfer coefficient in any specific cyclone separator. Increase in fluidizing velocity reduces the wall-to-bed heat transfer in heater due to poor heat conduction caused because of decrease in sand particles hold-up near the wall of the heater and subsequently near the wall of the cyclone separator, which causes decrease in (air + sand) mixture-to-cyclone's wall heat transfer due to conduction in cyclone separator, hence value of heat local heat transfer coefficient decreases with increase in non-dimensional velocity parameter (U*).

Figure 6.10 may be compared with Fig. 6.12 to study the effect of sand inventory on the axial distribution of local heat transfer coefficient in any specific cyclone separator. Heat transfer coefficient increases with increase in sand inventory per unit area of distributor plate from $P = 1750$ N/m^2 to 3050 N/m^2. This is because, solid hold-up near the wall of the heater and subsequently near the wall of the cyclone separator, which causes increase in (air + sand) mixture-to-cyclone wall heat transfer

TH-1848_Shankarrao

due to conduction in cyclone separator, hence value of local heat transfer coefficient increases with increase sand inventory. Trends reported in the Figures 6.10-6.13 were similar to those reported in the literature (Gupta and Nag, 2000).

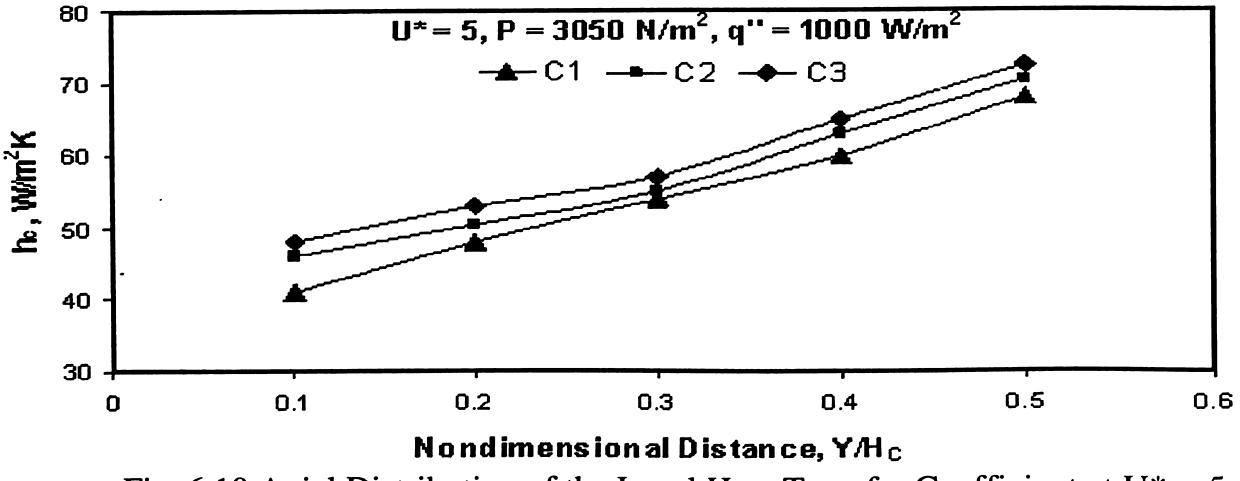

Fig. 6.10 Axial Distribution of the Local Heat Transfer Coefficient at U* = 5, P = 3050 N/m^2

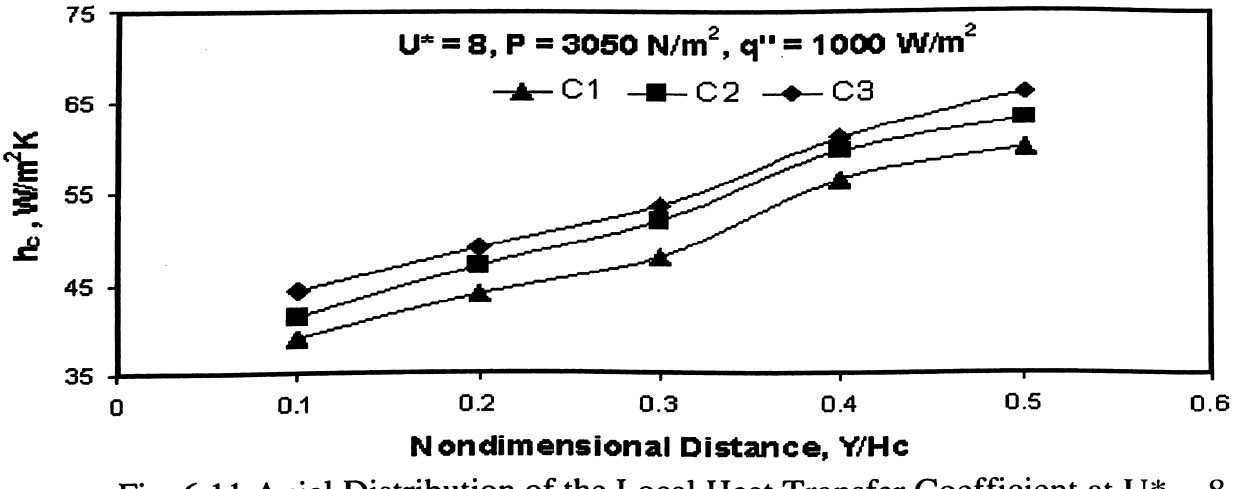

Fig. 6.11 Axial Distribution of the Local Heat Transfer Coefficient at U* = 8, P = 3050 N/m^2

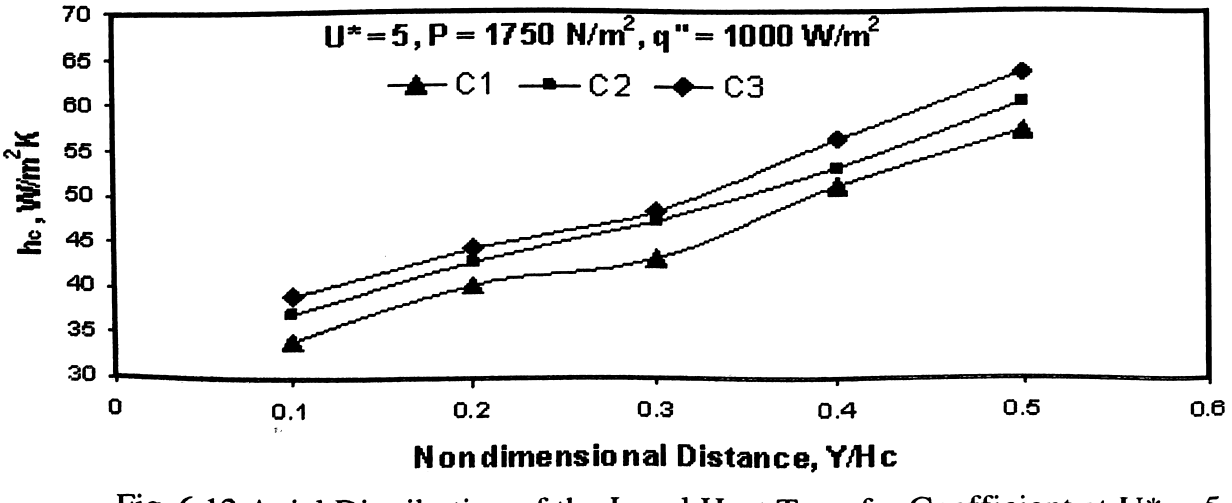

Fig. 6.12 Axial Distribution of the Local Heat Transfer Coefficient at U* = 5, P = 1750 N/m^2

TH-1848_Shankarrao

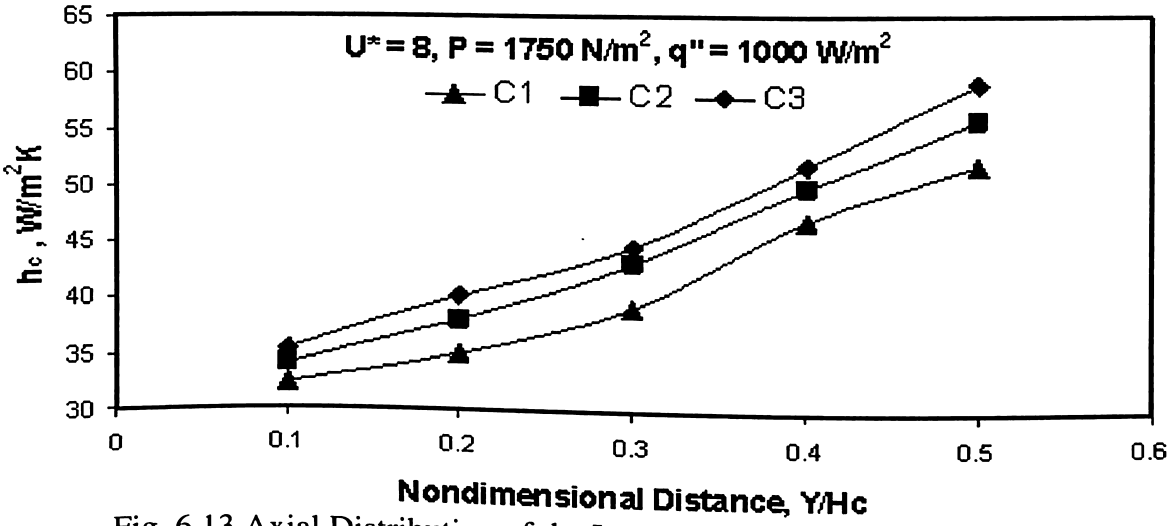

Fig. 6.13 Axial Distribution of the Local Heat Transfer Coefficient at U* = 8, P = 1750 N/m^2

6.4 Correlation

A dimensional analysis was made using Rayleigh's method and four non-dimensional numbers were obtained. Nusselt number and Reynolds number are the most important and widely used numbers. Also, two more non-dimensional numbers were obtained, non-dimensional density ratio [ρ_{sus}/ρ_g] (ratio of suspension density of sand particles to the density of gas i.e air) and non-dimensional geometrical parameter (Y/D_C) (ratio of the distance (Y) of the different thermocouples location with respect to T7-T11 as shown in Fig. 3.5, measured from the inlet of the cyclone, normalized with respect to barrel diameter of the cyclone separator). A best-fit equation involving these four non-dimensional numbers fitting experimental data were obtained with the help of FindFit function of Mathematica 5.2. The best-fit equation is as follows.

$$Nu_C = 5229.21[Re_C]^{-0.384}[\rho_{sus}/\rho_g]^{0.901}[Y/D_C]^{0.294} \qquad (6.1)$$

Correlation presented in eq. (6.1) is valid in the following range of experimental conditions: $15000 < Re_C < 42000$, $4 < (\rho_{sus}/\rho_g) < 18$, $0.2 < (Y/D_C) < 1$. The bed Nusselt number was in the range of 363.38 to 1350.00.

Figure 6.14 shows the comparison of the present experimental results with the prediction of the above correlation showing an rms deviation of ± 14.31%.

TH-1848_Shankarrao

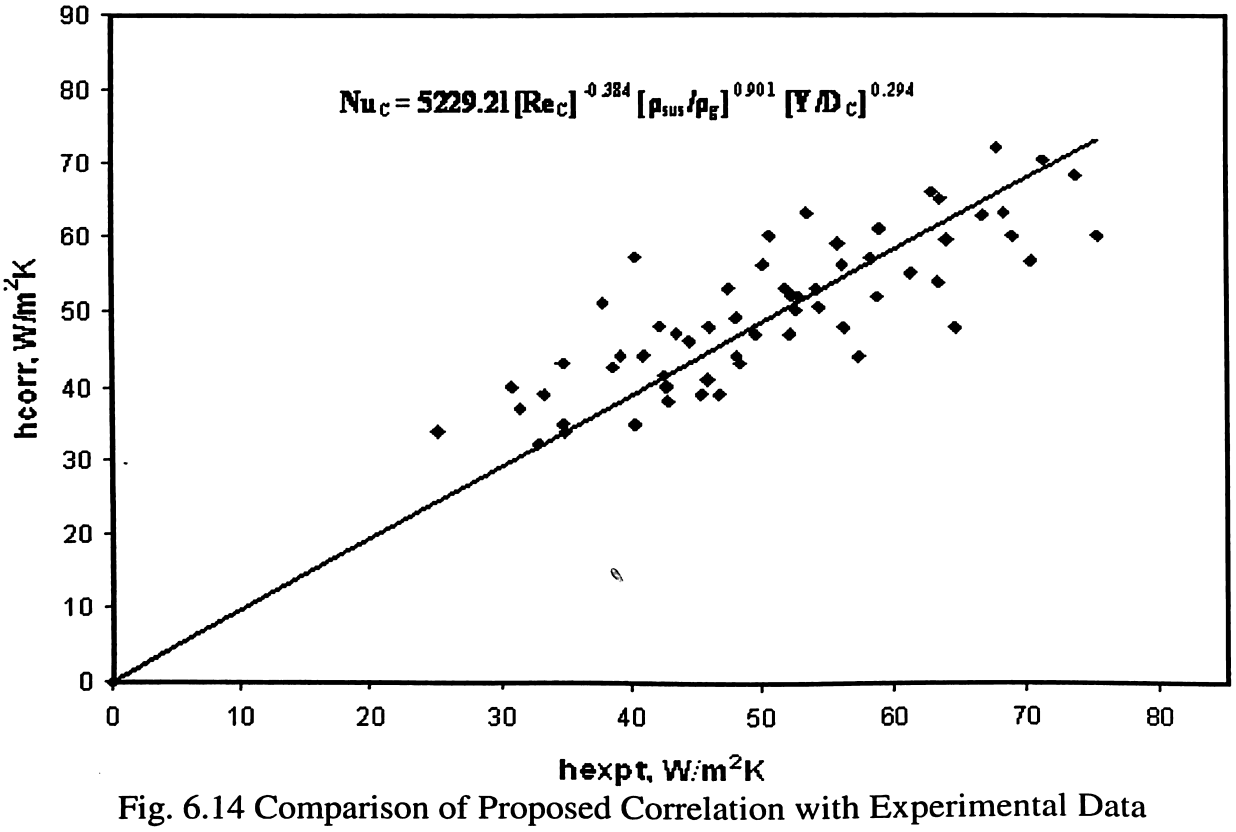

Fig. 6.14 Comparison of Proposed Correlation with Experimental Data

6.5 Summary

In the present study, effect of barrel diameter and other operating parameters on heat transfer characteristics was studied for cyclone separators of three different CFB setups. Experiments were conducted under similar operating conditions. Heat was supplied to the heater section placed in the riser column and consequently bed-to-wall heat transfer study was conducted in the cyclone separators. Present investigation is more realistic as far as the operation of CFB is concerned. Comparative studies were carried out to predict the effect of cyclone barrel diameters on heat transfer characteristics. Parametric study has been done to predict the effect of superficial velocity of air and sand inventory on distribution of temperature in the radial direction in individual cyclone separator and heat transfer coefficient along the height of each cyclone separator. In all the cyclone separators, it is observed that the temperature decreases with increase in size i.e increase in cyclone barrel diameter and superficial velocity of air. It increases with increase in sand inventory. Heat transfer coefficient increases with increase in size of the cyclone separator and inventory of sand. It decreases with increase in superficial velocity of air. Empirical correlation was developed to predict the Nusselt number.

TH-1848_Shankarrao

Chapter 7

Conclusions and Scope for Future Work

TH-1848_Shankarrao

Chapter 7

Conclusions and Scope for Future Work

7.1 Conclusions

Experimental and computational studies on heat transfer characteristics were accomplished on three circulating fluidized bed (CFB) risers and cyclone separators. Wall-to-bed as well as bed-to-wall heat transfer study has been completed on CFB risers and cyclone separators, respectively. Experiments were conducted under similar operating conditions on in-house fabricated CFB setups with height of 2.85 m and riser cross sections of 0.15 m × 0.15 m, 0.20 m × 0.20 m and 0.25 m × 0.25 m. Effect of superficial air velocity, sand inventory, and bed cross section, cyclone separators' barrel diameter on off-axial bed temperature distribution and axial distribution of local heat transfer coefficients have been predicted. Empirical correlations were developed to predict the heat transfer coefficient. Predicted heat transfer coefficients were compared with corresponding available experimental results. Computational study using Fluent 6.3.26 also has been conducted to study the effect particle size, bed cross section and other operating parameters like superficial velocity of air and sand inventory on heat transfer characteristics in CFB risers. Computational results were validated by comparing it with available experimental data.

A flow regime study was carried out on the CFB riser of cross section 0.15 m × 0.15 m. Effect of superficial velocity of air on variation of pressure drop and suspension density along the riser column was studied. In individual CFB riser, effect of superficial velocity (U* = 5, 5.5, 6, 6.6, 8) and sand inventory (P = 1750 N/m^2 and P = 3050 N/m^2) on distribution of bed temperature across the riser and heat transfer coefficient along the riser height was studied. In all the setups, it is observed that pressure drop and suspension density increases with increase in riser cross section area, decreases with increase in superficial velocity of the air in individual CFB riser. In all the setups, it is also observed that the bed temperature decreases with increase in

TH-1848_Shankarrao

cross section of the riser and superficial velocity of air in the riser column and increases with increases in sand inventory. Heat transfer coefficient increases with increase in cross section of the riser, sand inventory i.e suspension density and decreases with increase in superficial velocity of air.

Based on the experimental data, obtained from three CFB risers operated under similar operating conditions, empirical correlations were developed for lower splash region, middle splash region, and for entire riser height. A best-fit equation to predict bed Nusselt number involving different non-dimensional numbers fitting experimental data points were obtained with the help of FindFit function of Mathematica 5.2. Experimental results with the prediction of correlation showing rms deviation of ±15%, ±16% and ±22% for correlations obtained on lower splash region, middle splash region and entire riser, respectively. Hence this study will be more promising and helpful for design and fabrication of the new CFB risers.

CFD simulations on lower splash region of 0.15 m × 0.15 m CFB riser have been completed using Fluent 6.3.26. Effect of superficial velocity of air, sand inventory and particle size has been predicted and results obtained were compared with available experimental data. It is observed that bed temperature and heat transfer coefficient increases with increase in sand inventory and particle size. Bed temperature and heat transfer coefficient decreases with increase in superficial velocity of air. Further simulations on upper splash region of 0.15 m × 0.15 m and 0.30 m × 0.30 m CFB risers were done under similar operating conditions to predict the effect of bed cross section on heat transfer characteristics. Bed temperature decreases and heat transfer coefficient increases with increase in cross section area of risers. Results obtained from CFD simulations were validated by comparing with experimental data.

Effect of parameters such as superficial velocity of air and sand inventory on bed-to-wall heat transfer characteristics was also predicted for individual cyclone separator. Heat transfer coefficient along the height of cylindrical portion of cyclone separators were evaluated and compared under similar operating conditions. Also, bed temperature across the barrel diameter of all cyclone separators were measured and compared under similar operating conditions. In all the cyclone separators, it is observed that the bed temperature decreases with increase in size i.e increase in cyclone's barrel diameter, superficial velocity of air. It increases with increases in

TH-1848_Shankarrao

sand inventory. Heat transfer coefficient increases with increase in barrel diameter of cyclone separators and inventory of sand. It decreases with increase in superficial velocity of air. Empirical correlation was developed to predict the Nusselt number as function of different non-dimensional numbers fitting experimental data points in FindFit function of Mathematica 5.2. Experimental results with the prediction of correlation showing rms deviation of ± 14.31%.

7.2 Scope for Future Work

Present experimental study was limited to CFB riser of cross sectional area 0.25 m × 0.25m due to the involvement of high cost for fabrication of larger size CFB unit. Further, modelling and simulations were conducted in a CFB riser of bed cross sectional area of 0.30 m × 0.30 m. However, same could not be implemented in beds with higher cross sectional area due to the limitation of dynamic memory of the computer.

Therefore following are the scope for future work:

1. Work reported in the present study establishes a procedure based on which numerical scale-up studies to industrial sizes can be carried out using high memory computational facility, which will be useful for the design of industrial CFB units.
2. Present study is limited to cold bed units. However, comparative hot bed studies with combustion can be conducted on atmospheric and pressurized CFB units to study the effect of temperature.
3. Material used in the experimental investigations was sand, with average particle size of 460 μm. Future work may be accomplished using different materials like coal, wood chips, biomass, sand particles of different sizes to perform the study on the atmospheric and pressurized hot beds and empirical correlation model can be developed by the incorporation of Archimedes number.
4. A large pressure drop across the distributor plate was observed in the present study. Modification of the same can lead to the reduction of pressure drop across the distributor plate leading to better the hydrodynamics as well as heat transfer characteristics. Thus an alternate design of distributor plate and parametric study may be done.

THESIS
Lakshminath Bezbaroa Central Library
Indian Institute of Technology Guwahati
ACC. No. TH...1848.....
Date.....28/3/12.....

621.042
SHA/P
P11

References

TH-1848_Shankarrao

References

Almuttahar, A., Taghipour, F., 2008. Computational fluid dynamics of a circulating fluidized bed under various fluidization conditions. Chem. Eng. Sc. 63, 1696 - 1709.

Almuttahar, A., Taghipour, F., 2008. Computational fluid dynamics of high density circulating fluidized bed riser: Study of modeling parameters. Powder Technol.185, 11- 23.

Arastoopour, H., Pakdel, P., Adewumi, M., 1990. Hydrodynamic analysis of dilute gas - solids flow. Derivation of a drag coefficient from velocity-voidage correlation. U.S. Dept. of Energy, Office of Fossil Energy, National Energy Technology Laboratory, Morgantown, West Virginia.

Arena, U., Marzocchella, A., Massimilla, L., Malandrino, A., 1992. Hydrodynamics of circulating fluidized beds with risers of different shape and size. Powder Technol. 70, 237-247.

Avci, A., Karagoz, I., 2001. Theoretical investigation of pressure losses in cyclone separators. Inr. Comm. Heat Mass Trans., 28, 107-117.

Avci, A., Karagoz, I., 2003. Effects of flow and geometrical parameters on the collection efficiency in cyclone separators. Aerosol Sc. 34, 937 - 955.

Bader, R., Findlay, J., Knowlton, T., 1988. Gas/solid flow patterns in a 30.5-cm diameter circulating fluidized bed. In: P. Basu, J. Large (Eds.), Circulating Fluidized bed Technology II, Pergamon Press.

Bastos, J.C.S.C., Rosa, L.M., Mori, M., Marini, F., Martignoni, W.P., 2008. Modelling and simulation of a gas - solids dispersion flow in a highflux circulating fluidized bed (HFCFB) riser. Catalysis Today 130, 462 - 470.

TH-1848_Shankarrao

Basu, P., Nag, P.K., 1987. An investigation into heat transfer in circulating fluidized beds. Int. J. Heat Mass Trans. 30 (11), 2399-2409.

Basu, P., 1990. Heat transfer in high temperature fast fluidized beds, Chem. Eng. Sci. 3123-3136.

Basu, P., Fraser, S., 1991. Circulating Fluidized Bed Boilers. Butterworth Heinemann.

Basu, P., Nag, P.K., 1996. Heat transfer to walls of circulating fluidized bed furnace. Chem. Engg. Sc. 51 (1), 1-26.

Behjat, Y., Shahhosseini, S., Hashemabadi, S.H., 2008. CFD modeling of hydrodynamic and heat transfer in fluidized bed reactors. Int.Comm. in Heat and Mass Trans. 35, 357-368.

Benyahia, S. Arastoopour, H., Knowlton, T., Massah, H., 2000. Simulation of particles and gas flow behavior in the riser section of a circulating fluidized bed using the kinetic theory approach for the particulate phase. Powder Technol. 112, 24-33.

Chan, C., Guo, Y., Lau, K., 2005. Numerical modeling of gas–particle flow using a comprehensive kinetic theory with turbulent modulation. Powder Technol. 150, 42-55.

Chen, J. C., Grace, J.R., Gloriz, M.R., 2005. Heat transfer in fluidized beds: design methods. Powder Technol.150, 123-132.

Danziger, W.J., 1963. Heat transfer to fluidized gas-solid mixtures in vertical transport. Ind. Eng. Chem. Proc. Des. Dev. 2, 269.

Dietz, P. W., 1981. Collection efficiency of cyclone separator,.AIChE J. 27, 882-892.

Ding, J., Gidaspow, D., 1990. A bubbling fluidization model using kinetic theory of granular flow. AIChE J. 36, 523-538.

TH-1848_Shankarrao

Fluent 6.3.26 Manual.

Fraley, L.D., Lin, Y.Y., Hsiao, K.H., Solbakken, A., 1983. Heat transfer coefficient in circulating bed reactor. ASME 83-HT-92.

Fox, W.B., Grewal, N.S., Moen, D.A., 1999. Wall-to-bed heat transfer in circulating fluidized beds. Int. Commun. Heat Mass Trans. 26 (4), 499-508.

Gavali, M.V., 2005. Development of an experimental facility to study scale effects in circulating fluidized bed, M.Tech Thesis Report, IIT Guwahati, India.

Gidaspow, D., 1994. Multiphase flow and fluidization: continuum and kinetic theory description. Academic Press, Boston.

Gidaspow, D., Bezburuah, R., Ding, J., 1992. Hydrodynamics of circulating fluidized beds, kinetic theory approach. Fluidization VII, Proceedings of the 7th Engineering Foundation Conference on Fluidization, New York, pp. 75-82.

Glicksman, L.R., 1988. Circulating fluidized bed heat transfer. In: P.Basu, J.F. Large, (Eds.), Circulating Fluidized Bed Technology II. pp. 13-30.

Glicksman, L.R., Hyre, M., Woloshun, K., 1993. Simplified scaling relationships for fluidized beds. Powder Technol. 70, 237-247.

Goyal, M., 2009. Recent approaches in CO_2 fixation research in India and future prospectives towards zero emission coal based power generation. Current Sc. 97 (11).

Grulovic, G.R., Vragolovic, N.B., Grbavcic, Z., Arsenijevic, Z., 2008. Wall-to-bed heat transfer in vertical hydraulic transport and in particulate fluidized beds. Int. J. Heat Mass Trans. 51, 5942-5948.

Gungor, A., 2008. Predicting axial pressure profile of a CFB. Chem. Eng. Sci. 140, 448-456.

TH-1848_Shankarrao

Gungor, A., 2009. Second law analysis of heat transfer surfaces in circulating fluidized beds. App. Energy. 86, 1344-1353.

Gupta, A.V.S.S.K.S., Nag, P.K., 2000. Prediction of heat transfer coefficient in the cyclone separator of a CFB. Int. J. Energy Research, 24, 1065-1079.

Hartge, E.U., Ratschow, L.,Wischnewski, R., 2009. CFD-simulation of a circulating fluidized bed riser. Particuology. 7, 283-296.

He, J., Simonin, O., 1993. Non-equilibrium prediction of particle-phase stress tensor in vertical pneumatic conveying gas - solid flows. ASME FED, 166, 253-263.

http://mathbits.com/Mathbits/TISection/Statistics2/correlation.htm

http://forecasts.org/cc.htm

Kim, S.D, Kim, J.S., Nam, C.H., Kim, S.H., Kang, Y., 1999. Immersed heater-to-bed heat transfer in liquid–liquid–solid fluidized beds. Chem. Eng. Sci. 54 (21), 5173-5179.

Kline, S.J., Mcclintok, F. A., 1953. Describing uncertainties in single – sample experiments. Mech. Eng.

Kolar, A.K., 2000. Heat transfer in circulating fluidized bed boilers: perspective and issues. Proceedings of 4th ISHMT-ASME Heat and Mass Transfer Conference, New Delhi, India. pp. 105-116.

Kolar, A.K., Sundaresan, R., 2002. Heat transfer characteristics at an axial tube in a circulating fluidized bed riser. Int. J. Thermal Sci. 41, 673-681.

Kolar, A. K., Leckner, B., 2006. Scaling of CFB boiler hydrodynamics. Advances in Energy Research (AER – 2006): Proceedings of 1st National Conference on Advances in Energy Research, Bombay, India. pp. 34-40.

TH-1848_Shankarrao

Kunii, D., Levenspiel, O., 1991. Fluidization Engineering. Butterworth-Hememann, USA, pp. 313.

Masoumifard, N., Mostoufi, N., Hamidi, A.A., Gharebagh, R.S., 2008. Investigation of heat transfer between a horizontal tube and gas–solid fluidized bed. Int. Jr. of Heat and Fluid Flow. 29, 1504-1511.

Mathematica Software Version 5.2.

Meena K.L., 2004. Heat transfer characteristics on upper splash region and in cyclone separator of circulating fluidized bed unit. M. Tech. Thesis Report, Department of Mechanical Engineering, IIT Guwahati- India.

McKeen, T., Pugsley, T., 2003. Simulation and experimental validation of a freely bubbling bed of FCC catalyst. Powder Technol. 129. 139-152.

Mickley, H.S., Trilling, C.A., 1949. Heat transfer characteristics of fluidized beds. Ind. Eng. Chem. 41, 1135.

Miller, A., Gidaspow, D., 1992. Dense vertical gas–solid flow in a pipe. AIChE J. 38, 1801-1814.

Molerus, O.,Wirth, K.E., 1997. Heat transfer in fluidized beds. Powder Technol. Series, Chapman and Hall, London.

Moral, M. N. A., 1990. Some studies on heat transfer in circulating fluidized beds, Ph.D. Thesis, Indian Institute of Technology Kharagpur, India.

Nag, P.K., Moral, M.N.A., 1990. Effect of probe size on heat transfer at the wall in circulating fluidized beds, Int. J. Energy Res. 14, 965-974.

Nag, P.K., Singh, N.K., 1996. Heat transfer in the cyclone separator of a circulating fluidized bed, Preprints of CFB- V, 5th Int. Conf. on Circulating Fluidized Beds, Beijing, P.R. China, HM II.

Nag, P.K., Gupta, A.V.S.S.K.S., 1999. Fin heat transfer studies in a cyclone separator of a circulating fluidized bed, Heat Transfer Engg. 20, 28-34.

Nag, P.K., 1998. Power Plant Engineering: Steam and Nuclear. Tata McGraw-Hill.

Nag, P.K., 2007. Heat and Mass Transfer. Second Ed., Tata McGraw-Hill, New Delhi. pp. 300.

Neri, A., Gidaspow, D., 2000. Riser hydrodynamics: simulation using kinetic theory, AIChE J. 46, 52-67.

Noymer, P.D., Hyre, M.R., Glicksman, L.R., 2000. The effect of bed diameter on near-wall hydrodynamic in scale-model circulating fluidized bed. Int. J. Heat Mass Trans. 43, 3641-3649.

Orozco, J., Nguyen, T., 1993. An analysis of the heat transfer characteristics of the fin/refractory system in a cyclone furnace. Heat Transfer Engg. 14, 19-25.

Pagliuso, J.D., Lombardi, G., Jr., L.G, 2000. Experiments on the local heat transfer characteristics of a circulating fluidized bed. Expt. Thermal and Fluid Sc. 20, 170-179.

Patankar, S., 1980. Numerical Heat Transfer and Fluid Flow. Hemisphere Publishing Corp., Washington, DC.

Praghanmor, R.R., 2009. Study on heat transfer characteristics of cold circulating fluidized bed risers. M.Tech. Thesis Report, Department of Mechanical Engineering, IIT Guwahati, India.

Ranade, V., 2002. Computational flow modeling for chemical reactor engineering. Vol.5, Acad. Press, pp. 19-20.

TH-1848_Shankarrao

Schouten, J.C., Zijerveld, R.C., Bleek, C.M., 1999. Scale-Up of Bottom-Bed Dynamics and Solids-Distribution in Circulating Fluidized Beds of Geldart-B Particles. Chem. Eng. Sci. 54, 2103-2112.

Shi, D., Nicolai, R., Reh, L., 1998. Wall-to-bed heat transfer in circulating fluidized beds. Chem. Eng. Processing. (37), 287-293.

Singh, V., Sharma, P., 2008. Studies on hydrodynamics and heat transfer characteristics of the circulating fluidized bed. B.Tech. Project Report, Department of Mechanical Engineering, IIT Guwahati – India.

Singh, B., Mittal, C., 2009. Studies on hydrodynamic characteristics of the circulating fluidized beds and erecting the CFB setups. B.Tech. Project Report, Department of Mechanical Engineering, IIT Guwahati – India.

Stairmand, C. J., 1951. The design and performance of cyclone separators. Trans., Instn. Chem. Engg. 29, 356-383.

Subbarao, D., Basu, P., 1986. A model for heat transfer in circulating fluidized beds. Int. J. Heat Mass Trans. 29 (3), 487- 489.

Sundaresan, R., Kolar, A. K., 2002. Core heat transfer studies in a circulating fluidized bed. Powder Technol. 124, 138-151.

Taghipour, F., Ellis, N.,Wong, C., 2005. Experimental and computational study of gas–solid fluidized bed hydrodynamics. Chem. Eng. Sc. 60, 6857-6867.

Trefz, M., Muschelknautz, E., 1993. Extended cyclone theory for gas flows with high solid concentrations. Chem. Engg. Technol.16, 153-160.

Xiang, R. B., Lee, K.W., 2008. Effects of exit tube diameter on the flow field in cyclones. Particulate Sc. and Technol. 26, 467- 481.

TH-1848_Shankarrao

Yan, A., Ball, J., Zhu, J., 2005. Scale-up effect of riser reactors (3) axial and radial solids flux distribution and flow development. Chem. Eng.J. 10, 97-106.

Wen, C.Y., Miller, F. N., 1961. Heat transfer in solid-gas transport lines. Ind. Engg. Chem. 53, 51.

Wirth, K.E., 1995. Heat transfer in circulating fluidized beds. Chem. Eng. Sci. 50, 2137-2151.

Wu, R.L., Lim, C.J., Chaouki, J., Grace, J.R., 1987. Heat transfer from a circulating fluidized bed to membrane water wall cooling surfaces. AIChE J. 33 (11), 1888-1893.

Zheng, Y., Wan, X., Qian, Z., Wei, F., Jin, Y., 2001. Numerical simulation of the gas–particle turbulent flow in risers reactor based on $k–\varepsilon–k_p–\varepsilon_p–\Theta$ two fluid model. Chem. Eng. Sci. 56, 6813-6822.

Zhou, J.,Grace, J. R., Qin, S., Brereton, C. M. H., Lim, C. J., Zhu, J. 1994. Voidage profiles in a circulating fluidized bed of square cross-section. Chem. Eng. Sci. 49(19), 3217-3226.

Zhou, L.X., Soo, S.L., 1990. Gas - solid flow and collection of solids in a cyclone separator. Powder Technol. 63, 45-53.

TH-1848_Shankarrao

Appendix

TH-1848_Shankarrao

Appendix A

Specifications of Various Components

1. Motor

20 HP, Primo 3 phase induction motor

Voltage 445 volts 50 Hz

Amperes 27.6

Manufacture: Kirloskar

2. Blower

Twin lobe blower

Model 710

Serial No. 0503468

Pressure 2000 mm Hg

Speed 1300 RPM

Flow rate 1275 m^3/hr

Manufacturer: Everest transmission

3. Variac

Input: 240 volts

Output: 0-270 Volts

Type 6P-1

Capacity: 6 Amps

Manufacturer: Varivolt

4. Heating Element - Nichrome Wire

2000 W capacity

Resistance of the wire 29 Ohms

Diameter of the wire 0.6 mm

5. Fine wire mesh (BS 400) and cigarette filter is used at the pressure tapping ends to minimize the pressure fluctuations in the water filled 'U' tube manometer.

6. The Data Acquisition System (DAS)

It consists of two RS-232 converter modules, six analog input modules, each module has eight channels to connect thermocouples and the software named as VPL-EASYLAB 1.0. DAS is used to receive the data from various transducers or sensors and then transfer the data to computer, where output can be measured in the form of digital or analog or in the graphical form of signal. The software VPL-EASYLAB 1.0 is used to convert the data of DAS into required output.

TH-1848_Shankarrao

7. Distributor Plate

Figure A.1 represents the distributor plate used in the present study. Design calculations for the MS distributor plate are shown in Table A.1, where the thickness of the distributor plates and the diameter of orifices are taken as 5 mm and 4 mm, respectively. In the Table A.1, ΔP_d is the pressure drop across the distributor plate (kPa), ΔP_b is the pressure drop across the bed (kPa), D is the hydraulic diameter of the bed (m), Lm is the height of the fixed bed (m), t is the thickness of the distributor plate (m), d_{or} is the diameter of the orifice plate (m), $Cd_{,or}$ is the orifice coefficient, u_{or} is the velocity of gas through an orifice (m/s), N_{or} is the number of orifices per unit area of distributor (m^{-2}).

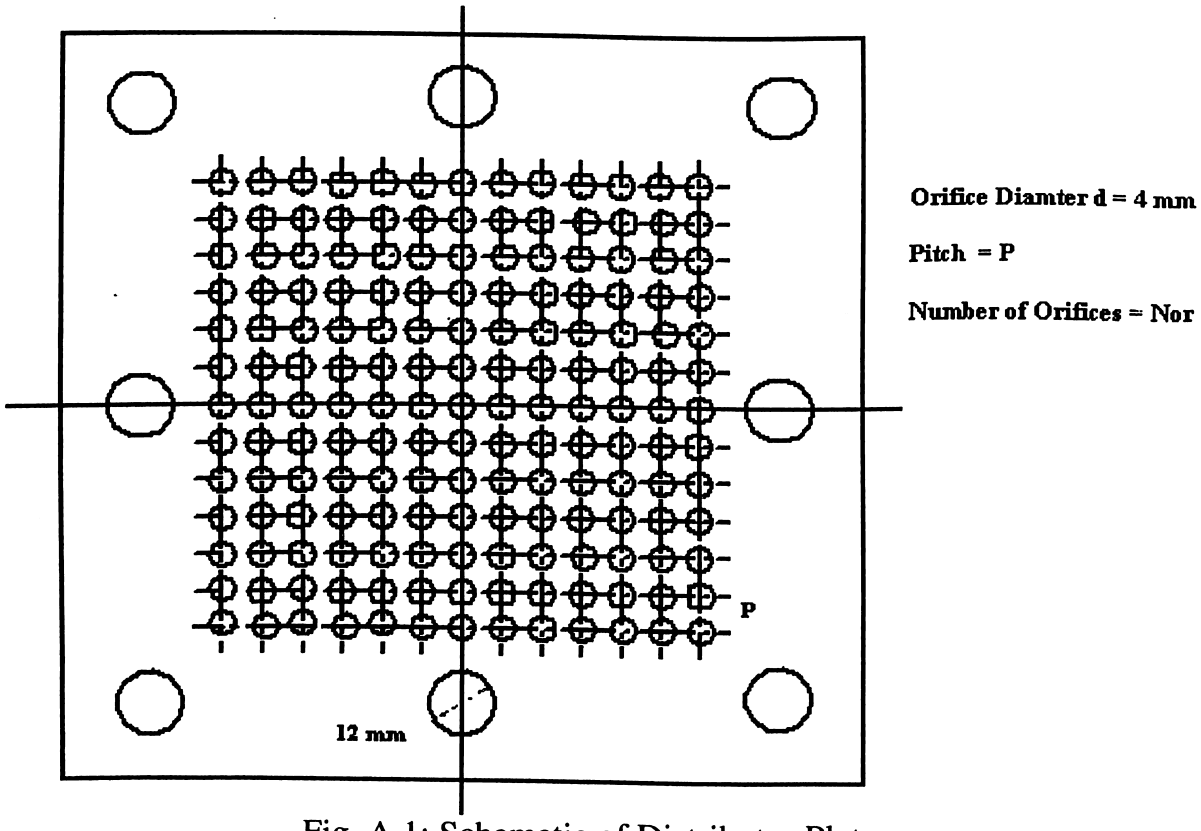

Fig. A.1: Schematic of Distributor Plate

Table A.1

Quantity	Formula	Bed of 0.25 m x 0.25 m	Bed of 0.20 m x 0.20 m	Bed of 0.15 m x 0.15 m
ΔP_d, kPa	$\Delta P_d = \Delta P_b \left[0.01 + 0.2 \left\{ 1 - \exp\left(\frac{-D}{2L_m} \right) \right\} \right]$	0.5	0.42	0.325
$C_{d,or}$	$C_{d,or} = 0.82 \left(\frac{t}{d_{or}} \right)^{0.13}$	0.8441	0.8441	0.8441
u_{or}, m/s	$u_{or} = C_{d,or} \left(\frac{2\Delta P_d}{\rho_g} \right)^{\frac{1}{2}}$	24.36	22.33	19.64
N_{or}, m^{-2}	$N_{or} = \frac{u_g}{u_{or}} X \frac{4}{\pi d_{or}^2}$	16329	17816	20256
Total number of holes	$N_{or} \times A_b$	1021	713	456
Pitch of the orifices, mm	$\frac{1}{(N_{or})^{1/2}}$	8	7.5	7.0
Open area in the distributor plate, m^2	$= \frac{\pi}{4} d_{or}^2 \; x \; (N_{or} \; x \; A_b)$	0.0128	8.95×10^{-3}	5.72×10^{-3}

TH-1848_Shankarrao

Appendix B

Measurement of Mean Particle Size of Sand

The actual sand particles are of varieties of shape and size. To measure the mean size of the particles following procedure has been followed (Kunii and Levenspiel, 1991).

Following assumptions have been made,

1. Volume remains same.
2. Surface area remains same.

Now, let there be:

n_1: Particles of diameter d1.

n_2: Particles of diameter d2.

n_3: Particles of diameter d3.

And so on.

From assumption no.1:

$$N \times \frac{\pi \bar{d}_p^{\,3}}{6} = n_1 \frac{\pi d_1^3}{6} + n_2 \frac{\pi d_2^3}{6} + n_3 \frac{\pi d_3^3}{6} + \ldots\ldots\ldots\ldots$$

Where N is the number of replaced, uniformly sized particles of diameter $\bar{d}_p$.

$$N \times \bar{d}_p^{\,3} = n_1 \times d_1^3 + n_2 \times d_2^3 + n_3 \times d_3^3 + \ldots\ldots\ldots\ldots$$

From assumption no.2:

$$N \times \pi \bar{d}_p^{\,2} = n_1 \pi d_1^2 + n_2 \pi d_2^2 + n_3 \pi d_3^2 + \ldots\ldots\ldots\ldots$$

or,

$$N \times \bar{d}_p^{\,2} = n_1 \times d_1^2 + n_2 \times d_2^2 + n_3 \times d_3^2 + \ldots\ldots\ldots\ldots$$

Let X_1 be the weight fraction of solids of diameter d_1.

TH-1848_Shankarrao

Therefore

$$X_1 = \frac{\frac{n_1 \times \bar{d}_1^{\,3}}{6} \times \rho_s}{\frac{N \times \bar{d}_p^{\,3}}{6} \times \rho_s} = \frac{n_1 \times d_1^3}{N \times \bar{d}_p^{\,3}}$$

where ρ_s represents the density of sand.

Similarly, $X_2 = \dfrac{n_2 \times d_2^3}{N \times \bar{d}_p^{\,3}}$

Hence, $n_1 \times d_1^2 = X_1 \times N \times \bar{d}_p^{\,3} / d_1$

$$n_2 \times d_2^2 = X_2 \times \bar{d}_p^{\,3} / d_2$$

$$N \times \bar{d}_p^{\,2} = n_1 \times d_1^2 + n_2 \times d_2^2 + n_3 \times d_3^2 + \ldots\ldots\ldots\ldots$$

$$= X_1 \times N \times \frac{\bar{d}_p^{\,3}}{\bar{d}_1} + X_2 \times N \times \frac{\bar{d}_p^{\,3}}{\bar{d}_2} + X_3 \times N \times \frac{\bar{d}_p^{\,3}}{\bar{d}_3}$$

or, $$\frac{1}{\bar{d}_p} = \frac{X_1}{d_1} + \frac{X_2}{d_2} + \frac{X_3}{d_3} + \ldots\ldots\ldots\ldots\ldots\ldots$$

or, $$\frac{1}{\bar{d}_p} = \sum \frac{X_i}{d_i}$$

or, $$\bar{d}_p = \frac{1}{\sum \frac{X_i}{d_i}}$$

Table B.1

Mesh (BSS)	Mean particle size (d_i), µm	Weight in grams	Weight fraction (Xi)	X_i / d_i
22-25	649	144	0.144	0.221×10^{-3}
25-30	549.5	126	0.126	0.229×10^{-3}
30-36	461	192	0.192	0.416×10^{-3}
36-44	388	192	0.192	0.494×10^{-3}
44-52	325.5	4	0.004	0.0113×10^{-3}
52-60	274	96	0.096	0.350×10^{-3}
60-pan	251	46	0.046	0.183×10^{-3}

Hence for Mean particle size calculation, following formula has been used

$$\bar{d}_p = \frac{1}{\Sigma \frac{X_i}{d_i}}$$

Thus, mean particle size = 460 µm.

Appendix C

Formulae, Sample Calculations on Operating Parameters, Heat Transfer Coefficient

1. Non-dimensional Superficial Velocity of air (U*)

Non-dimensional form (U*) is given as

$$U^* = \frac{U'}{U_{mf}} \qquad \text{(C.1)}$$

where (U') and (U_{mf}) are superficial air velocity and minimum fluidizing air velocity respectively. The superficial velocity (U') is defined as the volume flow rate of air per unit cross-section of the bed.

$$U' = \frac{Volume\ flow\ rate\ of\ air\ through\ bed}{Cross-sectional\ area\ of\ bed} = \frac{Q_o}{A_b}$$

where A_b is the cross section area of bed and Q_o is the discharge through orifice meter ($A_b \times U'$)

$$Q_o = \frac{C.a_1\left(2.\rho_w.g.\Delta h\right)^{1/2}}{\left\{\rho_g.(1-\beta^4)\right\}^{1/2}} = 0.035\sqrt{\Delta h}$$

where C = Discharge coefficient = 0.6082

a_1 = Cross-section area of orifice = 0.004417 m^2

β = Diameter ratio = d/D = 0.5

Δh = Difference between pressure head (manometer reading), cm

For example, for 0.15 m × 0.15 m bed, at seven kg of sand inventory on the distributor plate or P = 3050 N/m^2 (static pressure due to weight of sand on the distributor plate), superficial velocity of air is calculated as below.

$Q_o = 0.035\sqrt{\Delta h} = 0.09\ m^3/s = A_b \times U'$

Therefore, $U' = 0.09 / (0.15 \times 0.15) = 4$ m/s

Similarly U_{mf} was evaluated = 0.5 m/s, hence $U^* = \frac{U'}{U_{mf}} = 8.$

In this way, U* = 5, 5.5, 6, 6.6, 8 may be calculated for three CFB units for two sand inventories, P = 3050 N/m^2 and P = 1750 N/m^2. Experiments were conducted in three CFB setups at U'= 2.5 m/s, 2.75 m/s, 3 m/s, 3.3 m/s, and 4 m/s when static pressure due to weight of sand on the distributor plate (P) = 3050 N/m^2, and at U'= 2.36 m/s, 2.47 m/s, 2.63 m/s, 2.8 m/s and 3.03 m/s, U_{mf} = 0.47 m/s when P = 1750 N/m^2.

2. Weight of Sand per Unit Area of Distributor Plate, (P)

For 0.15 m × 0.15 m bed, two sand inventories at which experiments were conducted were 7 kg and 4 kg i.e experiments were conducted at 3050 N/m^2 and 1750 N/m^2 due to weight of sand per unit area of distributor plate of riser column respectively.

For example, P = (4 kg × 9.81 m/s^2) / (0.15 m × 0.15 m) = 1750 N/m^2 (approx.). In this way, also for other two CFB units, weight of sand inventory per unit area of distributor plate was maintained as 3050 N/m^2 and 1750 N/m^2.

3. Suspension Density

The suspension density of the bed (ρ_{sus}) can be evaluated by the equation (Kunni and Levenspiel, 1991)

$$\rho_{sus} = \rho_s (1-\varepsilon) + \varepsilon \rho_g \qquad \text{(C.2)}$$

where voidage (ϵ) is defined as the volume fraction of the bed by occupied by air bubbles. The bed voidage (ϵ) at any cross-section of riser has been estimated from the measured pressure drop (ΔP_b) from a differential water filled U-tube manometer connected across two pressure taps separated by a distance 0.6 m along the height of the riser. ρ_g is the density of air in kg/m^3.

Voidage (ϵ) is given by

$$\varepsilon = 1 - \frac{10\Delta h}{\rho_s L_m} \qquad \text{(C.3)}$$

where Δh is difference of height in manometric fluid, measured in cm of water, L_m is the distance between two consecutive pressure taps (0.6 m approx. for all CFB units)

TH-1848_Shankarrao

across which pressure drop, hence voidage has to be determined, ρ_s is the density of sand (2600 kg/m^3).

Let us take a case for which suspension density has to be determined at a height 0.9 m above the distributor plate - for CFB setup B1 operated at P = 3050 N/m^2, superficial velocity U'= 4 m/s (refer Fig. 4.2 and Fig. 4.4). Suspension density has been calculated by using eq. (C.2),

Suspension density = 2600 $(1-\varepsilon)$ + ε (1.22) = 122 kg/m^3 (Refer Fig. 4.4)

where ε = 0.9535 is obtained using eq. (C.3) by substituting Δh = 7.25 cm (refer Fig. 4.2), ρ_s = 2600 kg/m^3, L_m = 0.6 m (distance between two taps connected on portion L of Fig. 3.1)

4. Solid Circulation Rate

Solid circulation rate (G_s) i.e (solid mass flux) is given by

$$G_s = \frac{\rho_s L_a A_D (1-\varepsilon_{mf})}{A_B . t} \qquad \text{(C.4)}$$

where L_a is accumulation height in m, t is the time elapsed in *s* after closing the butterfly valve to gain L_a in graduated column of down-comer, ρ_s is the density of sand in kg/m^3, A_B and A_D are cross sectional area of riser column and graduated column or sand height measuring section in m^2, respectively, as shown in Fig. 3.1, ε_{mf} is the voidage at minimum fluidization. In the present study, $A_B = A_D$ in each CFB unit.

Consider a case, CFB unit B1 was operated at P = 3050 N/m^2, U* = 8. Solid circulation rate using eq. (C.4) is estimated as below

G_s = 2600 × 0.15 × (1 − 0.5) / 10 sec = 19.50 kg/m^{2}s. (refer Fig. 4.16)

Solid circulation rate for CFB unit B2 and B3 was almost same (varying between 19-20 kg/m^{2}s) for the same operating conditions. Solid circulation rate for three CFB units for the operating conditions, P = 3050 N/m^2, U* = 5 was 12.19 kg/m^{2}s, at P = 17050 N/m^2, U* = 5 was 8.16 kg/m^{2}s and at P = 17050 N/m^2, U* = 8 was 10.47 kg/m^{2}s. For P = 1750 N/m^2, ε_{mf} was 0.4 for all CFB units.

5. Local Heat Transfer Coefficient (h_{local} or h) – Riser

The local heat transfer coefficient (h) is calculated by

$$h = \frac{Q}{A_S (T_S - T_B)} \qquad (C.5)$$

where Q is rate of heat supplied to the heater measured using calibrated wattmeter. T-type calibrated thermocouples (Appendix D) and data acquisition system with Easy Lab software version 1.0 were used to measure the surface temperature (T_S) and (bulk mean) bed temperature (T_B), A_S is the surface area of the heater.

Consider a case for CFB unit B1 (0.15 m × 0.15 m), U* = 5, P = 1750 N/m^2 at D = 2.24 m above the distributor plate. (Refer Fig. 4.6). Bed temperature measured at non-dimensional distance [X/b] of 0.1, 0.3, 0.5, 0.7, 0.9 across the bed at a height 2.24 m above the distributor plate was 40.79^{0}C, 41.58^{0}C, 41.05^{0}C, 40.53^{0}C, 47.11^{0}C, respectively.

Therefore bulk mean temperature (T_B) across the heater - riser for any CFB unit is calculated by (Refer Fig. C.1)

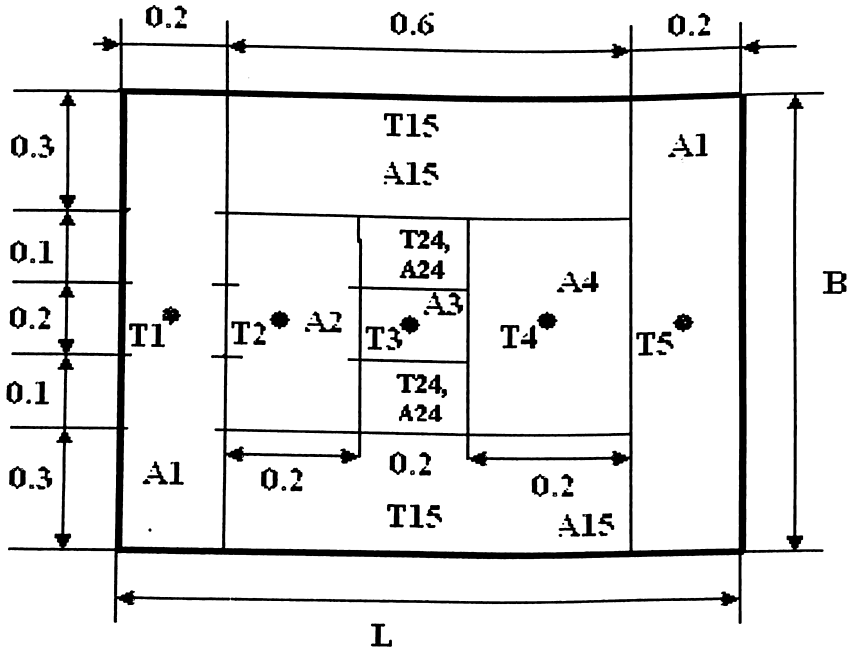

Fig. C.1 Bulk Mean Temperature Measurement across Heater - Riser

$T_B = \{ A1 (T_1 + T_5) + 2 A_{15} . T_{15} + A_2 (T_2 + T_4) + 2 A_{24} (T_{24}) + A_3 T_3 \} / A$

Where A = L × B as shown in Fig. C.1 and $T_{15} = (T_1 + T_5) / 2$, $T_{24} = (T_2 + T_4) / 2$

$T_B = 0.38 (T_1 + T_5) + 0.1 (T_2 + T_4) + 0.04 (T_3)$

$T_B = 0.38 (40.79 + 47.11) + 0.1 (41.58 + 40.53) + 0.04 (41.05)$

Therefore $T_B = 43.25\ ^0C$.

TH-1848_Shankarrao

Surface temperature (T_S) of heater at 2.24 m above the distributor plate was 137 ^{0}C. Heat flux applied at the wall of the heater of small CFB unit B1 having surface area 0.36 m^2 was 1000 W/m^2. Heat supplied at the wall of the heater is measured using Wattmeter. Therefore, local heats transfer coefficient value at 2.24 m above the distributor plate (refer eq. D.5) = 1000 / (137 – 43.25) = 10.66 W/m^2. In this way local heat transfer coefficient has been calculated for all the CFB units.

6. Local Heat Transfer Coefficient (h_c) – Cyclone Separator

Local heat transfer coefficient (h_c) along the height of cyclone separator is calculated by

$$h_c = q'' / (T_{Bc} - T_{Sc}) \qquad \text{(C.6)}$$

where T_{Bc} and T_{Sc} represent the bed (air + sand mixture) and wall temperature of the cyclone separator, respectively. Heat flux (q") in each cyclone separator is calculated by

$$q'' = (q_1 - (q_2 + q_3) / As_c \qquad \text{(C.7)}$$

where q_1 is the amount heat carried by air and sand mixture which was calculated at the inlet of cyclone separator (refer Fig. 3.5), As_c is the surface area of cyclone separator, q_2 and q_3 is the heat carried by air and sand in W from the top outlet of cyclone separator - chimney and bottom outlet of cyclone separator respectively (refer Fig. 3.5). Speed and temperature of air at outlet of cyclone separator was measured using anemometer.

Consider a case if U* = 8, P = 3050 N/m^2 is the operating condition for smaller CFB unit of 0.15 m × 0.15 m. Let us consider a case to determine the bulk mean temperature and local heat transfer coefficient value at the non-dimensional distance (Y/H_C) of 0.1 at operating condition of U* = 8, P = 3050 N/m^2 (refer Fig. 6.4, Fig. 6.7, and Fig. 6.11 with respect to C1). Bed temperature distribution at the non-dimensional distance (Y/H_C) of 0.1, in the radial direction with non-dimensional distance (r/R) - 0.9, - 0.5, 0.0, 0.5, 0.9 (refer Fig. 3.5) was 37^{0}C, 37.10^{0}C, 37.85^{0}C, 37.40^{0}C, 37.10^{0}C respectively. T_{Bc} in eq. (C.6) represents the bulk mean bed temperature across the section taken at the non-dimensional distance (Y/H_C) of 0.1 in the cyclone separator C1. Refer Fig. C.2 with respect to formula to be derived to

obtain bulk mean temperature in a radial direction of cyclone separator C1 having barrel diameter 0.27 m at the non-dimensional distance (Y/H_C) of 0.1.

Cross sectional area of cylindrical portion of cyclone separator C1 having barrel diameter 0.27 m, A3 = π $(0.135)^2$. Therefore A2 = π $(0.081)^2$ and A1 = π $(0.027)^2$ as shown in Fig. C.2. Therefore, A3' = A3 – A2 = 0.0366 m^2, A2' = A2 – A1 = 0.0183 m^2, and A1' = A1 = 0.00229 m^2.

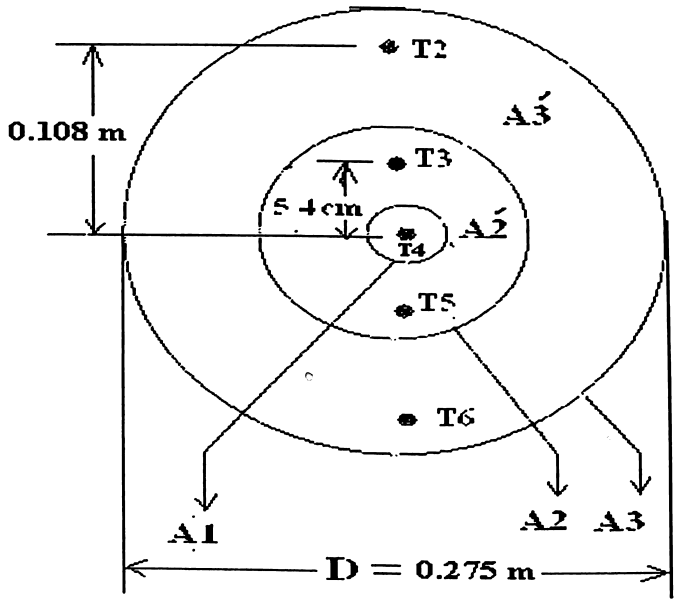

Fig. C.2 Bulk Mean Temperature Measurement

Therefore bulk mean temperature (T_{Bc}) is calculated by

T_{Bc} = (T2 + T6) × (A3'/ 2) + (T3 + T5) × (A2'/ 2) + T4A1 / {(π / 4) D^2}

T_{Bc} = 0.32 × (T2 + T6) + 0.16 × (T3 + T5) + 0.04 × T4

Therefore, T_{Bc} = 0.32 × (37 + 37.10) + 0.16 × (37.10 + 37.40) + 0.04 × 37.85

T_{Bc} = 37.14 ^{0}C and As_c is the surface area of cyclone separator C1 = 0.744 m^2. In the similar way, bulk mean temperature may be obtained across section taken at any location in the cylindrical portion of any cyclone separator.

Now q_2 of eq. (C.7) is calculated by, $q_2 = \rho_{air} \cdot A_{chimeny} \cdot U_{chimney} \cdot Cp_{air} \cdot (T_{b2} - T_{atm})$ = 1.2 × ({π /4}. $(0.07)^2$) × 23.46 × 1005 × (34.15 – 21.3) = 1388.55 W, where $U_{chimney}$ and T_{b2} are measured using anemometer at the just above the chimney.

Now q_1 of eq. (C.7) is calculated by, $q_1 = \rho_{sus} \cdot A_b \cdot U_1' \cdot Cp_{as} \cdot (T_{b1} - T_{atm})$ = 3.18 × (0.15 ×0.15) × 8 × 1005 × (37.14 – 21.3) = 9112.15 W, where $Cp_{as} = C_{p\text{-sand}}$ (1

TH-1848_Shankarrao

- ε_1) + $C_{p\text{-}air}$. ε_1 = 835 (1 – 0.999) + 1005 × 0.999 = 1005 J/kg.K (approx.), and ρ_{sus} = ρ_{sand} (1 - ε_1) + ρ_{air} . ε_1 = 2600 (1 – 0.999) + 1005 × 0.999 = 3.18 kg/m^3, U_1' is obtained from Fluent Simulations at 2.85 m above the distributor plate in the riser column = 8 m/s, ε_1 is the voidage measured with help of pressure tapping provided over tangential inlet of cyclone separator of length 0.3 m and of cross section 0.135 m × 0.0675 m.

Now q_3 of eq. (C.7) is calculated by $q_3 = \rho_{sus} . A_{cbo} . U_{cbo} . Cp_{as} . (T_{b3} - T_{atm})$ = 6 × ({π /4}. (0.07)^2) × 23.46 × 1004.36 × (34.87 – 21.3) = 7383.06 W, where A_{cbo} and U_{cbo} is the cross section area of the bottom outlet of cyclone separator and velocity of sand respectively. U_{cbo} is calculated by ({A_b . U_1'} – {$A_{chimeny}$. $U_{chimney}$}) / A_{cbo}, and $Cp_{as} = C_{p\text{-}sand}$ (1 – ε_3) + $C_{p\text{-}air}$. ε_3 = 835 (1 – 0.998) + 1005 × 0.998 = 1004.36 J/kg.K, ρ_{sus} = ρ_{sand} (1 - ε_3) + ρ_{air} . ε_3 = 2600 (1 – 0.998) + 1005 × 0.998 = 6 kg/m^3, ε_3 is the voidage = 1 – {(10 × Δh) / (ρ_{sand} × L)} measured with help of pressure tapping 1 and 2 as shown in Fig. 3.5 provided over bottom outlet of cyclone separator, separated by distance (L) 0.1 m.

Therefore, h_c = q" / (T_{Bc} – T_{Sc}) W/m^2.K (refer eq. C.6 and eq. C.7) Substituting values, h_c = 461.74 / (37.14 – 25.3) = 39 W/m^2.K (refer Fig. 6.11, Y/H_C = 0.1, cyclone separator C1). In the similar way, heat flux, local heat transfer coefficient has been obtained along the height of the cylindrical portion of any cyclone separator.

TH-1848_Shankarrao

Appendix D

Calibration of T - type Thermocouple

Calibration of thermocouple was done using the oil heater calibration machine. One junction of the thermocouple is kept in atmosphere while the other end is subjected to changing oil temperature. The device gives a continuous temperature reading of the oil. The oil is heated to a temperature upto 100 ^{0}C and then cooled back to room temperature. Voltage is read through multimeter during both heating and cooling. Following data has been obtained.

Table D.1

Sr. No.	Voltage in mV (Y_i)	Oil Temperature,^{0}C	Reference Temperature,^{0}C	Temperature Difference (X_i)
1	0.045	21.87	21	0.87
2	0.07	26	21	5
3	0.09	30	21	9
4	0.16	35	21	9
5	0.35	40	21	19
6	0.58	45	21	24
7	0.87	50	21	29
8	1.07	55	21	34
9	1.22	60	21	39
10	1.41	65	21	44
11	1.59	70	21	49
12	1.76	75	21	54
13	1.94	80	21	59
14	2.07	85	21	64
15	2.29	90	21	69
16	2.47	95	21	74
17	2.50	100	21	79
Total	$\sum Y_i$ = 20.485			$\sum X_i$ = 660.87

TH-1848_Shankarrao

Also, $\sum X_i^2 = 35950.76$, $\sum Y_i^2 = 37.15$, $(\sum X_i)^2 = 436749.20$, $(\sum Y_i)^2 = 419.63$, $\sum X_i Y_i = 1152.61$, N = 17 data points

Using regression analysis,

$$A = N \sum X_i Y_i - (\sum X_i \times \sum Y_i) / N \sum X_i^2 - (\sum X_i)^2 = 0.033$$

$$B = \sum Y_i \times \sum X_i^2 - (\sum X_i Y_i \times \sum X_i) / N \sum X_i^2 - (\sum X_i)^2 = -0.144$$

As $Y = a X + b$, $Y = 0.033 X - 0.144$ or $X = 30.30 Y + 4.363$.

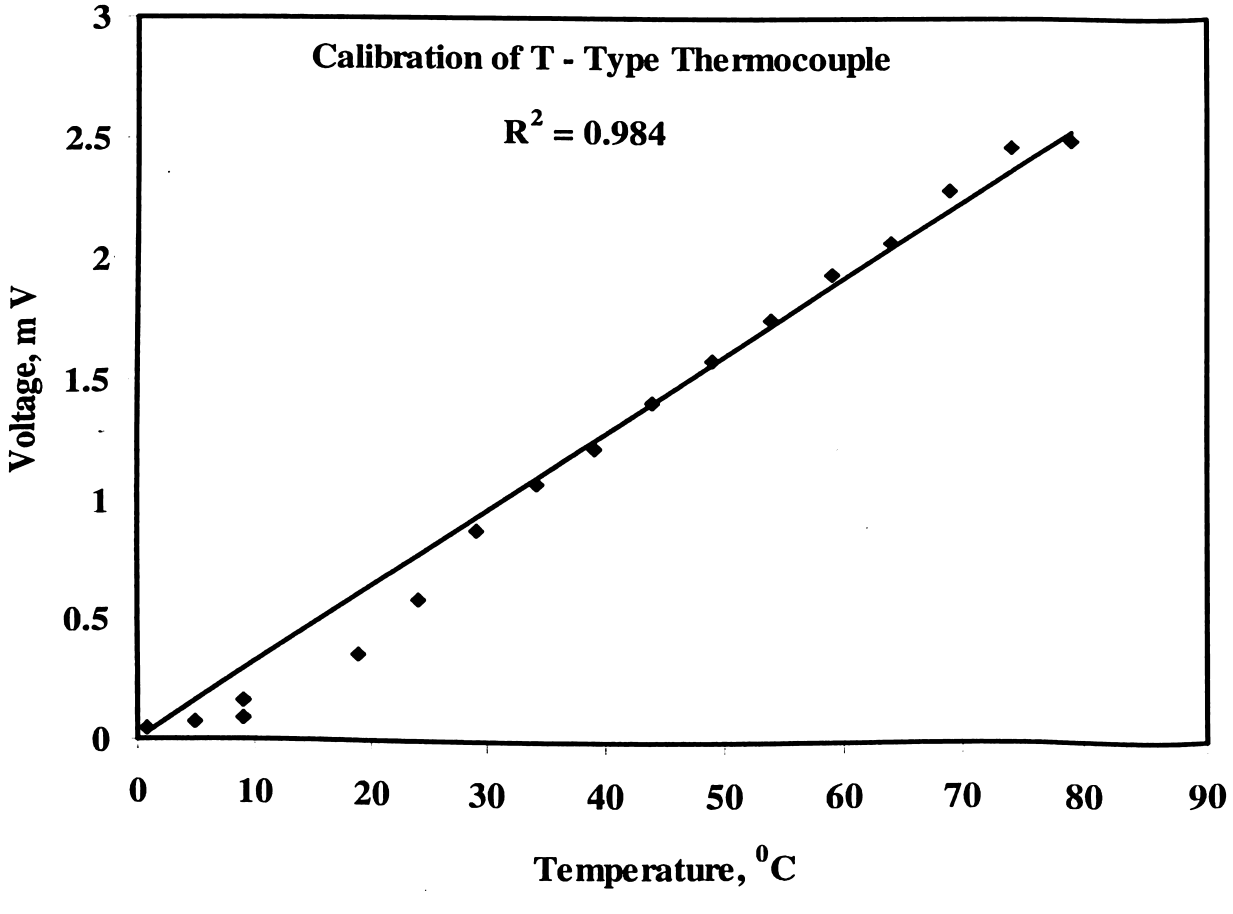

Fig. D.1 Calibration of Thermocouple

Appendix E

Uncertainty Analysis

Percent uncertainty in the heat transfer coefficient can be determined by using Kline and McClintok method (Kline and McClintok, 1953).

The local heat transfer coefficient along the riser column may be evaluated using

$$h = q / [A_S \,.\, (T_S - T_b)] \quad W.m^{-2}.K^{-1} \qquad (E.1)$$

where

q: Heat supplied, W

H: Height of heated section, m

B: Width of heated section, m

T_b: Bed temperature, °C

T_S: Surface temperature, °C

Now,

$$h = f(q, H, B, T_S, T_b)$$

$$\therefore \text{Percentage uncertainty} = \frac{\text{Error}}{h} \times 100\%$$

$$= 100 \times \sqrt{\left(\frac{w_1}{q}\right)^2 + \left(\frac{-w_2}{B}\right)^2 + \left(\frac{w_3}{H}\right)^2 + \left(\frac{-w_4}{T_s - T_b}\right)^2 + \left(\frac{w_5}{T_s - T_b}\right)^2} \qquad (E.2)$$

Here, w_1, w_2, w_3, w_4, w_5 are uncertainties associated with independent variables q, B, H, T_S, T_B, respectively. The sample calculation for 0.15 m × 0.15 m CFB setup, bed inventory 7 kg, superficial velocity U* = 5.5, for lower splash region has been illustrated.

For this case, refer Table E.1, Sr.no.9,

$T_{b9} = 34.21 \pm 0.5$ °C

$T_{s9} = 60.26 \pm 0.5$ °C

$q = 360 \pm 5$ W

TH-1848_Shankarrao

$$B = 0.6 \pm 0.001 \text{ m}$$

$$H = 0.6 \pm 0.001 \text{ m}$$

Thus,

Percent uncertainty

$$= 100 \times \sqrt{\left(\frac{5}{360}\right)^2 + \left(\frac{-0.001}{0.6}\right)^2 + \left(\frac{0.001}{0.6}\right)^2 + \left(\frac{-0.5}{60.26-34.21}\right)^2 + \left(\frac{0.5}{60.26-34.21}\right)^2}$$

= 3.06 % (Refer Table E.1, Sr. No. 9)

For 0.20 m × 0. 20 m CFB setup at lower splash region,

$$q = 480 \pm 6 \text{ W}$$

$$B = 0.8 \pm 0.001 \text{ m}$$

$$H = 0.6 \pm 0.001 \text{ m}$$

For 0.25 m × 0.25 m CFB setup at lower splash region,

$$q = 600 \pm 7 \text{ W}$$

$$B = 1 \pm 0.001 \text{ m}$$

$$H = 0.6 \pm 0.001 \text{ m}$$

Table E.1 Sample Calculation Results for Uncertainties (%) for 0.15 m × 0.15 m CFB Setup

Sr. No.	U* = 5.5 I = 7 kg	U* = 6.6 I = 7 kg	U* = 5.5 I = 4 kg	U* = 6.6 I = 4 kg
1	1.65	1.61	1.63	1.64
2	1.69	1.65	1.65	1.66
3	1.71	1.70	1.68	1.68
4	1.73	1.76	1.70	1.70
5	1.72	1.75	1.69	1.69
6	1.81	1.87	1.73	1.73
7	1.94	2.04	1.79	1.78
8	2.28	2.46	2.00	1.97
9	3.06	3.50	2.46	2.36
10	4.81	6.95	3.03	2.80
Root mean square value of uncertainty for 0.15 m × 0.15 m CFB setup = 2.37%				

TH-1848_Shankarrao

Table E.2 Sample Calculation Results for Uncertainties (%) for 0.20 m × 0.20 m CFB Setup

Sr. No.	U* = 5.5 I = 12.5 kg	U* = 6.6 I = 12.5 kg	U* = 5.5 I = 7 kg	U* = 6.6 I = 7 kg
1	3.34	4.04	3.48	4.10
2	2.16	2.34	1.70	1.72
3	2.49	2.86	1.71	1.73
4	2.90	3.63	2.08	2.90
5	2.51	2.88	1.69	1.73
6	2.62	2.95	1.70	1.79
7	3.63	4.04	1.86	2.11
8	4.80	5.68	2.10	2.46
9	6.24	8.01	4.26	3.10
10	10.49	9.29	10.61	9.85
Root mean square value of uncertainty for 0.20 cm × 0.20 m CFB setup = 4.5%				

Table E.3 Sample Calculation Results for Uncertainties (%) for 0.25 m × 0.25 m CFB Setup

Sr. No.	U* = 5.5 I = 19.5 kg	U* = 6.6 I = 19.5 kg	U* = 5.5 I = 11 kg	U* = 6.6 I = 11 kg
1	1.98	2.26	1.89	1.99
2	1.95	2.09	1.70	1.78
3	1.89	1.80	1.56	1.62
4	1.95	1.65	1.49	1.55
5	2.06	2.46	1.58	1.64
6	2.40	2.74	1.69	1.80
7	4.36	2.80	1.83	2.06
8	6.22	3.52	2.43	2.70
9	8.48	9.04	3.64	4.30
10	7.09	7.56	7.77	8.64
Root mean square value of uncertainty for 0.25 m × 0.25 m CFB setup = 3.92%				

TH-1848_Shankarrao

Thus uncertainty has been predicted at thirty different locations including lower, middle and upper splash region where thermocouples have been attached in the heated section of the riser. In the same way, uncertainty was also evaluated for U* = 5, 6, 8 at P = 1750 N/m^2 and P = 3050 N/m^2 for 3 CFB units. Uncertainty is depending upon connections of thermocouples, accuracy of T type thermocouple, wattmeter accuracy, accuracy in length measurement etc. The root mean square value of uncertainty for total experiments conducted on 0.15 m × 0.15 m, 0.20 m × 0.20 m, and 0.25 m × 0.25 m CFB setup was 4.73%, 6.65%, 6.22%, respectively.

TH-1848_Shankarrao

Appendix F

Rayleigh's Method to Obtain Non-dimensional Numbers

1. CFB Risers and Cyclone Separators

For CFB riser, let us take local heat transfer coefficient is the function of operating parameters like superficial velocity of air (U), suspension density (ρ_{sus}), density of air (ρ_{air}), geometrical parameter like hydraulic diameter of riser / heater (B), height of the heater (H), and terms indicating other properties of mixture (air and sand mixture) like specific heat of mixture (Cp_{gs}), thermal conductivity of mixture (k_{gs}) and kinematic viscosity of air (μ_g).

$h = C\ U^a\ \rho_{sus}^{\ b}\ \rho_{air}^{\ c}\ B^d\ H^e\ Cp_{gs}^{\ f}\ k_{gs}^{\ g}\ \mu_g^{\ i}$ ....(F.1)

Where 'C' is constant.

Expressing the quantities in terms of fundamental dimensions M, L, t and T.

$Mt^{-3}T^{-1} = (Lt^{-1})^a\ (ML^{-3})^b\ (ML^{-3})^c\ (L)^d\ (L)^e\ (L^2t^{-2}T^{-1})^f\ (MLt^{-3}T^{-1})^g\ (ML^{-1}t^{-1})^i$

$= M^{b+c+g+i}\ L^{a-3b-3c+d+e+2f+g-i}\ t^{-a-2f-3g-i}\ T^{-f-g}$

For dimensional homogeneity of

M: $b + c + g + i = 1$ .....(F.2)

L: $a - 3b - 3c + d + e + 2f + g - i = 0$ .....(F.3)

t: $- a - 2f - 3g - i = - 3$.....(F.4)

T: $-f - g = -1$.....(F.5)

Equation (F.5) becomes, $f + g = 1$.....(F.6)

Equation (F.4) becomes, $a + 2f + 3g + i = 3$

$a + 2(f + g) + g + i = 3$

$a + g + i = 1$ or $a + i = 1 - g$ or $a + i = f$ .....(F.7)

Equation (F.2) becomes, $b + c = a$ .....(F.8)

Equation (F.3) becomes, $a - 3(a) + d + e + f + f + g - i = 0$

$-2a + d + e + f - i = -1$

$2a - d - e - f + i = 1$

TH-1848_Shankarrao

$$a - d - e = 1 \quad \text{.....(F.9)}$$

Therefore eq. (F.1) may be written as

$$h = C\, U^{a}\, \rho_{sus}^{\,b}\, \rho_{air}^{\,a-b}\, B^{a-1-e}\, H^{e}\, Cp_{gs}^{\,f}\, k_{gs}^{\,1-f}\, \mu_{g}^{\,f-a}$$

$$h = C\, U^{a}\, \rho_{air}^{\,a}\, B^{a}\, \mu_{g}^{\,-a} \times \rho_{sus}^{\,b}\, \rho_{air}^{\,-b} \times B^{-e}\, H^{e} \times Cp_{gs}^{\,f}\, k_{gs}^{\,-f}\, \mu_{g}^{\,f} \times B^{-1}\, k_{gs}^{\,1}$$

$$\frac{hB}{k_{gs}} = Nu_{B} = C\left[\frac{\rho_{g} BU}{\mu_{g}}\right]^{a}\left[\frac{\rho_{sus}}{\rho_{g}}\right]^{b}\left[\frac{H}{B}\right]^{e}\left[\frac{\mu_{g} Cp_{gs}}{k_{gs}}\right]^{f} = C\left[\mathrm{Re}_{B}\right]^{a}\left[\frac{\rho_{sus}}{\rho_{g}}\right]^{b}\left[\mathrm{Pr}\right]^{f}\left[\frac{H}{B}\right]^{e} \quad \text{.....(F.10)}$$

Above eq. (F.10) is the correlation used in chapter 4, section 4.4.4, eq. (4.6). However Prandtl number (Pr) has been omitted there because variation of Pr was not significant ($0.71 < Pr < 0.76$).

In the similar way Rayleigh method has been used to obtain the non-dimensional numbers used in the correlation for cyclone separator (refer chapter 6, eq. 6.1) and also for correlations on lower splash, middle splash region and entire riser (refer chapter 4, eqs. 4.3, 4.4 and 4.5 respectively). For cyclone separator, heat transfer coefficient was a function of, $h_c = f\{U, \rho_{sus}, \rho_{air}, D_C, Y, Cp_{gs}, k_{gs}, \mu_g\}$. For eqs. 4.3, 4.4 and 4.5 of chapter 4, heat transfer coefficient was the function of, $h = f\{U, U_{mf}, \rho_{air}, Cp_{gs}, k_{gs}, \mu_g, A_B, A_S, H_m, Hr, H_B, H_D\}$

2. Use of Findfit Function of Mathematica Version 5.2 to Obtain the Exponents of Non-dimensional Numbers

2.1 Correlation for Lower Splash Region

Steps to follow

In Mathematica 5.2, using following information, data.

Table F.1

U*	Re_B	A_B / A_S	H_m / Hr	H_B / H_D	Nu_B
5	23739.80	0.0625	0.40	0.833	111.63
5	23739.80	0.0625	0.32	0.833	122.60
5	23739.80	0.0625	0.22	0.833	236.21
8	30479.49	0.0625	0.40	0.833	80.82
8	30479.49	0.0625	0.32	0.833	97.12
8	30479.49	0.0625	0.22	0.833	414.42
5	25148.09	0.0625	0.40	1.466	124.46
5	25148.09	0.0625	0.32	1.466	139.09

TH-1848_Shankarrao

Table F.1 Cont....

U*	Re_B	A_B / A_S	H_m / Hr	H_B / H_D	Nu_B
5	25148.09	0.0625	0.22	1.466	374.00
8	35710.79	0.0625	0.40	1.466	104.07
8	35710.79	0.0625	0.32	1.466	118.69
8	35710.79	0.0625	0.22	1.466	618.28
5	31653.07	0.0833	0.40	0.625	187.93
5	31653.07	0.0833	0.32	0.625	194.62
5	31653.07	0.0833	0.22	0.625	641.07
8	40639.32	0.0833	0.40	0.625	197.02
8	40639.32	0.0833	0.32	0.625	203.71
8	40639.32	0.0833	0.22	0.625	749.33
5	33530.79	0.0833	0.40	1.1	205.61
5	33530.79	0.0833	0.32	1.1	221.23
5	33530.79	0.0833	0.22	1.1	923.88
8	47613.73	0.0833	0.40	1.1	244.62
8	47613.73	0.0833	0.32	1.1	392.56
8	47613.73	0.0833	0.22	1.1	969.09
5	39566.34	0.1041	0.40	0.5	199.38
5	39566.34	0.1041	0.32	0.5	227.68
5	39566.34	0.1041	0.22	0.5	1963.5
8	50799.15	0.1041	0.40	0.5	270.14
8	50799.15	0.1041	0.32	0.5	298.45
8	50799.15	0.1041	0.22	0.5	1660.64
5	41913.49	0.1041	0.40	0.88	272.93
5	41913.49	0.1041	0.32	0.88	326.13
5	41913.49	0.1041	0.22	0.88	1889.9
8	59516.17	0.1041	0.40	0.88	287.50
8	59516.17	0.1041	0.32	0.88	340.70
8	59516.17	0.1041	0.22	0.88	2813.5

data={{5,23739.8,0.0625,0.403509,0.833,111.6322},{5,23739.8,0.0625,0.326316,0.8
33,122.6033},{5,23739.8,0.0625,0.22807,0.833,236.219},{8,30479.49,0.0625,0.4035

TH-1848_Shankarrao

09,0.833,80.82645},{8,30479.49,0.0625,0.326316,0.833,97.1281},{8,30479.49,0.062
5,0.22807,0.833,414.4215},{5,25148.09,0.0625,0.403509,1.466,124.4628},{5,25148.
09,0.0625,0.326316,1.466,139.0909},{5,25148.09,0.0625,0.22807,1.466,374.0083},{
8,35710.79,0.0625,0.403509,1.466,104.0702},{8,35710.79,0.0625,0.326316,1.466,11
8.6983},{8,35710.79,0.0625,0.22807,1.466,618.2851},{5,31653.07,0.0833,0.403509,
0.625,187.9339},{5,31653.07,0.0833,0.326316,0.625,194.6281},{5,31653.07,0.0833,
0.22807,0.625,641.0744},{8,40639.32,0.0833,0.403509,0.625,197.0248},{8,40639.3
2,0.0833,0.326316,0.625,203.719},{8,40639.32,0.0833,0.22807,0.625,749.3388},{5,
33530.79,0.0833,0.403509,1.1,205.6198},{5,33530.79,0.0833,0.326316,1.1,221.2397
},{5,33530.79,0.0833,0.22807,1.1,923.8843},{8,47613.73,0.0833,0.403509,1.1,244.6
281},{8,47613.73,0.0833,0.326316,1.1,392.562},{8,47613.73,0.0833,0.22807,1.1,96
9.0909},{5,39566.34,0.1041,0.403509,0.5,199.3802},{5,39566.34,0.1041,0.326316,0
.5,227.686},{5,39566.34,0.1041,0.22807,0.5,1963.533},{8,50799.15,0.1041,0.40350
9,0.5,270.1446},{8,50799.15,0.1041,0.326316,0.5,298.4504},{8,50799.15,0.1041,0.2
2807,0.5,1660.64},{5,41913.49,0.1041,0.403509,0.88,272.9339},{5,41913.49,0.1041
,0.326316,0.88,326.1364},{5,41913.49,0.1041,0.22807,0.88,1889.97},{8,59516.17,0.
1041,0.403509,0.88,287.5},{8,59516.17,0.1041,0.326316,0.88,340.7025},{8,59516.1
7,0.1041,0.22807,0.88,2813.533}}

$$expr = c * U^{*a} * Re^{b} * A^{d} * H^{e} * Asp^{f}$$

$A^{d}\,As^{f}\,c\,H^{e}\,Re^{b}\,U^{a}$

pars={c,a,b,d,e,f}

{c,a,b,d,e,f}

vars={U^{*},Re,A,H,As_p}

{U^{*},Re,A,H,As_p}

FindFit[data,expr,pars,vars]

TH-1848_Shankarrao

{c→0.0000272107, a→-0.721379, b→1.65208, d→2.07818, e→-4.3543, f→0.169056}

Note: for example, data = {5, 23739.8, 0.0625, 0.403509, 0.833, 111.6322}

= {U^*, Re_B, A^*, H*, A_{Sp}, $Nu_{B\text{ - experimental}}$}.

Where U^* = 5, Non-dimensional superficial velocity of air , as defined in Appendix C.

= 2.36 / 0.47 = 5

Re_B = 23739.8, bed Reynolds number

= {$\rho_{air} \times U' \times$ Hydraulic diameter of riser column / μ_{air}}

= {$1.2 \times 2.36 \times 0.15 / 1.7894 \times 10^{-5}$} = 23739.8

A = A_B / A_S = Cross section of riser / surface area of heater

= $0.15 \times 0.15 / \{(4 \times 0.15) \times 0.60\}$ = 0.0625

H^* = H_m / H_r = Ratio of height from the distributor plate to location of thermocouple in the heater to total height of the riser

= 1.14 / 2.85 = 0.403

As_p = H_B / H_D = Ratio of height of the static sand inventory of the fluidized bed to the hydraulic diameter of bed

= 0.125 / 0.15 = 0.833

$Nu_{B\text{ - experimental}}$ = h × H_D / Thermal conductivity of air

= $17.86 \times 0.15 / 0.024 = 111.63$ W/m^2K

2.2 Correlation for Middle Splash Region

data={{23739.8,5,0.0625,0.614035,0.833,65.33058},{23739.8,5,0.0625,0.536842,0.833,71.71488},{23739.8,5,0.0625,0.438596,0.833,185.3306},{30479.49,8,0.0625,0.614035,0.833,59.44215},{30479.49,8,0.0625,0.536842,0.833,81.40289},{30479.49,8,0.0625,0.438596,0.833,274.8347},{25148.09,5,0.0625,0.614035,1.466,88.38843},{25148.09,5,0.0625,0.536842,1.466,94.77273},{25148.09,5,0.0625,0.438596,1.466,212.2934},{35710.79,8,0.0625,0.614035,1.466,84.97934},{35710.79,8,0.0625,0.536842,1.466,109.5248},{35710.79,8,0.0625,0.438596,1.466,313.5124},{31653.07,5,0.0833,0.614035,0.625,87.02479},{31653.07,5,0.0833,0.536842,0.625,104.814},{31653.07,5,

0.0833,0.438596,0.625,380.2686},{40639.32,8,0.0833,0.614035,0.625,109.5248},{4
0639.32,8,0.0833,0.536842,0.625,129.4835},{40639.32,8,0.0833,0.438596,0.625,405
.9298},{33530.79,5,0.0833,0.614035,1.1,136.1777},{33530.79,5,0.0833,0.536842,1.
1,158.5537},{33530.79,5,0.0833,0.438596,1.1,420.6818},{47613.73,8,0.0833,0.6140
35,1.1,138.843},{47613.73,8,0.0833,0.536842,1.1,187.7913},{47613.73,8,0.0833,0.4
38596,1.1,453.0372},{39566.34,5,0.1041,0.614035,0.5,130.4132},{39566.34,5,0.104
1,0.536842,0.5,144.7934},{39566.34,5,0.1041,0.438596,0.5,448.2645},{50799.15,8,
0.1041,0.614035,0.5,152.9132},{50799.15,8,0.1041,0.536842,0.5,169.8967},{50799.
15,8,0.1041,0.438596,0.5,582.5207},{41913.49,5,0.1041,0.614035,0.88,145.8223},{
41913.49,5,0.1041,0.536842,0.88,177.7438},{41913.49,5,0.1041,0.438596,0.88,633.
8802},{59516.17,8,0.1041,0.614035,0.88,203.4917},{59516.17,8,0.1041,0.536842,0.
88,265.1033},{59516.17,8,0.1041,0.438596,0.88,692.1694}}

$expr = c * Re^a * U^{*b} * A^d * H^e * Asp^f$

$A^d As^f c H^e Re^a U^b$

pars={c,a,b,d,e,f}

{c,a,b,d,e,f}

vars={Re,U^*,A,H,As_p}

{Re,U,A,H,As_p}

FindFit[data,expr,pars,vars]

{c→138.986, a→0.139965, b→0.26453, d→1.84654, e→-4.54952, f→0.347764}

Table F.2

U*	Re_B	A_B / A_S	H_m / Hr	H_B / H_D	Nu_B
5	23739.8	0.0625	0.61	0.833	65.33
5	23739.8	0.0625	0.53	0.833	71.71
5	23739.8	0.0625	0.43	0.833	185.33
8	30479.49	0.0625	0.61	0.833	59.44
8	30479.49	0.0625	0.53	0.833	81.40
8	30479.49	0.0625	0.43	0.833	274.83

TH-1848_Shankarrao

Table F.2 Cont....

U*	Re_B	A_B / A_S	H_m / Hr	H_B / H_D	Nu_B
5	25148.09	0.0625	0.61	1.466	88.38
5	25148.09	0.0625	0.53	1.466	94.77
5	25148.09	0.0625	0.43	1.466	212.29
8	35710.79	0.0625	0.61	1.466	84.97
8	35710.79	0.0625	0.53	1.466	109.52
8	35710.79	0.0625	0.43	1.466	313.51
5	31653.07	0.0833	0.61	0.625	87.024
5	31653.07	0.0833	0.53	0.625	104.81
5	31653.07	0.0833	0.43	0.625	380.26
8	40639.32	0.0833	0.61	0.625	109.52
8	40639.32	0.0833	0.53	0.625	129.48
8	40639.32	0.0833	0.43	0.625	405.92
5	33530.79	0.0833	0.61	1.1	136.17
5	33530.79	0.0833	0.53	1.1	158.55
5	33530.79	0.0833	0.43	1.1	420.68
8	47613.73	0.0833	0.61	1.1	138.84
8	47613.73	0.0833	0.53	1.1	187.79
8	47613.73	0.0833	0.43	1.1	453.03
5	39566.34	0.1041	0.61	0.5	130.41
5	39566.34	0.1041	0.53	0.5	144.79
5	39566.34	0.1041	0.43	0.5	448.26
8	50799.15	0.1041	0.61	0.5	152.91
8	50799.15	0.1041	0.53	0.5	169.89
8	50799.15	0.1041	0.43	0.5	582.52
5	41913.49	0.1041	0.61	0.88	145.82
5	41913.49	0.1041	0.53	0.88	177.74
5	41913.49	0.1041	0.43	0.88	633.88
8	59516.17	0.1041	0.61	0.88	203.49
8	59516.17	0.1041	0.53	0.88	265.10
8	59516.17	0.1041	0.43	0.88	692.16

2.3 First Correlation for Entire Riser

data={{25148.1,5,0.0625,0.32,1.466,177.31},{25148.1,5,0.0625,0.53,1.466,121.44},
{25148.1,5,0.0625,0.74,1.466,91.25},{33530.8,5,0.0833,0.32,1.1,360.08},{33530.8,5
,0.0833,0.53,1.1,290.25},{33530.8,5,0.0833,0.74,1.1,214.58},{41913.5,5,0.1041,0.32
,0.88,549.9},{41913.5,5,0.1041,0.53,0.88,443.54},{41913.5,5,0.1041,0.74,0.88,335.4
2},{28165.9,5.6,0.0625,0.32,1.466,181.56},{28165.9,5.6,0.0625,0.53,1.466,127.53},
{28165.9,5.6,0.0625,0.74,1.466,95.05},{37554.5,5.6,0.0833,0.32,1.1,386.01},{37554
.5,5.6,0.0833,0.53,1.1,296.22},{37554.5,5.6,0.0833,0.74,1.1,220.03},{41662.,5.6,0.1
041,0.32,0.88,594.85},{41662.,5.6,0.1041,0.53,0.88,465.79},{41662.,5.6,0.1041,0.74
,0.88,347.67},{30177.7,6,0.0625,0.32,1.466,184.39},{30177.7,6,0.0625,0.53,1.466,1
29.1},{30177.7,6,0.0625,0.74,1.466,95.48},{40237.,6,0.0833,0.32,1.1,403.68},{4023
7.,6,0.0833,0.53,1.1,300.85},{40237.,6,0.0833,0.74,1.1,223.68},{44637.9,6,0.1041,0.
32,0.88,624.97},{44637.9,6,0.1041,0.53,0.88,480.64},{44637.9,6,0.1041,0.74,0.88,3
55.84},{33195.5,6.6,0.0625,0.32,1.466,188.64},{33195.5,6.6,0.0625,0.53,1.466,133.
67},{33195.5,6.6,0.0625,0.74,1.466,98.02},{44260.6,6.6,0.0833,0.32,1.1,429.28},{4
4260.6,6.6,0.0833,0.53,1.1,306.08},{44260.6,6.6,0.0833,0.74,1.1,229.13},{49101.7,6
.6,0.1041,0.32,0.88,669.8},{49101.7,6.6,0.1041,0.53,0.88,502.9},{49101.7,6.6,0.104
1,0.74,0.88,368.09},{35710.3,8,0.0625,0.32,1.466,198.56},{35710.3,8,0.0625,0.53,1.
466,144.38},{35710.3,8,0.0625,0.74,1.466,103.94},{47613.7,8,0.0833,0.32,1.1,489.7
5},{47613.7,8,0.0833,0.53,1.1,319.83},{47613.7,8,0.0833,0.74,1.1,241.83},{59517.2
,8,0.1041,0.32,0.88,774.69},{59517.2,8,0.1041,0.53,0.88,554.38},{59517.2,8,0.1041,
0.74,0.88,396.67},{23739.8,5,0.0625,0.32,0.833,147.5},{23739.8,5,0.0625,0.53,0.83
3,97.13},{23739.8,5,0.0625,0.74,0.833,73.75},{31653.1,5,0.0833,0.32,0.625,290.42}
,{31653.1,5,0.0833,0.53,0.625,213.58},{31653.1,5,0.0833,0.74,0.625,152.17},{3956
6.3,5,0.1041,0.32,0.5,441.15},{39566.3,5,0.1041,0.53,0.5,337.5},{39566.3,5,0.1041,
0.74,0.5,250.52},{24846.3,5.6,0.0625,0.32,0.833,149.55},{24846.3,5.6,0.0625,0.53,0
.833,100.63},{24846.3,5.6,0.0625,0.74,0.833,80.08},{33128.4,5.6,0.0833,0.32,0.625,
294.25},{33128.4,5.6,0.0833,0.53,0.625,220.24},{33128.4,5.6,0.0833,0.74,0.625,163
.52},{41410.5,5.6,0.1041,0.32,0.5,450.04},{41410.5,5.6,0.1041,0.53,0.5,348.91},{41
410.5,5.6,0.1041,0.74,0.5,266.83},{26455.8,6,0.0625,0.32,0.833,150.92},{26455.8,6,
0.0625,0.53,0.833,102.97},{26455.8,6,0.0625,0.74,0.833,84.33},{35274.4,6,0.0833,0
.32,0.625,296.81},{35274.4,6,0.0833,0.53,0.625,224.71},{35274.4,6,0.0833,0.74,0.6
25,170.34},{44093.,6,0.1041,0.32,0.5,456.},{44093.,6,0.1041,0.53,0.5,356.56},{440

93.,6,0.1041,0.74,0.5,277.76},{28165.9,6.6,0.0625,0.32,0.833,152.96},{28165.9,6.6,0.0625,0.53,0.833,106.46},{28165.9,6.6,0.0625,0.74,0.833,90.65},{37554.5,6.6,0.0833,0.32,0.625,300.63},{37554.5,6.6,0.0833,0.53,0.625,231.36},{37554.5,6.6,0.0833,0.74,0.625,181.19},{46943.1,6.6,0.1041,0.32,0.5,464.87},{46943.1,6.6,0.1041,0.53,0.5,367.94},{46943.1,6.6,0.1041,0.74,0.5,294.07},{30479.5,8,0.0625,0.32,0.833,157.75},{30479.5,8,0.0625,0.53,0.833,114.63},{30479.5,8,0.0625,0.74,0.833,105.44},{40639.3,8,0.0833,0.32,0.625,309.58},{40639.3,8,0.0833,0.53,0.625,246.92},{40639.3,8,0.0833,0.74,0.625,206.58},{50799.2,8,0.1041,0.32,0.5,485.63},{50799.2,8,0.1041,0.53,0.5,394.58},{50799.2,8,0.1041,0.74,0.5,332.08}}

$expr = c * Re^{a} * U^{*b} * A^{d} * H^{e} * Asp^{f}$

$A^{d}\, As^{f}\, c\, H^{e}\, Re^{a}\, U^{b}$

pars={c,a,b,d,e,f}

{c,a,b,d,e,f}

vars={Re,U^{*},A,H,As_p}

{Re,U^{*},A,H,As_p}

FindFit[data,expr,pars,vars]

{c→103.404, a→0.569282, b→0.0576903, d→2.23951, e→-0.636267, f→0.450281}

Table F.3

U*	Re_B	A_B / A_S	H_m / Hr	H_B / H_D	Nu_B
5	25148.1	0.0625	0.32	1.466	177.31
5	25148.1	0.0625	0.53	1.466	121.44
5	25148.1	0.0625	0.74	1.466	91.250
5	33530.8	0.0833	0.32	1.1	360.08
5	33530.8	0.0833	0.53	1.1	290.25
5	33530.8	0.0833	0.74	1.1	214.58

TH-1848_Shankarrao

Table F.3 Cont....

U*	Re_B	A_B / A_S	H_m / Hr	H_B / H_D	Nu_B
5	41913.5	0.1041	0.32	0.88	549.90
5	41913.5	0.1041	0.53	0.88	443.54
5	41913.5	0.1041	0.74	0.88	335.42
5.6	28165.9	0.0625	0.32	1.466	181.56
5.6	28165.9	0.0625	0.53	1.466	127.53
5.6	28165.9	0.0625	0.74	1.466	95.050
5.6	37554.5	0.0833	0.32	1.1	386.01
5.6	37554.5	0.0833	0.53	1.1	296.22
5.6	37554.5	0.0833	0.74	1.1	220.03
5.6	41662.0	0.1041	0.32	0.88	594.85
5.6	41662.0	0.1041	0.53	0.88	465.79
5.6	41662.0	0.1041	0.74	0.88	347.67
6	30177.7	0.0625	0.32	1.466	184.39
6	30177.7	0.0625	0.53	1.466	129.10
6	30177.7	0.0625	0.74	1.466	95.480
6	40237.0	0.0833	0.32	1.1	403.68
6	40237.0	0.0833	0.53	1.1	300.85
6	40237.0	0.0833	0.74	1.1	223.68
6	44637.9	0.1041	0.32	0.88	624.97
6	44637.9	0.1041	0.53	0.88	480.64
6	44637.9	0.1041	0.74	0.88	355.84
6.6	33195.5	0.0625	0.32	1.466	188.64
6.6	33195.5	0.0625	0.53	1.466	133.67
6.6	33195.5	0.0625	0.74	1.466	98.020
6.6	44260.6	0.0833	0.32	1.1	429.28
6.6	44260.6	0.0833	0.53	1.1	306.08
6.6	44260.6	0.0833	0.74	1.1	229.13
6.6	49101.7	0.1041	0.32	0.88	669.80
6.6	49101.7	0.1041	0.53	0.88	502.90
6.6	49101.7	0.1041	0.74	0.88	368.09

TH-1848_Shankarrao

Table F.3 Cont....

U*	Re_B	A_B / A_S	H_m / Hr	H_B / H_D	Nu_B
8	35710.3	0.0625	0.32	1.466	198.56
8	35710.3	0.0625	0.53	1.466	144.38
8	35710.3	0.0625	0.74	1.466	103.94
8	47613.7	0.0833	0.32	1.1	489.75
8	47613.7	0.0833	0.53	1.1	319.83
8	47613.7	0.0833	0.74	1.1	241.83
8	59517.2	0.1041	0.32	0.88	774.69
8	59517.2	0.1041	0.53	0.88	554.38
8	59517.2	0.1041	0.74	0.88	396.67
5	23739.8	0.0625	0.32	0.833	147.50
5	23739.8	0.0625	0.53	0.833	97.13}
5	23739.8	0.0625	0.74	0.833	73.75}
5	31653.1	0.0833	0.32	0.625	290.42
5	31653.1	0.0833	0.53	0.625	213.58
5	31653.1	0.0833	0.74	0.625	152.17
5	39566.3	0.1041	0.32	0.5	441.15
5	39566.3	0.1041	0.53	0.5	337.50
5	39566.3	0.1041	0.74	0.5	250.52
5.6	24846.3	0.0625	0.32	0.833	149.55
5.6	24846.3	0.0625	0.53	0.833	100.63
5.6	24846.3	0.0625	0.74	0.833	80.080
5.6	33128.4	0.0833	0.32	0.625	294.25
5.6	33128.4	0.0833	0.53	0.625	220.24
5.6	33128.4	0.0833	0.74	0.625	163.52
5.6	41410.5	0.1041	0.32	0.5	450.04
5.6	41410.5	0.1041	0.53	0.5	348.91
5.6	41410.5	0.1041	0.74	0.5	266.83
6	26455.8	0.0625	0.32	0.833	150.92
6	26455.8	0.0625	0.53	0.833	102.97
6	26455.8	0.0625	0.74	0.833	84.330

TH-1848_Shankarrao

Table F.3 Cont....

U*	Re_B	A_B / A_S	H_m / Hr	H_B / H_D	Nu_B
6	35274.4	0.0833	0.32	0.625	296.81
6	35274.4	0.0833	0.53	0.625	224.71
6	35274.4	0.0833	0.74	0.625	170.34
6	44093.0	0.1041	0.32	0.5	456.00
6	44093.0	0.1041	0.53	0.5	356.56
6	44093.0	0.1041	0.74	0.5	277.76
6.6	28165.9	0.0625	0.32	0.833	152.96
6.6	28165.9	0.0625	0.53	0.833	106.46
6.6	28165.9	0.0625	0.74	0.833	90.65}
6.6	37554.5	0.0833	0.32	0.625	300.63
6.6	37554.5	0.0833	0.53	0.625	231.36
6.6	37554.5	0.0833	0.74	0.625	181.19
6.6	46943.1	0.1041	0.32	0.5	464.87
6.6	46943.1	0.1041	0.53	0.5	367.94
6.6	46943.1	0.1041	0.74	0.5	294.07
8	30479.5	0.0625	0.32	0.833	157.75
8	30479.5	0.0625	0.53	0.833	114.63
8	30479.5	0.0625	0.74	0.833	105.44
8	40639.3	0.0833	0.32	0.625	309.58
8	40639.3	0.0833	0.53	0.625	246.92
8	40639.3	0.0833	0.74	0.625	206.58
8	50799.2	0.1041	0.32	0.5	485.63
8	50799.2	0.1041	0.53	0.5	394.58
8	50799.2	0.1041	0.74	0.5	332.08

2.4 Correlation for Cyclone Separators

data={{15001,4,0.2,382.50},{15001,4,0.4,450.00},{15001,4,0.6,483.75},{15001,4,0.8,573.75},{15001,4,1,641.25},{19260,6,0.2,363.38},{19260,6,0.4,393.75},{19260,6,0.6,438.75},{19260,6,0.8,528.75},{19260,6,1,585.00},{15891,8,0.2,461.25},{15891,8,0.4,540.00},{15891,8,0.6,607.50},{15891,8,0.8,673.59},{15891,8,1,765.00},{2542

TH-1848_Shankarrao

5,10,0.2,438.75},{25426,10,0.4,495.00},{25426,10,0.6,540.00},{25426,10,0.8,635.63},{25426,10,1,675.00},{20001,8,0.2,555.00},{20002,8,0.4,637.50},{20002,8,0.6,705.00},{20002,8,0.8,795.00},{20002,8,1,900.00},{25680,10,0.2,510.00},{25680,10,0.4,570.00},{25680,10,0.6,645.00},{25680,10,0.8,750.00},{25680,10,1,840.00},{21188,12,0.2,690.00},{21188,12,0.4,757.50},{21188,12,0.6,825.00},{21188,12,0.8,943.11},{21188,12,1,1054.97},{33901,14,0.2,619.50},{33901,14,0.4,705.00},{33901,14,0.6,780.00},{33901,14,0.8,892.50},{33901,14,1,945.00},{25002,12,0.2,731.25},{25002,12,0.4,825.00},{25002,12,0.6,900.00},{25002,12,0.8,1050.00},{25002,12,1,1181.25},{32100,14,0.2,656.25},{32100,14,0.4,750.00},{32100,14,0.6,825.00},{32100,14,0.8,975.00},{32100,14,1,1106.25},{26485,16,0.2,900.00},{26485,16,0.4,993.75},{26485,16,0.6,1068.75},{26485,16,0.8,1218.75},{26485,16,1,1350.00},{42376,18,0.2,825.00},{42376,18,0.4,918.75},{42376,18,0.6,993.75},{42376,18,0.8,1143.75},{42376,18,1,1237.50}}

$expr = c * Rec^{a} * Ro^{*b} * L^{*d}$

$c\ L^{d}\ Re^{a}\ Ro^{b}$

pars={c,a,b,d}

{c,a,b,d}

vars={Re_c,Ro^{*},L^{*}}

{Re_c,Ro^{*},L^{*}}}

where, $Ro^{*} = \rho_{sus}/\rho_g$, (ratio of suspension density to the density of air) and $L^{*} = Y/D_C$, (ratio of the distance (Y) of the different thermocouples location with respect to T7-T11 as in Fig. 3.5, measured from the inlet of the cyclone separator, normalized with respect to barrel diameter of the cyclone separator).

FindFit [data,expr,pars,vars]

{c→5229.21, a→-0.384964, b→0.901322, d→0.294613}

Table F.4

Re_C	ρ_{sus}/ρ_g	Y / D_C	Nu_C
15001	4	0.2	382.50

Table F.4 Cont....

Re_C	ρ_{sus}/ρ_g	Y / D_C	Nu_C
15001	4	0.4	450.00
15001	4	0.6	483.75
15001	4	0.8	573.75
15001	4	1	641.25
19260	6	0.2	363.38
19260	6	0.4	393.75
19260	6	0.6	438.75
19260	6	0.8	528.75
19260	6	1	585.00
15891	8	0.2	461.25
15891	8	0.4	540.00
15891	8	0.6	607.50
15891	8	0.8	673.59
15891	8	1	765.00
25425	10	0.2	438.75
25426	10	0.4	495.00
25426	10	0.6	540.00
25426	10	0.8	635.63
25426	10	1	675.00
20001	8	0.2	555.00
20002	8	0.4	637.50
20002	8	0.6	705.00
20002	8	0.8	795.00
20002	8	1	900.00
25680	10	0.2	510.00
25680	10	0.4	570.00
25680	10	0.6	645.00
25680	10	0.8	750.00
25680	10	1	840.00
21188	12	0.2	690.00

TH-1848_Shankarrao

Table F.4 Cont....

Re_C	ρ_{sus}/ρ_g	Y / D_C	Nu_C
21188	12	0.4	757.50
21188	12	0.6	825.00
21188	12	0.8	943.11
21188	12	1	1054.97
33901	14	0.2	619.50
33901	14	0.4	705.00
33901	14	0.6	780.00
33901	14	0.8	892.50
33901	14	1	945.00
25002	12	0.2	731.20
25002	12	0.4	825.00
25002	12	0.6	900.00
25002	12	0.8	1050.0
25002	12	1	1181.2
32100	14	0.2	656.25
32100	14	0.4	750.00
32100	14	0.6	825.00
32100	14	0.8	975.00
32100	14	1	1106.2
26485	16	0.2	900.00
26485	16	0.4	993.75
26485	16	0.6	1068.75
26485	16	0.8	1218.75
26485	16	1	1350.0
42376	18	0.2	825.00
42376	18	0.4	918.75
42376	18	0.6	993.75
42376	18	0.8	1143.7
42376	18	1	1237.5

TH-1848_Shankarrao

2.5 Second Correlation for Entire Riser

data={{25148.09,130,4,198.56},{25148.09,030,4,144.38},{25148.09,7.5,4,103.94},{28165.86,120,4,188.64},{28165.86,025,4,133.67},{28165.86,7.2,4,098.02},{30177.71,113,4,184.39},{30177.71,022,4,129.10},{30177.71,6.9,4,95.480},{33195.48,107,4,181.56},{33195.48,021,4,127.53},{33195.48,6.5,4,095.05},{35710.29,100,4,177.31},{35710.29,020,4,121.44},{35710.29,006,4,091.25},{23739.80,120,4,157.75},{23739.80,025,4,114.62},{23739.80,6.5,4,105.43},{24846.31,115,4,152.96},{24846.31,022,4,106.46},{24846.31,006,4,090.65},{26455.79,109,4,150.92},{26455.79,020,4,102.97},{26455.79,5.8,4,084.33},{28165.86,100,4,149.55},{28165.86,015,4,100.63},{28165.86,5.4,4,080.08},{30479.49,090,4,147.50},{30479.49,010,4,97.125},{30479.49,005,4,073.75},{33530.79,200,3,489.75},{33530.79,060,3,319.83},{33530.79,016,3,241.83},{37554.48,180,3,429.28},{37554.48,050,3,306.08},{37554.48,014,3,229.13},{40236.94,160,3,403.68},{40236.94,040,3,300.85},{40236.94,012,3,223.68},{44260.64,150,3,386.01},{44260.64,033,3,296.22},{44260.64,010,3,220.03},{47613.73,140,3,360.08},{47613.73,030,3,290.25},{47613.73,008,3,214.58},{31653.06,190,3,309.58},{31653.06,055,3,246.91},{33128.42,175,3,300.63},{33128.42,047,3,231.36},{33128.42,013,3,181.19},{35274.39,156,3,296.81},{35274.39,038,3,224.71},{35274.39,10.8,3,170.3},{37554.48,143,3,294.25},{37554.48,036,3,220.24},{37554.48,8.9,3,163.52},{40639.32,130,3,290.41},{40639.32,020,3,213.58},{40639.32,007,3,152.16},{41913.49,270,02.4,775},{41913.49,90,2.4,554.4},{41913.49,24.5,2.4,397},{41662.012,240,2.4,670},{41662.012,075,2.4,503},{44637.87,207,02.4,625},{44637.87,058,2.4,480.64},{44637.87,17.1,2.4,355.84},{49101.65,193,2.4,594.85},{49101.65,045,2.4,465.79},{49101.65,13.5,2.4,347.67},{59517.16,180,2.4,549.9},{59517.16,040,2.4,443.54},{59517.16,010,2.4,335.42},{39566.33,260,2.4,485.62},{39566.33,085,2.4,394.58},{39566.33,23.5,2.4,332.08},{41410.52,235,2.4,464.87},{41410.52,072,2.4,367.94},{41410.52,020,2.4,294.07},{44092.99,203,2.4,456},{44092.99,056,2.4,356.56},{44092.99,15.8,2.4,277.76},{46943.10,186,2.4,450.04},{46943.10,057,2.4,348.91},{46943.10,12.4,2.4,266.83},{50799.15,170,2.4,441.14},{50799.15,030,2.4,337.5},{50799.15,009,2.4,250.52}}

$$expr = c * Re_B^{a} * Ro^{*b} * L^{*d}$$

$c\, L^{d}\, Re^{a}\, Ro^{b}$

pars={c,a,b,d}

{c,a,b,d}

vars={Re,Ro^*,L^*}

{Re,Ro^*,L^*} where, $Ro^* = \rho_{sus}/\rho_g$, (ratio of suspension density to the density of gas i.e air) and $L^* = H/B$, (ratio of height of the heater to the hydraulic diameter of the bed).

FindFit[data,expr,pars,vars]

{c→59.3494, a→0.2238481, b→0.241789, d→-1.70789}

Table F.5

Re_B	ρ_{sus}/ρ_g	H / B	Nu_B
25148.09	130	4	198.56
25148.09	030	4	144.38
25148.09	7.5	4	103.94
28165.86	120	4	188.64
28165.86	025	4	133.67
28165.86	7.2	4	098.02
30177.71	113	4	184.39
30177.71	022	4	129.10
30177.71	6.9	4	95.480
33195.48	107	4	181.56
33195.48	021	4	127.53
33195.48	6.5	4	095.05
35710.29	100	4	177.31
35710.29	020	4	121.44
35710.29	006	4	091.25
23739.80	120	4	157.75
23739.80	025	4	114.62
23739.80	6.5	4	105.43
24846.31	115	4	152.96
24846.31	022	4	106.46

Table F.5 Cont....

Re_B	ρ_{sus}/ρ_g	H / B	Nu_B
24846.31	006	4	090.65
26455.79	109	4	150.92
26455.79	020	4	102.97
26455.79	5.8	4	084.33
28165.86	100	4	149.55
28165.86	015	4	100.63
28165.86	5.4	4	080.08
30479.49	090	4	147.50
30479.49	010	4	97.125
30479.49	005	4	073.75
33530.79	200	3	489.75
33530.79	060	3	319.83
33530.79	016	3	241.83
37554.48	180	3	429.28
37554.48	050	3	306.08
37554.48	014	3	229.13
40236.94	160	3	403.68
40236.94	040	3	300.85
40236.94	012	3	223.68
44260.64	150	3	386.01
44260.64	033	3	296.22
44260.64	010	3	220.03
47613.73	140	3	360.08
47613.73	030	3	290.25
47613.73	008	3	214.58
31653.06	190	3	309.58
31653.06	055	3	246.91
33128.42	175	3	300.63
33128.42	047	3	231.36
33128.42	013	3	181.19

TH-1848_Shankarrao

Table F.5 Cont....

Re_B	ρ_{sus}/ρ_g	H / B	Nu_B
35274.39	156	3	296.81
35274.39	038	3	224.71
35274.39	10.8	3	170.30
37554.48	143	3	294.25
37554.48	036	3	220.24
37554.48	8.9	3	163.52
40639.32	130	3	290.41
40639.32	020	3	213.58
40639.32	007	3	152.16
41913.49	270	2.4	775.00
41913.49	90	2.4	554.40
41913.49	24.5	2.4	397.00
41662.01	240	2.4	670.00
41662.01	075	2.4	503.00
44637.87	207	2.4	625.00
44637.87	058	2.4	480.64
44637.87	17.1	2.4	355.84
49101.65	193	2.4	594.85
49101.65	045	2.4	465.79
49101.65	13.5	2.4	347.67
59517.16	180	2.4	549.90
59517.16	040	2.4	443.54
59517.16	010	2.4	335.42
39566.33	260	2.4	485.62
39566.33	085	2.4	394.58
39566.33	23.5	2.4	332.08
41410.52	235	2.4	464.87
41410.52	072	2.4	367.94
41410.52	020	2.4	294.07
44092.99	203	2.4	456.00

TH-1848_Shankarrao

Table F.5 Cont....

Re_B	ρ_{sus}/ρ_g	H / B	Nu_B
44092.99	056	2.4	356.56
44092.99	15.8	2.4	277.76
46943.10	186	2.4	450.04
46943.10	057	2.4	348.91
46943.10	12.4	2.4	266.83
50799.15	170	2.4	441.14
50799.15	030	2.4	337.50
50799.15	009	2.4	250.52

TH-1848_Shankarrao

Publications from Present Work

TH-1848_Shankarrao

Publications from Present Work

International Journals

1. R. S. Patil, M. Pandey, P. Mahanta, "Effect of Scale-up of Lower and Middle Splash Region on Heat Transfer Characteristics of Circulating Fluidized Bed Risers", Journal of Power and Energy (IMechE Part A, Sage Publications), 224 (8), 1059-1068, 2010.

2. R. S. Patil, M. Pandey, P. Mahanta, "Parametric Studies and Effect of Scale-up on Wall-to-Bed Heat Transfer Characteristics of Circulating Fluidized Bed Risers", Experimental Thermal and Fluid Science - International Journal of Experimental Heat Transfer, Thermodynamics, and Fluid Mechanics (Elsevier), 35 (3), 485-494, 2011.

3. R. S. Patil, P. Mahanta, M. Pandey, "Effect of Scale-up on Heat Transfer Characteristics of Cyclone Separators of Circulating Fluidized Beds", International Energy Journal, 11 (3), 123-130, 2010.

4. R. S. Patil, M. Pandey, P. Mahanta, "Effect of Scale-up on Heat Transfer Characteristics in Upper Splash Region of Circulating Fluidized Bed Risers", Journal of Energy and Power Engineering, 04 (6), 9-15, 2010.

5. P. Mahanta, R. S. Patil, M. Pandey "Effect of Particle size and Bed Inventory on Wall-to-Bed Heat Transfer Characteristics of Circulating Fluidized Bed Risers" Lecture Notes in Engineering and Computer Science, 2184 (1), 1495-1500, 2010.

International / National Conferences

6. R. S. Patil, M. Pandey, P. Mahanta, "Study on the Heat Transfer Characteristics in the Lower Splash Region of Circulating Fluidized Bed Riser", 7th World Conference on Experimental Heat Transfer, Fluid Mechanics and Thermodynamics, (ExHFT-7) Proceedings, Krakow, Poland, 28th June – 3rd July, 2009, pp. 555-561. (ISBN: 978-83-7464-235-4).

7. R. S. Patil, M. Pandey, P. Mahanta, "CFD Simulation for Heat Transfer and Hydrodynamics Characteristics of Circulating Fluidized Bed Riser", 1st International Conference on Energy Engineering and Eco- Balance (IC-EEE), MITR Pune, India, 16-18th February, 2009.

8. R. S. Patil, M. Pandey, P. Mahanta, K.L. Meena, Y.V. Singh, and P. Sharma, "Studies on Bed to Wall Heat Transfer in the Cyclone Separators of Circulating Fluidized Beds", International Conference on Energy Security and Climate Change: Issues, Strategies and Options (ESCC), AIT and RERIC Bangkok, Thailand, 6-8th August, 2008.

TH-1848_Shankarrao

9. R. S. Patil, M. Pandey, P.Mahanta, "Studies on Hydrodynamic Characteristics along the Riser of Circulating Fluidized Bed", IISC Centenary – International Conference on Advances in Mechanical Engineering (IC-ICAME), IISC Bangalore, India, 2-4th July, 2008.

10. Ranjit S. Patil, Manmohan Pandey, Pinakeswar Mahanta, "Study on Wall-to-Bed Heat Transfer Characteristics in the Upper Splash Region of Cold Circulating Fluidized Bed Risers", 9th International ISHMT-ASME Heat and Mass Transfer Conference (ISHMT-ASME), IIT Bombay, Mumbai, India, 4-6th January, 2010.

11. P. Mahanta, R. S. Patil, M. Pandey "Effect of Particle size and Bed Inventory on Wall-to-Bed Heat Transfer Characteristics of Circulating Fluidized Bed Risers", International Association of Engineers (IAENG)-World Congress on Engineering 2010, International Conference of Mechanical Engineering (ICME'10) London, UK, 30th June -2nd July, 2010.

12. Manmohan Pandey, Pinakeswar Mahanta, Patil Ranjit S., Gawali Mahesh Vijay, "Development of an Experimental Facility for the Study of Scale Effects in Circulating Fluidized Beds", National Conference on Recent Advances in Mechanical Engineering (NCRAME), NIT Silchar, India, 20-21st December, 2008.

621.042
SHA/P
PL1

THESIS
Lakshminath Bezbaroa Central Library
Indian Institute of Technology Guwahati
ACC. No. TH...1848.....
Date.....28/3/12.....